Gallium isotope fractionation during adsorption on clay and oxide minerals: implications for using gallium isotopes as a geochemical tracer

by

John Ulkem

A thesis

presented to the University of Waterloo

in fulfillment of the

thesis requirement for the degree of

Master of Science

in

Earth Sciences

Waterloo, Ontario, Canada, 2022

Author's Declaration

I hereby declare that I am the sole author of this thesis. This is a true copy of the thesis, including any required final revisions, as accepted by my examiners.

I understand that my thesis may be made electronically available to the public.

Abstract

Increasing climate change leads to the imbalance between silicate, sulfide, and carbonate weathering fluxes, influencing the global carbon budget. Thus, understanding this balance is critical for understanding future global warming. Gallium (Ga) concentration is low in carbonates, moderate in silicates, and high in some sulfides (e.g., sphalerite). Other significant fluxes of Ga into the environment are acid mine drainage streams caused by sulfide mineral oxidation and waste effluents from the semi-conductor industry. Thus, Ga isotopes can be a promising environmental tracer. However, utilization of Ga isotopes as tracer requires a comprehensive understanding of its mobility and isotope fractionation processes. Thus, this study focused on adsorption and how this process fractionates the isotope composition of Ga. Laboratory experiments were conducted with clay (kaolinite and Ca-montmorillonite) and oxide minerals (silica, aluminum oxide, and goethite) to determine the effects of pH, ionic strength, Al competition, and low temperature on Ga adsorption. Experimental results together with Ga speciation and adsorption modeling provide insight onto the Ga adsorption mechanisms and associated Ga isotope fractionation process. Ga isotope ratio analyses were conducted for samples from the adsorption experiments on clay minerals and aluminum oxide, as a function of pH and ionic strength at room temperature (21°C) by Multi-collector Inductively Coupled Plasma Mass Spectrometry (MC-ICP-MS). At low concentration (50 μg/L), Ga adsorption on kaolinite was highest (adsorbed Ga = 63%) at pH 4.8 and lowest at alkaline pH (adsorbed Ga = 0) at pH = 9 which was attributed to the formation of the SO_4Ga^{1-} surface complex at all pH values. Conversely, during adsorption on Ca-montmorillonite, ionic exchange and surface complexation ($SOH_2Ga(OH)_4$ and $SOGa(OH)_3^{1-}$) caused high Ga sorption in acidic solutions, but adsorption also decreased with increasing pH, where only surface complexation of $SOGa(OH)_3^{1-}$ occurred. At high concentrations (1000 μg/L and 3000 μg/L), Ga precipitation ($\alpha - GaOOH$) was observed at both 21°C and 5°C. In contrast with clay minerals, adsorption on oxide minerals was highest at mildly acidic to circumneutral pH (4 – 7). Ga adsorption on silica was highest (adsorbed Ga = 98%) at pH 4 where $SOGa(OH)_3^{1-}$ was formed, and lowest (adsorbed Ga = 44%) at pH 9 where $SOH(Ga(OH)_4^{1-})_2^{2-}$ was formed. Conversely, Ga adsorption on goethite was greater than 95% at pH 4 – 7 and lowest at pH 3 (adsorbed Ga = 14%), due to a single surface complex ($SOGa(OH)_2$). Ga adsorption on aluminum oxide was highest (adsorbed Ga ≈ 80%) at circumneutral pH (4 – 7), and lowest (adsorbed Ga = 24%) at pH 3. For all oxides, moderate Ga adsorption (adsorbed Ga ≈ 45%) occurred at alkaline pH (9).

Analysis of in-house reference standards for gallium isotopes demonstrated that there was a constant shift in the isotope data from the expected values. Analyzing the stock solution throughout the study shows a consistent value (2.04 ± 0.09‰, 2SD; n = 10). This is 0.6‰ higher than the δ^{71}Ga of the pure Ga solution used to prepare the experimental Ga stock solutions (δ^{71}Ga = 1.44 ± 0.09‰, 2SD; n = 21). This isotope fractionation is likely caused by the incomplete purification of the sample matrix and/or interfering elements that affect the accuracy of isotope ratio measurement. However, the degree of fractionation appears relatively constant within samples having similar matrix loading. Therefore, the isotopic data of the experimental samples can be interpreted with the assumption that the fractionation due to the isotopic analysis was somewhat consistent among experimental samples and in-house standards, given that their matrix element contents were also similar.

For Ga adsorption on clay and aluminum oxide minerals, the lighter isotope (^{69}Ga) was preferentially adsorbed on the solid phase, leaving the solution enriched in the heavier isotope (^{71}Ga). Ga isotope fractionation during adsorption on kaolinite, Ca-montmorillonite, and aluminum oxide followed the closed-system equilibrium model. For all minerals, fractionation factors (α) did not vary with solution pH, suggesting pH independent isotope fractionation. Ga isotope fractionation ($\Delta_{solution\text{-}solid}$) was greatest following adsorption on Ca-montmorillonite (1.70 ± 0.63‰, 2SD; n = 4) and was lowest after adsorption on aluminum oxide (0.62 ± 0.97‰, n = 6). Following Ga adsorption on kaolinite, $\Delta_{solution\text{-}solid}$ was 0.94 ± 0.37‰, 2SD; n = 5. Ga adsorption on kaolinite at pH 3 decreased with increasing ionic strength, but ionic strength had negligible effects on δ^{71}Ga values (1.78 ± 0.06‰, 2SD; n = 6). In experiments testing influence of adsorption on Ga/Al ratios, under acidic conditions (pH 3 and pH 5), Ga/Al remained unchanged whereas Ga/Al increased significantly at pH 7 due to the preferential adsorption of Ga and precipitation of Al as gibbsite. This study demonstrates that Ga adsorption on common aquifer minerals such as clays and oxides induces a relatively large fractionation between δ^{71}Ga in the solution and solid (1.70‰ for Ca-montmorillonite and 0.62‰ for aluminum oxide). Future studies can focus on other processes such as dissolution of primary minerals and precipitation of secondary minerals to provide a more comprehensive understanding on Ga isotope fractionation by chemical weathering processes. Overall, Ga isotopes can potentially be used as a geochemical tracer of chemical weathering due to the association of Ga with rocks whose weathering directly affects the global carbon budget. Ga isotopes may also be useful for tracing point sources of Ga from the technology industry which consumes large quantities of Ga, whose wastes can contaminate the environment.

Acknowledgements

Thank you to my supervisor Dr. Thai Phan for your support and mentorship which has undoubtedly pushed me to be better. This research was supported by the Natural Sciences and Engineering Research Council of Canada (NSERC) Discovery grant to Phan (RGPIN-2020-05442). This research would not be possible without the Metal Isotope Geochemistry Laboratory facilities at the University of Waterloo. The Metal Isotope Geochemistry Laboratory at Waterloo was funded by the Canada Foundation for Innovation, Ontario Research Fund, and University of Waterloo.

Also, thank you to Dr. Thai Phan and my co-supervisor Dr. Fereidoun Rezanezhad for giving me the opportunity to work on the lepidolite byproduct project in Summer 2019, helping to prepare me for my research and the grad program at UW. That research was funded by a research grant from Lepidico Ltd. to Rezanezhad and Phan, and NSERC Partnership Grants with Knight Piésold Ltd (Engage Grant to Rezanezhad: EGP-533973-18) and the University of Waterloo starter grant to Phan.

Thank you to Dr. Brian Kendall for allowing me to work in your lab and your generosity with storage space and lab supplies/equipment. Also, thank you for allocating generous time slots to our group during the COVID-19 pandemic. Thank you to Drs. Thai Phan, Fereidoun Rezanezhad, and Brian Kendall for offering your valuable comments, feedback, and suggestions during my proposal defense and committee meetings. Thank you to Dr. Sherry Schiff for agreeing to serve as my committee member despite having short notice. Also, thank you for your guidance in EARTH 622 which has helped me understand my isotope data better. Finally, thank you to our department coordinator, Sue Fisher, for providing the necessary administrative support along the way.

Dedication

Thank you to my parents for always loving, supporting, and believing in me- without you, it would not be possible. Thank you to Azin for listening to me talk about gallium and having a plate ready after those twelve-hour lab days. You guys kept me going and made this experience much more enjoyable. This thesis is dedicated to you.

Table of Contents

List of Figures

List of Tables

Chapter 1
Introduction and Study Objectives

1.1 Introduction

Chemical weathering of continental rocks is one of many important processes that determine the planetary fate of nutrients, geomorphology, ocean chemistry, and climate. Carbonate, sulfide, and silicate weathering controls the chemical constituents that regulate the dynamics of Earth's surface. While silicate weathering partly regulates Earth's climate due to fixing CO_2 from the atmosphere, carbonate weathering releases more CO_2 back into the atmosphere (Frings & Buss, 2019). Acid generation from sulfide weathering, especially in mining environments , can greatly enhance carbonate weathering, potentially offsetting CO_2 sinking by silicates (Jennings et al., 2000; Spence & Telmer, 2005) In addition, sulfide weathering can liberate toxic metals to the environment which poses a major threat to humans and ecosystems (Root et al., 2015).

Increasing climate change leads to the imbalance between silicate, sulfide, and carbonate weathering, influencing the global carbon budget. Thus, understanding the balance of the weathering fluxes and dominant weathering processes is critical for understanding future global warming. Naturally occurring isotopes can be powerful geochemical tracers. Recently, there is strong interest in developing new isotope systems to provide further insights on chemical weathering regimes under a changing climate. Gallium (Ga) is potentially a useful tracer for several reasons. Ga is very low in carbonate minerals (average 0.06 ppm; Burton et al., 1959; Gray et al., 2013) and present at a considerable amount in silicate and sulfide minerals (Gray et al., 2013). Ga isotope composition is homogenous in silicate rocks. So, Ga isotope fractionation during chemical weathering is not likely affected by silicate lithologies (Kato et al., 2017). Aluminum (Al) is one of main rock forming elements and is geochemically similar to Ga (Diakonov, 1995; Yuan et al., 2018). As such, Ga and Al are considered chemical analogs, behaving similarly during rock weathering and interactions with secondary minerals such as clays (Yuan et al., 2018). Al is a known toxin to ecological systems at elevated level. Tracing principle processes controlling Al mobility is a challenge because it is monoisotopic (Derry, 2017). However, Ga can be a potential geochemical tracer of Al as it can act as its pseudo-isotope (Derry, 2017). Ga concentrations are generally high in acidic hot springs, which are features associated with oxidative sulfide weathering (Ogawa et al., 2012). Therefore, understanding Ga mobility can lend insight on distinguishing sulfide and silicate weathering processes. Moreover, mining of sulfide containing ores is a major source releasing Ga and other contaminants into the environment (Akcil &

Koldas, 2006). Other anthropogenic sources include electronic waste, coal fly ash, zinc and Al industry by-products in which Ga can be released both from manufacture and end-of-life of these products (Lu et al., 2017). In this regard, understanding Ga mobility can also assess the fate of Ga as an environmental contaminant.

Adsorption in aquatic environments is a major reaction affecting Ga concentration and isotope composition. However, geochemical processes controlling Ga mobility and its isotope fractionation have not been extensively studied. This is partly because Ga isotope analysis by Multicollector Inductively Coupled Plasma Mass Spectrometer (MC-ICP-MS) has only been recently possible owing to lack of high precision analytical instruments. One prior study reported appreciable Ga isotope fractionation due to adsorption on calcite and goethite under a range of pH values. However, the influence of other environmental factors such as ionic strength, competition with Al, and temperature on Ga isotope fractionation have not been studied. Likewise, Ga isotope fractionation by the adsorption on other minerals remains unknown. The current state of knowledge of Ga isotope fractionation processes is lacking which necessitates more studies to facilitate the use of Ga isotopes as a geochemical tracer. Therefore, the overarching goal of this research aims to evaluate the influence of environmental factors on the adsorption of Ga on common aquifer minerals and Ga isotope fractionation process.

1.2 Study Objectives

Ga can be a potential chemical weathering tracer and contaminant due to its increasing use in high technology industries. To address the gaps in the state of knowledge, this study aims to experimentally determine Ga isotope fractionation mechanisms and magnitudes during adsorption on clay and oxide minerals. Specific objectives are outlined below.

- Determine the Ga isotope fractionation during adsorption on kaolinite (KGa-2) under varying pH values, temperature, and ionic strengths.
- Evaluate the role of pH on Ga isotope fractionation during adsorption on Ca-montmorillonite (Saz-1), silica, aluminum oxide, and goethite.
- Experimentally determine pH induced fractionation of the Ga/Al ratio during adsorption on each of the study minerals.

Chapter 2
Literature Review

2.1 Gallium Geochemistry

2.1.1 Concentration of Gallium in the Environment

Ga is a moderately volatile and rare trace metal existing in low concentrations throughout the Earth's crust. (Kato et al., 2017). Ga has three oxidation states: +1 (rare), +3, and elemental Ga (Ga^0), which is uncommon in nature (Moskalyk, 2003; Shaw, 1957; Yuan et al., 2016). A group 13 element, Ga behaves similarly with Al during igneous differentiation – both elements share the same valence (+3), and similar ionic radii and ionization potentials (De Argollo & Schilling, 1978; Kato et al., 2017). Consequently, Ga has a tendency to replace Al under such rock-forming conditions (Kato et al., 2017; Schulte & Foley, 2014). For the same reasons, Ga also replaces Fe^{3+} under oxidizing conditions (Kato et al., 2017). Ga has an average crustal abundance of 17 ppm (Wood & Samson, 2006; Yuan et al., 2016). The two stable isotopes of Ga are ^{71}Ga and ^{69}Ga, having average terrestrial abundances of 39.89% and 60.11%, respectively (Meija et al., 2016). Ga is mostly associated with Al oxide minerals such as bauxite and corundum. However, Ga concentrations are moderate to low in these minerals (Gray et al., 2013; Schulte & Foley, 2014). Primary Ga minerals such as gallite or ishiharaite are scarce and are mostly found in two sulfide ore deposits in Africa (Payne, 2016). Ga is also associated with Zn-rich polymetallic sulfide ores (Gray et al., 2013). Generally, Ga is highest in sulfides, moderate in silicates, and low in carbonates (Figure 2.1).

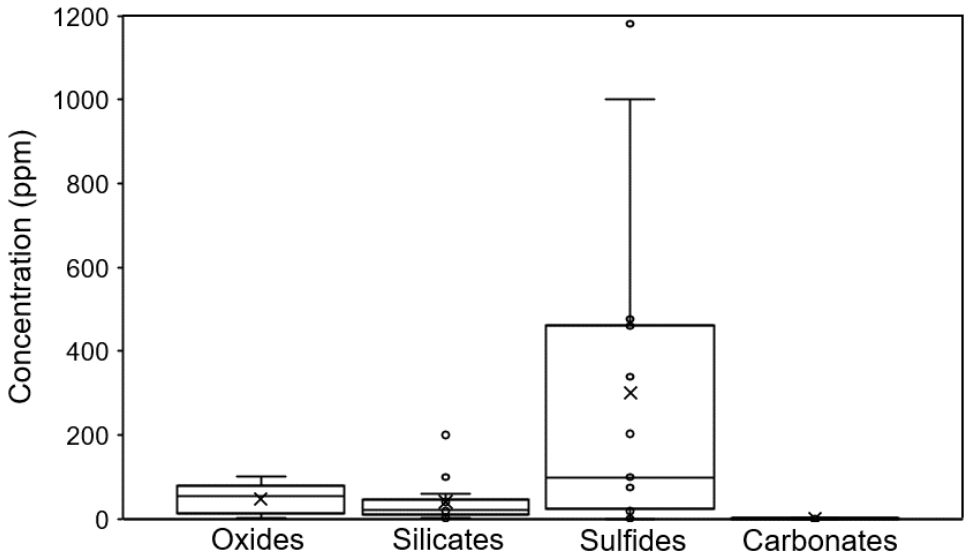

Figure 2.1. Ga abundances in major mineral groups

(Ball & Gilkes, 1987; Horbe & Anand, 2011; Sahlström et al., 2017; Schulte & Foley, 2014).

Although Ga can form many compounds, Ga is mostly a trace constituent and typically does not amass in any specific geological setting (Gray et al., 2013). Ga concentrations in several minerals are described in Table 2.1. Ga abundance is generally highest in sulfide minerals, though on a wide range. For example, sphalerite can contain up to 1181 ppm Ga, while pyrite contains only 0.4 ppm. Carbonates have virtually no association with Ga, with only 0.1 ppm Ga concentration in calcite. Oxides can have a maximum of 100 ppm Ga in minerals such as corundum, while minerals such as hematite and limonite have less than 5 ppm. Silicates generally contain less Ga than oxides, however, an exception to this is muscovite, containing 200 ppm Ga. Conversely, quartz lies on the low range of silicates with less than 1 ppm Ga.

Table 2.1. Ga abundances in different minerals.

Mineral	Type	[Ga] (ppm)	Mineral	Type	[Ga] (ppm)
Calcite[3]	Carbonate	0.1	Microcline[3]	Silicate	40
Cryolite[3]	Fluoride	3	Muscovite[3]	Silicate	200
Bauxite[3]	Oxide	90	Nepheline[3]	Silicate	20
Chromite[3]	Oxide	18	Oligoclase[3]	Silicate	10
Corundum[3]	Oxide	100	Olivine[3]	Silicate	2
Franklinite[3]	Oxide	10	Orthoclase[3]	Silicate	10
Hematite[3]	Oxide	1	Phlogopite[3]	Silicate	50
Limonite[3]	Oxide	3	Quartz[3]	Silicate	<1
Magnetite[3]	Oxide	30	Sodalite[3]	Silicate	100
Andesite (JA-3)[1]	Silicate	17	Spodumene[3]	Silicate	60
Albite[3]	Silicate	40	Rhyolite (JR-2) [1]	Silicate	18.2
Almandine[3]	Silicate	20	Jarosite[3]	Sulfate	8–23
Biotite[3]	Silicate	40	Barite[4]	Sulfide	0.4
Diopside[3]	Silicate	5	Pyrite[4]	Sulfide	0.2
Granite (JG-2) [1]	Silicate	19	Sphalerite[3]	Sulfide	1-1000
Hornblende[3]	Silicate	10	Sphalerite[2]	Sulfide	460
Lepidolite[3]	Silicate	100	Sphalerite[4]	Sulfide	1181

*Ando et al., 1987[1]; Fleischer, 1955[2]; Gray et al., 2013[3]; Sahlström et al., 2017[4]

In the bulk silicate earth (BSE), mantle xenoliths have been used to determine that the BSE Ga concentration is approximately 4 ppm (Kato et al., 2017; O'Neill & C., 1998). Consequently, Ga was relatively excluded from the Earth's core (Kato et al., 2017; McDonough, 2003). Meteorites and planets are depleted in Ga (6 – 10 ppm), and the mantle is even more-so, with comparable Ga abundance to the BSE (Kato et al., 2017; O'Neill & C., 1998). Ga abundance in planetary crusts is higher relative to the mantle because Ga tends to substitute Al during igneous differentiation (Kato et al., 2017). With nearly negligible Ga in the core according to mass balance, the Ga concentration of the bulk earth is around 2.7 ppm (Kato et al., 2017). The average seawater and stream water concentrations are 0.03 ppb and 0.15 ppb, respectively (Yu & Liao, 2011). Average groundwater Ga concentrations are less than 1 ppb (Yu & Liao, 2011). In geothermal waters, Ga concentrations are variable, but overall, they are

significantly higher than those in groundwater and surface water. Generally, average Ga concentrations in hot springs tend to be in the 2 – 3 ppb range, but can be as high as 120 ppm (Payne, 2016). In soils, Ga abundance ranges from 5 – 300 ppm, though it is normally between 5 and 70 ppm (Połedniok, 2008). Ga present in soils exists mainly by sorption to trivalent Fe and Mn oxides or organics in silty soils and to a less extent carbonate minerals in carbonate rich soils (Połedniok, 2008). Soils and groundwater near industrial areas are susceptible to a significant accumulation of Ga (Chen, 2006; Połedniok, 2008; Ringering et al., 2019). Most of the global Ga supply originates from bauxite and hydrothermal Pb-Zn resource mining in which the primary source of Ga is the byproduct of bauxite extraction for Al (Lu et al., 2017; Schulte & Foley, 2014). Zn ores also embody a significant Ga reservoir, having similar Ga concentrations with bauxite (Table 2.2). Coal represents the largest terrestrial reservoir of Ga (Table 2.2), in which the Ga is mostly present in kaolinite and boehmite (Lu et al., 2017). Worldwide Ga production was projected by the USGS to be 273 metric tons in 2012; main producers being Ukraine, China, Kazakhstan, and Germany (Schulte & Foley, 2014; Jaskula, 2013). Annually, Ga production is increasing by 7.4%, with 375 tons produced in 2016 also according to the USGS (Jaskula, 2017). By the year 2030, the global demand for Ga is anticipated to be twenty times that of 2012 (Gladyshev et al., 2015; Lu et al., 2017).

Table 2.2. Ga reserve estimates.

Raw material	Estimated reserve (10^9 tons)	Average [Ga] (ppm)
Bauxite	55 - 75	50
Zinc ore[a]	1.9	50[a]
Coal[b]	>1000	10

[a]Study refers to the Ga content of U.S. zinc ore due to lack of average [Ga] in global Zn resources

[b]Coal reserve estimated to a depth of ~1000 m

(BP, 2015; Frenzel et al., 2016; Jaskula, 2017; Lu et al., 2017; Thakur, 2017)

Industrial Ga consumption is rising rapidly, as it has become a cornerstone of the technology industry for its superior semiconducting characteristics (Erdmann & Graedel, 2011; European Commission & Ad-hoc Working Group, 2014; Frenzel et al., 2016; Ringering et al., 2019). Subsequently, the Ga containing wastes can eventually be leached into natural waters and interact with humans and other organisms. For this reason, it is especially important to understand Ga mobility in those environments.

2.1.2 Gallium Contamination in the Environment

Since Ga mobility and toxicity are not fully understood, water and air quality guideline for Ga concentrations has not been established (Yu & Liao, 2011). With low solubility and environmental abundance, background Ga concentrations in aquatic settings are also low (Yu & Liao, 2011). However, higher Ga levels (two orders of magnitude) were reported in groundwater samples proximal to an industrial area than those from a background site (Yu & Liao, 2011). Therefore, groundwater and surface water are potential routes for Ga contamination to reach organisms. In semiconductor factories, workplace air samples have been shown to have higher Ga concentrations than air from other parts of the facility (Yu & Liao, 2011). These factories mostly produce GaAs wafers, where up to 93 % of GaAs material is discarded (Torrance et al., 2010). The fate of this waste is typically in backside waste slurries containing up to 2,200 ppm Ga (Torrance et al., 2010). In fossil fuels, Ga is also present up to 1.2 ppm and 35 ppm in oil and coal, respectively (Yu & Liao, 2011). Therefore, in addition to semiconductor manufacturing, combustion of fossil fuel also releases Ga into the atmosphere. Ga is also released from acid mine drainage of sulfide mines, Al & Zn processing, and electronic waste (Akcil & Koldas, 2006; Lu et al., 2017). Ultimately, Ga accumulates in soils over time via sorption and can subsequently be taken up by plants (Jensen et al., 2018). Generally though, this uptake is relatively low in comparison to that of other metals (Jensen et al., 2018). Therefore, there is a higher health risk from directly ingesting high-Ga soil than ingesting high-Ga plants (Jensen et al., 2018). Regardless, the degree of Ga uptake by plants can vary for different plants and environmental conditions, making this risk variable. For example, paddy rice significantly uptakes Ga under acidic condition (Syu et al., 2020). In the same conditions but with Al presence, paddy rice was found to preferentially uptake Al instead of Ga (Syu et al., 2020). This example highlights the importance of studying the relationship between Ga and Al because they are usually present together and their relative mobilities can vary by environment.

2.1.3 Aqueous Geochemistry of Gallium

2.1.3.1 Ga in Aqueous Environments

Ga is only stable as Ga^{3+} in aqueous form and thus is not redox sensitive (Hacht, 2008; Kloo et al., 2002; Payne, 2016). However, redox conditions can directly affect Ga speciation by changing the anion species in solution available for complexation. Ga has low solubility and tends to precipitate several insoluble species (Benedicto et al., 2014; Stumm & Morgan, 2012). Moreover, Ga mobility in groundwater has neither been reported, nor is it well understood (Ringering et al., 2019). In water, Ga

readily undergoes hydrolysis. Due to its amphoterism, Ga is able to remain soluble at higher concentration in alkaline solutions (Lu et al., 2017) due to the formation of negatively-charged complexes with hydroxyl ions (Benedicto et al., 2014; Lu et al., 2017).

In natural environments, Ga can be released from chemical weathering of continental rocks. While Ga is transported via surface and groundwater, Ga interacts with many secondary minerals in soils that have high adsorption affinities, which is why adsorption is the focus of this study. However, many other environmental factors can also influence Ga mobility including pH, temperature, ionic strength, competing cations, etc. Thus, studying and understanding these processes is also important as they are fundamental in nature and highly relevant to Ga mobility and transport.

2.1.3.2 Aqueous Gallium Speciation

The aqueous speciation of Ga at low ionic strength (0.01M NaCl) and high Ga concentration (3800 µg/L) is illustrated in Figure 2.2. In aqueous environments, Ga^{3+} is the dominant species at pH<3. Between pH 2 and 6, five hydroxide species are formed, and only $Ga(OH)_4^-$ is present above pH 6 (Benedicto et al., 2014). Between pH 3.5 and 5.6, the precipitation of $Ga(OH)_{3,am}$ is predicted along with the presence of a small amount of aqueous $Ga(OH)_3$. Generally, $Ga(OH)_{3,am}$ is the likely Ga precipitate to form in lieu of $\alpha - GaOOH$, which is the other possible Ga precipitate (Baes Jr & Mesmer, 1976). Though the $\alpha - GaOOH$ precipitate is more stable than $Ga(OH)_{3,am}$, formation of $\alpha - GaOOH$ is not as thermodynamically favored as $Ga(OH)_{3,am}$ (Persson et al., 2006).

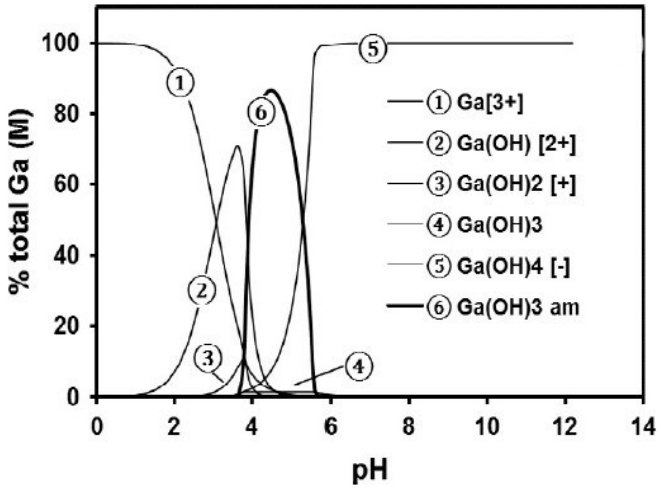

Figure 2.2. Ga speciation ([Ga] = 3800 µg/L) at 0.01 M NaCl (Benedicto et al., 2014).

To date, the understanding regarding gallium precipitate morphologies ($\alpha - GaOOH$ vs. $Ga(OH)_{3,am}$) remains unclear. This is generally simplified by applying the assumption that $\alpha - GaOOH$ doesn't initially form. So, Ga speciation models tend to only consider the precipitation of $Ga(OH)_{3,am}$ in the calculations. However, since this assumption has not been confirmed, the nature of Ga precipitation is still unclear. The stability regimes of $Ga(OH)_{3,am}$ and $\alpha - GaOOH$ are starkly different. $\alpha - GaOOH$ forms on a much wider range (from pH 3 – 8) with significantly more abundance (>99 %) than the $Ga(OH)_{3,am}$ for most of these pH values (Persson et al., 2006). Ga loss from precipitation as gallium oxyhydroxide cannot be clearly differentiated from other processes such as adsorption at high Ga concentrations, because they can occur at similar circumneutral pH values of natural water. However, hydrolysis is the main reaction that leads to the precipitation of Ga in those conditions. In hydrothermal environments, for example, Ga can also co-precipitate in high concentrations (900 μg/g) within the lattice of sulfide minerals such as sphalerite (Zhang et al., 2021).

The hydrolysis of cations can be influenced by ionic strength. In marine waters (pH > 7.7, 0.6 M NaCl), the primary Ga hydrolysis product is $Ga(OH)_4^-$ as reported by Savenko & Savenko, (2010); the same as in 0.01M NaCl. However, Ga complexation with chloride ions may lower the abundance of $Ga(OH)_4^-$ in solutions with high ionic strengths. This is important because soluble Ga in aqueous environments is usually in the form of hydrolysis products. When chloride complexation is significant, reactions that depend on hydrolyzed Ga species (such as adsorption) would be increasingly limited, thus affecting Ga mobility. Ga complexation with chloride has not been studied extensively in the context of Ga hydrolysis or adsorption. With an increasing flux of Ga into waters with a wide range of characteristics, further study regarding the influence of ionic strengths is needed.

2.1.3.3 Environmental Factors Controlling Gallium Adsorption

Adsorption is the process by which an atom or molecule within a matrix adheres to the surface of a solid, which in this study, is a mineral. The solute atoms and solid are called the adsorbate and adsorbent, respectively. Adsorption is important because it affects many chemical processes occurring at the solid-liquid interface. For example, adsorption impacts the electrostatic features of adsorbents (surface charge), the dispersal of matter, as well as surface reactivity of adsorbents (Stumm & Morgan, 1996). Many chemical reactions can occur at the interface between solids and liquids, depending on the materials' properties.

A) Influence of pH

In natural environment, aqueous Ga mobility is largely controlled by surface complexation with hydrolyzed Ga species. In fact, Ga's affinity to hydrolyze is a property associated with its sorption onto clay minerals and oxides (Benedicto et al., 2014). Since hydrolyzed species contain the same or similar ligands (oxide/hydroxide) as a hydrated solid's surface (water-hydroxide/oxide interface), the same bonds can be shared with Ga hydroxide species which are the dominant form of Ga in aqueous environments. The charge of aqueous Ga species also impacts surface complexation. The interaction of attractive and repulsive forces affects the ability of ions to approach the surface for bonding. This is further complicated by pH, where H^+ and OH^- ions in solution control Ga hydrolysis as well as the surface charge of the solid. The effects of pH on Ga adsorption tend to be significant. For example, at pH $\leq$ 3.1, $Ga(OH)_4^-$ was found to be preferentially adsorbed to goethite despite making less than 1% of total Ga species (Yuan et al., 2018). This is likely from the repulsion of Ga^{3+} and $Ga(OH)^{2+}$ by $>Fe(OH)_2^+$ which is goethite's dominant surface species at this pH range (Yuan et al., 2018). Furthermore, OH^- ions are attracted towards the layer of water immediately at the goethite surface, which is positively charged. At low pH, this attraction of OH^- facilitates the formation of $Ga(OH)_4^-$ in this layer by hydrolyzing Ga^{3+} (Hiemstra & Van Riemsdijk, 2006; Tamura et al., 2001; Yuan et al., 2018). Ga adsorption has previously shown pH dependence for several different minerals (Benedicto et al., 2014; Chegrouche & Bensmaili, 2002; Pokrovsky et al., 2004; Yuan et al., 2018). With most studied minerals, the majority of Ga adsorption occurs under mildly acidic to neutral pH, and less adsorption occurs in highly acidic or alkaline environments. Under such conditions, the extreme surface charges repel the available Ga species preventing them from being adsorbed. This adsorption behavior was observed for gallium adsorption on oxide minerals such as birnessite and goethite (Pokrovsky et al., 2004; Yuan et al., 2018). Under alkaline pH conditions, adsorption on magnesite and calcite also decreases (Pokrovsky et al., 2004), the same being true for the clay minerals illite and montmorillonite (Benedicto et al., 2014). Adsorption on magnesite and calcite at pH less than 5 has not been reported due to the high solubility of those minerals at lower pH. However, higher Ga adsorption was observed with illite and montmorillonite under acidic pH values (Benedicto et al., 2014). Ga adsorption on kaolinite was studied by Takahashi et al., (1999). This study demonstrated a peak adsorption of Ga at pH 5, decreasing with increasing acidity and alkalinity. Unlike illite and montmorillonite, Ga was not preferentially adsorbed on kaolinite under acidic pH values. Despite all being aluminosilicate clays, kaolinite is different in that it is a 1:1 clay; its structure has one tetrahedral Si-O sheet (SiO_4) and one

octahedral Al-O sheet (AlO_6). Illite and montmorillonite are 2:1 clays, where the Al-O sheet is between two Si-O sheets. The structures for 1:1 and 2:1 clays are illustrated in Figure 2.3.

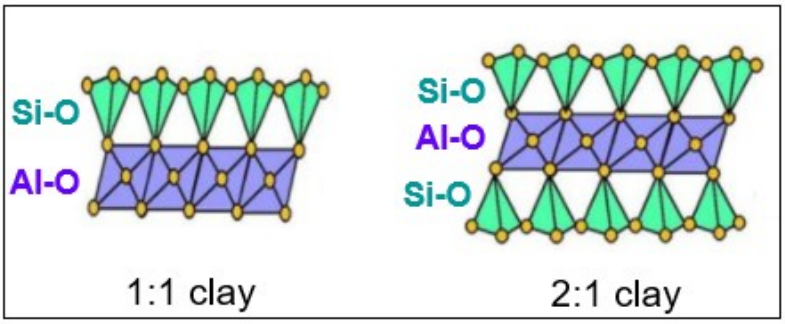

Figure 2.3. Mineral structures of 1:1 and 2:1 clays, adapted from Marchuk (2016).

Clay minerals can have variable charge sites, permanently charged sites, or a combination of both. The substitution of Al and Si in 2:1 clays such as montmorillonite and illite creates permanently negative charged sites in addition to the existing variable charge sites (Benedicto et al., 2014). Even in a highly protonated environment, these permanently negative sites would form, capable of exchanging Ga^{3+} with the central cation (Al or Si) by a process called ionic exchange. The lack of permanently negative sites in 1:1 clays explains why kaolinite is unable to preferentially adsorb Ga in acidic environments. In those minerals, the positive charge induced by protons in variable charge sites is not compensated by permanently negative sites. In that case, Ga^{3+} ions are mostly repelled instead of adsorbed.

B) Influence of Ionic Strength

There are very limited works studying the effects of ionic strength on Ga adsorption. Benedicto et al (2014) reported that Ga adsorption under acidic pH (2.5 – 5) on illite and montmorillonite at ionic strength of 0.2 M was significantly less than at 0.01 M. However, no measurable difference was observed at other pH values. This suggests that Ga adsorption is only ionic strength dependent under acidic conditions. In this study, the influence of ionic strength on Ga adsorption was studied for kaolinite, providing additional insights on how ionic strength affects Ga adsorption.

C) Influence of Temperature

Current understanding of temperature dependence for Ga adsorption is also limited and previous studies have only explored the effects of high temperatures. Between 20° and 80°C, Ga adsorption on bentonite has displayed an inverse relationship with temperature, decreasing by 60% as temperature increased

(Chegrouche & Bensmaili, 2002). In contrast, the Ga adsorption capacity of nano-TiO_2 increased from 2° to 40°C (Zhang et al., 2010). Adsorption behavior in relation to temperature is indicative of the reaction thermodynamics. If adsorption increases with temperature, the reaction is endothermic and the intermolecular forces between adsorbent and adsorbate are greater. If adsorption decreases with temperature as with bentonite, the forces are weaker because the reaction is exothermic.

2.2 Applications of the Ga/Al ratio as a Geochemical Tracer

2.2.1 Chemical Weathering Processes

Ga and Al are chemical analogs because they have comparable ionic radii, same coordination number, and same valence (Schier, 2021). Thus, they generally incorporate into minerals similarly, with a narrow range of Ga/Al ratios observed in most sediments, clastic sedimentary, and igneous rocks (Schier, 2021). The primary source of both Ga and Al to oceans is atmospheric dust which has a similar Ga/Al ratio with that of continental rocks (Schier, 2021). When atmospheric dust enters marine waters, Ga behavior is the same as with continental rock weathering where it dissolves more readily than Al (Schier, 2021). During chemical dissolution, the Ga-Al "pair" uncouples, resulting in distinct changes of the Ga/Al ratio (Schier et al., 2021). This is evident by observing distinct Ga/Al ratios in riverine waters compared with catchment area lithologies. Ga/Al ratios in riverine waters have been used to gauge intensity or extent of chemical weathering of their source rocks. Generally, weathering dominant (transport limited) environments have the Ga/Al ratios that are similar with their source rocks (Shiller, 1988; Shiller & Frilot, 1996). Much higher ratios are observed in weathering limited (transport dominated) areas (Shiller, 1988; Shiller & Frilot, 1996). This is caused by the preferential dissolution of Ga compared with Al because of larger ionic radius and greater hydrolysis constants of Ga (Schier et al., 2021; Shiller, 1988; Shiller & Frilot, 1996). Al only forms anionic complexes at pH > 8 whereas Ga does at pH > 5.3. Thus, Ga is less likely to undergo organic complexation in natural waters than Al. As a result, Ga/Al ratios progressively increase as riverine waters traverse into the oceans (Schier, 2021; Shiller, 1988; Shiller & Frilot, 1996). Furthermore, organic particles in marine water are negatively charged and they likely bond more easily with the abundant, neutral-charged $Al(OH)_3$ (Schier, 2021). Conversely, the dominant, anionic Ga species ($Ga(OH)_4^-$) would likely repel organic particles in marine waters. Thus, Ga has a longer residence time in seawater than Al which is more susceptible to adsorption onto particles (Schier, 2021; Shiller, 1988). Nevertheless, this observation about Ga and Al organic complexation does not always hold, with some organic ligands preferentially complexing with

Ga over Al. In that case, this effect could vary regionally and should be considered in that manner, as organic complexation has potential to fractionate Ga/Al ratios differently. The ratio of Ga/Al is also tied with lateritic weathering and weathering of its products: kaolinite and gibbsite (Hieronymus et al., 2001). In this case, the increased attraction of Ga to Fe (+3) oxides (Hieronymus et al., 2001) would lower the Ga/Al ratio in waters associated with lateritic weathering. The relationship is opposite for the weathering (dissolution) of kaolinite and gibbsite, where Al more readily precipitates than Ga, resulting in a higher Ga/Al ratio in the solution (Hieronymus et al., 2001). In this environment, the presence of Fe (III) oxides and oxyhydroxides leads to a higher Ga/Al ratio in the lateritic weathering products than in the source rocks.

2.2.2 High Temperature Geological Processes

Due to the geochemical similarity of Ga and Al, Ga/Al ratios do not fractionate during igneous differentiation (partial melting) or the late stages of crystallization (De Argollo & Schilling, 1978; Kato & Moynier, 2017). This is evidenced by the homogenous Ga/Al ratios found in a variety of silicate lithologies making up the BSE (Kato et al., 2017). Beside the atmospheric dusts and riverine fluxes (Section 2.2.1), the highly acidic, high temperature conditions in hydrothermal systems can significantly affect the fractionation of the Ga/Al ratios of marine waters due to aggressive interaction with continental rocks and sediments. Hydrothermal dissolution and precipitation can contribute to varying Ga/Al fluxes into seawater and result in Ga/Al fractionations. For this reason, it is important to understand the role of hydrothermal alteration of Ga/Al in marine water.

In two hydrothermal fields (Yuhuang and Duanquiao) of the Southwest Indian Ridge, a wide range of Ga/Al ratios were observed in the seafloor sediments (Zhang et al., 2021). The sediments were primarily calcareous, with the presence of Fe, Mn hydroxides. The carbonate phase in the calcareous sediments was found to contain a negligible amount of Ga (Zhang et al., 2021). Since Ga was associated with Fe in seafloor sediments, it is clear that Ga in the sediments was scavenged from seawater by the Fe and Mn oxides/hydroxides (Zhang et al., 2021). Fe and Mn oxides/hydroxides are generally known as hydrogenetic ferromanganese crusts which are sediments that precipitate slowly in ambient marine conditions at ocean ridges and plateaus (Schier, 2021). Due to their high surface area and surface properties, Fe and Mn oxides/hydroxides scavenge several trace elements including Ga (Schier et al., 2021; Schmidt et al., 2014). In this regard, the studies by Zhang et al. (2021) and Hieronymus et al., (2001) demonstrate that Fe and Mn oxides/hydroxides are likely to concentrate Ga. Therefore,

hydrothermal dissolution of Fe and Mn oxides/hydroxides could potentially be a significant source of Ga into seawater. Nonetheless, as reported by Yuan et al. (2018), goethite (Fe oxyhydroxide) is insoluble at pH 2.5, so dissolution of such minerals and releasing Ga is unlikely. As a result, adsorption on goethite decreases regional Ga/Al ratios due to their affinity for Ga. Although Ga is preferentially adsorbed Ga by Fe and Mn oxides/hydroxides, Ga/Al ratios were significantly lower than their respective seawaters, which were not expected (Schier, 2021). This is possibly attributed to lack of Ga available for adsorption due to preferential Ga complexation with certain organic particulates in marine water (Schier et al., 2021). This corroborates with the higher stability constants of Ga complexation with certain organic ligands than those of Al. As a result, Ga complexes with organics would be preferentially formed (Schier, 2021). So, the presence and nature of organic complexation with both Ga and Al must be fully considered to adequately evaluate the overall processes controlling the Ga/Al ratios.

Ga occurrence in the seafloor sulfides of the Southwest Indian Ridge hydrothermal fields was mainly present via isomorphic substitution in sphalerite (Zhang et al., 2021). Similar Ga isotope compositions between the sulfides and MORBs suggests that most Ga in the sulfides originates from MORBs (Zhang et al., 2021). Regardless, the association of Ga with massive seafloor sulfides makes them a potential Ga source into marine environments via hydrothermal dissolution. Due to the similar behavior of Ga and Al, it is possible for some extent of isomorphic Al substitution into the sphalerite structure during the formation of sulfides. However, the Ga substitution is preferential. Ga/Al ratios of the sulfides were not reported (Zhang et al., 2021), so the effect of their dissolution on seawater Ga/Al ratios is unknown. Overall, hydrothermal Al inputs are unlikely to have global significance to overall Al fluxes in the oceans, though regional importance may be observed (Ho et al., 2019). Conversely, hydrothermal input of Ga is somewhat similar to atmospheric Ga flux, which does have global significance (Ho et al., 2019).

2.3 Gallium Isotope Fractionation Processes

2.3.1 Adsorption

Adsorption is a major control on Ga mobility (Benedicto et al., 2014; Persson et al., 2006; Pokrovsky et al., 2004; Yuan et al., 2018). Still, the understanding regarding adsorption induced Ga isotope fractionation is very limited. To date, a laboratory study by Yuan et al. (2018) is the only study reporting Ga isotope fractionation due to adsorption on calcite and goethite. For both minerals, the lighter isotope

(^{69}Ga) was preferentially adsorbed, leaving the solution enriched in the heavier isotope (^{71}Ga). The results showed a large fractionation between the solution and solid phase, $\Delta_{solution\text{-}solid}$ = 1.27‰ and 0.89‰ for adsorption on calcite and goethite, respectively (Yuan et al., 2018). In both cases, the Ga isotope fractionations did not depend on the solution pH values. With adsorption on goethite, the isotope fractionation was due to the preferential adsorption/formation of $Ga(OH)_4^-$ at the goethite-water interface at all pH values, even where other Ga species were dominant. For calcite, only alkaline conditions were tested wherein $Ga(OH)_4^-$ was the only Ga hydroxide. Ga isotope fractionation by adsorption on calcite is due to difference (increase) in Ga–O bond length, and coordination number leap between $Ga(OH)_4^-$ in solution and the Ga–Ca complex on the calcite surface (Yuan et al., 2018). The coordination number and bond length both increase respectively from 4 and 1.84 Å in $Ga(OH)_4^-$, to 6 and 1.94 Å in the Ga–Ca complex (Yuan et al., 2018). In fact, coordination and bond length increased similarly with the Ga–Fe complex on the goethite surface. At isotopic equilibrium, heavier isotopes of an element generally concentrate in the phase where it can make shorter (stronger) bonds (Schauble, 2004). The findings by Yuan et al., 2018 illustrate this mechanism with calcite and goethite, reporting isotopically heavier solutions after adsorption. In this case, the shortest bonds (Ga–O) are in $Ga(OH)_4^-$ which preferentially incorporates ^{71}Ga. Thus, adsorption on these minerals is of a closed system equilibrium nature, illustrated by the linear trend of $\delta^{71}Ga_{solution}$ with the fraction of Ga removed from solution (Yuan et al., 2018). Closed system equilibrium processes are reversible, suggesting that Ga desorption could occur with both minerals. This is easily shown by calcite, whose dissolution in mildly acidic conditions would easily liberate sorbed Ga. Likewise, dissolution of Ga absorbed goethite could also liberate Ga, though under more acidic conditions due the resistance to acidic dissolution of goethite.

2.3.2 Precipitation and Dissolution

The influence of precipitation and dissolution on Ga isotopes remains unknown, with only one previous study discussing it. Ga in the sulfides from the Yuhuang and Duanquiao hydrothermal fields was found to mainly originate from MORB debris leaching, with negligible contribution from seawater (Zhang et al., 2021). This is supported by very similar average δ^{71}Ga values between the sulfides (+0.93 ‰ to +1.57 ‰) and MORBs (+1.2 ‰) whereas a much larger range observed in seawater (+1.92 ‰ to + 2.36 ‰). In addition, Ga concentrations in seawater is significantly lower than in MORBs (Zhang et al., 2021). The determination of the hydrothermal source (MORBs leachates) of Ga in sulfide minerals is

by assuming that the partial dissolution of MORBs or the precipitation with sulfides minimally fractionates Ga isotopes. It is noteworthy to mention that a much wider range of δ^{71}Ga of the sulfides from both hydrothermal fields were observed (+0.93 ‰ to +1.57 ‰), compared with δ^{71}Ga of MORBs which were homogenous (Zhang et al., 2021). This is probably due to sulfide formation processes, where sulfides rapidly precipitate and the different stages of sulfide formation can mix together in the hydrothermal environment (Zhang et al., 2021). Such processes could likely integrate the Ga from MORB debris leachates differently, resulting in the fractionation of Ga isotopes during partial dissolution and/or precipitation, explaining their range of δ^{71}Ga values.

In the same hydrothermal fields, Zhang et al. (2021) also studied Ga isotope ratios of calcareous seafloor sediments with different Ga concentrations, observing a narrow range of δ^{71}Ga (+1.28 ‰ to +1.47 ‰). In this case, it is evident that Ga isotopes can display slight fractionations during sediment formation (Zhang et al., 2021). As discussed earlier (Section 2.2.1) (Section 2.2.1), these sediments obtained the majority of their Ga from Fe and Mn oxides/hydroxides due to their ability to scavenge Ga easily from seawater. Though they could be a significant source of Ga, their contribution to seawater is unlikely due to their low solubility, even under highly acidic conditions. Also, since they preferentially incorporate Ga's lighter isotope (Yuan et al., 2018), they are likely to leave surrounding waters isotopically enriched in ^{71}Ga. This is supported by the overall higher δ^{71}Ga values in the regional seawater (+1.92 ‰ to + 2.36 ‰).

2.3.3 High Temperature Geological Processes

Even though high temperature processes are not the focus of this study, the discussion in this section provides comprehensive processes that induce Ga isotope fractionation to date. On Earth, the δ^{71}Ga of the bulk silicate earth (BSE) was determined to be homogenous, indicating that high temperature processes during the formation of silicate lithologies do not fractionate Ga isotopes (Kato et al., 2017). At extreme temperatures, however, light and heavy isotopes of an element may behave differently during volatilization, which is usually a kinetic isotope fractionation process. This is illustrated by the difference between isotope signatures of the Moon and Earth. During the impact that formed the Moon, extreme conditions caused the volatilization of many elements, including the moderately volatile Ga. As a result, lunar (mare) basalts are generally enriched in the heavier isotope of moderately volatile elements compared with Earth (Kato & Moynier, 2017). Kato & Moynier, (2017) investigated the volatile loss of Ga on the Moon by comparing δ^{71}Ga of the BSE and various mare basalts. Mare basalts

were found to be comparatively enriched in ^{71}Ga (by up to 0.57 ‰), and unlike the BSE, $\delta^{71}Ga$ values were heterogeneous (Kato & Moynier, 2017). Similar isotope enrichments were also observed with other elements, supporting the theory that volatile depletion of their lighter isotopes was caused by a large scale event (Kato & Moynier, 2017). During a massive impact, different processes can contribute to isotope fractionations. For example, as magma rises, pressure differences release gases enriched in ^{69}Ga which condense and deposit on the surface of lunar pyroclastic green glass (Kato & Moynier, 2017). The glass' surface thus has lower $\delta^{71}Ga$ values compared with its interior and the mare basalt (Kato & Moynier, 2017). Variability in the $\delta^{71}Ga$ values of lunar basalts could be attributed to source magma heterogeneity or secondary regional volatilization processes that redistributed Ga (Kato & Moynier, 2017). Wimpenny et al. (2020) tested the influence of extreme temperatures on Ga isotopes by laser-bombarding silicate rich soil (rhyolite) and comparing with the original rhyolite. In this study, Ga isotope fractionation followed the Rayleigh model, confirming that Ga volatilization is a kinetic isotope fractionation process (Wimpenny et al., 2020). However, those results did not correlate well with measured $\delta^{71}Ga$ of lunar basalts, suggesting that post-accretion (secondary) volatilization events further fractionated Ga isotopes (Wimpenny et al., 2020), supporting the hypothesis of Kato & Moynier (2017). In this regard, Ga isotopes can be used to trace extreme temperature events due to the isotope fractionations caused by volatilization. However, average $\delta^{71}Ga$ in these systems (such as the bulk silicate Moon) are not representative due to heterogeneity within lunar basaltic lithologies.

2.4 Adsorption Models

2.4.1 Non-Electrostatic vs. Electrostatic Models

Adsorption modeling can be categorized into two types: non-electrostatic and electrostatic (surface complexation) (US. EPA, 1999). Non-electrostatic models such as the Langmuir and Freundlich isotherms describe the relationship between the fractions of the adsorbed phase and the aqueous phase at chemical equilibrium. These models are relatively simple and do not provide insight about the chemical reactions occurring at surfaces. Instead, they describe the equilibrium adsorption capacity of the adsorbent for various adsorbate concentrations and provide indications about the homogeneity or heterogeneity of the solid surface. Though this can be useful, isotherms were not a focus of this research and thus are not further discussed.

Conversely, electrostatic models such as the CCM (Constant Capacitance Model), DLM (Diffuse Layer Model), and TLM (Triple Layer Model) describe the surface complexation reactions that occur during adsorption by performing thermodynamic calculations. They rely on thermodynamic databases and various system parameters for reliable results, and they differ by the assumptions they impose. For less studied systems, it is common for databases to lack necessary information such as certain chemical reactions and their equilibrium constants. For example, there is currently no database that includes complexation reactions between Ga and kaolinite. In this case, the modeling effort begins by studying previous research that studied adsorption on kaolinite with similar elements (such as Al). In many cases, the chemical reactions are identical or similar, and can be used as a starting point to describe the new system. The standard practice in SCMs is the use of mathematical techniques to optimize chemical reactions and equilibrium constants with other model parameters using software. Such software include Parameter Estimation (PEST); a program that uses the iterative Levenberg-Marquardt algorithm (LMA) which identifies the minimum value of an equation of the sum of squares for a nonlinear function (Lourakis, 2005). Using the most appropriate electrostatic model is important so the system is adequately characterized. Electrostatic models differ significantly in their assumptions and considerations, so it is important to understand their differences and apply them correctly. Accurate geochemical modeling clarifies the mechanisms behind isotope fractionations during adsorption, making surface complexation modeling (SCM) a powerful tool with great value.

2.4.2 The Electric Double Layer (EDL)

The electric double layer (EDL) refers to the complete ionic system illustrated in Figure 2.4 and is comprised of the charged mineral surface, uniformly charged Stern layer (inner-sphere), and the diffuse sublayer (outer-sphere) (Mojid, 2011). In the Stern layer, a linear relationship is observed between surface potential (ψ) and distance from the surface (x). Beyond the Stern layer, this relationship is no longer linear.

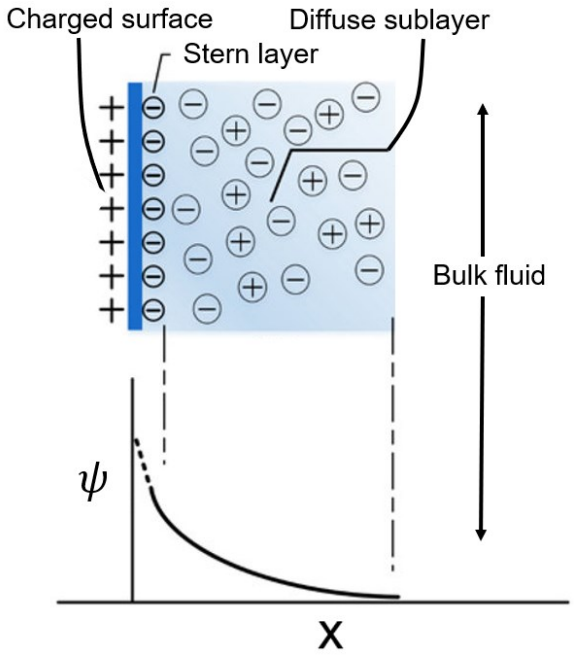

Figure 2.4. Diagram of the EDL and mineral surface (modified from Zhong et al. (2018).

Immediately outside the Stern layer is the neutrally charged diffuse sublayer, where ions of opposite polarity gather (Mojid, 2011). The diffuse sublayer neutralizes all net surface charge to 0. Depending on the system, ions may form inner-sphere or outer-sphere complexes, or both. Inner-sphere complexes are mostly formed by covalent bonding between cations and oxygen ions, and are formed in the Stern layer (Stumm, 1995). For simplicity, outer-sphere complexation can be considered to occur on an additional Stern layer. Jon Petter Gustafsson (2011) described this as the Stern layer split in two.

2.4.3 Constant Capacitance Model (CCM)

The CCM is a relatively simple SCM because it assumes that all surface complexes are inner-sphere. Further, no complexes are formed with the background electrolyte, and a linear relationship exists between surface charge density and surface potential through a constant capacitance (Equation 1) (Goldberg, 1992). The complexes form at the mineral's surface where ψ is greatest in the Stern layer (x = 0 or the "o" plane). The CCM's linear surface potential gradient in the Stern layer is illustrated in Figure 2.5.

$$\sigma = \kappa\psi \tag{1}$$

where $\sigma =$ surface charge $(\mathrm{C/m^2})$, $\kappa =$ capacitance $(\mathrm{F/m^2})$, $\psi =$ surface potential (V).

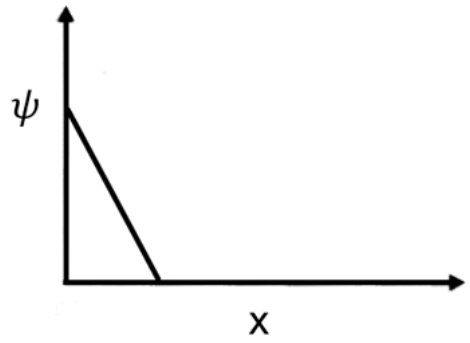

Figure 2.5. Surface potential (ψ) gradient in the Stern layer adapted from Goldberg (1992).

In the CCM, surface charge is given by Equation (2) where the net charge of protons and inner-sphere surface complexes are added in a simple expression.

$$\sigma_o = \sigma_{\mathrm{H}} + \sigma_{\mathrm{is}} \tag{2}$$

where σ_{H} and σ_{is} signify the net proton charge and charge of inner-sphere complexes, respectively.

There are many complexation reactions that can be considered at the solid-liquid interface. In the CCM, the core reactions considered are described in Equations (3, 4, 5, 6) adapted from (Hohl et al., 1980). In general, SCMs also account for the surface complexation with ligands, however, since they are all hydroxyl groups in this study, those reactions are excluded from discussion. With Ga, many complexes involve its hydrolyzed species, so water is commonly another reactant in Equation (5) to produce the Ga hydroxide surface complex. The CCM is a 2-pK model, where it accounts for double protonation of surface functional groups ($\mathrm{SO^-}$) indicated in Equation (3).

$$\mathrm{SOH} + \mathrm{H^+} \Leftrightarrow \mathrm{SOH_2^+} \quad (3)$$

$$\mathrm{SOH} - \mathrm{H^+} \Leftrightarrow \mathrm{SO^-} \quad (4)$$

$$\mathrm{SOH} - \mathrm{H^+} + \mathrm{M^{m+}} \Leftrightarrow \mathrm{SOM^{(m-1)}} \quad (5)$$

$$2\mathrm{SOH} - 2\mathrm{H^+} + \mathrm{M^{m+}} \Leftrightarrow \mathrm{(SO)_2M^{(m-1)}} \quad (6)$$

where M = adsorbate cation, m^+ is adsorbate charge, SOH = adsorbent's surface functional group.

In surface groups (SOH, SOM, etc.), "S" represents a metal ion of the mineral surface that is hydrolyzed (Goldberg, 1992). The equilibrium constant (K) expressions for these complexation reactions are described by Equations 7, 8, and 9, respectively. In the CCM, there is no rigid surface charge balance (Goldberg, 1992). Instead, the equilibrium constant expressions are defined by extrapolation of a net 0 surface charge (Goldberg, 1992).

$$\mathrm{K_{(+)}} = \frac{[\mathrm{SOH_2^+}]}{[\mathrm{SOH}][\mathrm{H^+}]} \exp\left[\frac{\mathrm{F}\psi}{\mathrm{RT}}\right] \quad (7)$$

$$\mathrm{K_{(-)}} = \frac{[\mathrm{SO^-}][\mathrm{H^+}]}{[\mathrm{SOH}]} \exp\left[\frac{-\mathrm{F}\psi}{\mathrm{RT}}\right] \quad (8)$$

$$\mathrm{K_{(m)}} = \frac{[\mathrm{SOM^{(m-1)}}][\mathrm{H^+}]}{[\mathrm{SOH}][\mathrm{M^{m+}}]} \exp\left[\frac{(\mathrm{m}-1)\mathrm{F}\psi}{\mathrm{RT}}\right] \quad (9)$$

where F = Faraday's constant (C/mol), ψ = surface potential (V), R = gas constant (J/mol*K), T = absolute temperature (K), m = cation charge.

All SCMs are based on net surface charge of a mineral in aqueous environments equaling to 0, also called a "balance of surface charge" expression (Goldberg, 1992). This expression considers the charge contribution of the EDL layers described in Figure 2.4. Thus, to include the effect of surface charge in

thermodynamic calculations, complexation models contain one or more "coulombic correction factor(s)" (i.e. Boltzmann factor(s) (Goldberg, 1992). In the CCM, the coulombic correction factors are of the form $\exp(\pm F\psi/RT)$ and can be seen multiplied by the equilibrium expressions of surface complexes. Based on the assumptions of different models, the correction factors differ and are not all the same. Theory aside, in practice, Boltzmann factors serve as activity coefficients for the solid phase, used to correct for the charges of the surface species (Goldberg, 1992). In modeling software such as Visual MINTEQ, the Boltzmann factor is available as an "electrostatic component" added as a reactant in complexation reactions, where its coefficient represents the charge of the surface complex.

2.4.3.1 Gallium Adsorption CCM Modeling

The CCM has been previously used to model Ga adsorption. Yuan et al. (2018) and Persson et al. (2006) both modeled Ga adsorption on goethite using the CCM. The results of modeling and experiments agree in those studies, suggesting that Ga adsorbs to goethite mostly at the inner sphere where the $FeOGa(OH)_2$ complex is formed. Both studies consistently report that most Ga adsorption occurs at mildly acidic to mildly basic conditions (pH 4 – 8). However, their experiments and results are slightly different. Yuan et al. (2018) modeled Ga adsorption at low ionic strength (0.01M NaCl) and Persson et al. (2006) modeled at 0.1M NaCl. Under acidic conditions (pH < 3.5) with similar Ga/m^2 (Ga per unit surface area of goethite) in both studies, Yuan et al. (2018) observed significantly less adsorption, whereas Persson et al. (2006) observed similar adsorption with higher pH values. In other words, experiments with higher ionic strength observed greater adsorption in acidic conditions compared with the experiments with lower ionic strength. A possible explanation for this is neutralization by Cl^- of the positive surface charge induced by protons in highly acidic conditions. At higher ionic strength, increased concentration of Cl^- may lessen the otherwise repulsion of Ga^{3+} (in lower ionic strength solutions), allowing it to be adsorbed. For other pH values (pH < 3.5), Ga adsorption behavior was comparable between both studies.

The CCM has also been used to model Ga adsorption on carbonates and other oxide minerals. Pokrovsky et al. (2004) studied Ga adsorption on calcite, magnesite, birnessite, and amorphous silica, and Yuan et al. (2018) also studied Ga adsorption on calcite. Both studies found that the CCM was able to accurately predict all experimental results and agreed on the findings for Ga adsorption on calcite.

The affinity of a cation to form complexes at the inner-sphere increases with ionic potential (the ratio of valence to ionic radius) or for simplicity, with increasing valence, though this is also determined by

its electron configuration (Sposito, 1984; US. EPA, 1999). In general, complexation of cations with higher valence is likely to be described well by the CCM. Since this model characterizes systems only involving inner-sphere complex formation, it is simple and relies on few parameters to perform calculations. According to previous studies, Ga complexation clearly occurs at the inner-sphere. Thus, the CCM has been successful at modeling Ga adsorption.

2.4.3.2 Gallium Adsorption DLM and TLM Modeling

Though the CCM is proven successful for Ga adsorption modeling, it is only one of many SCM's. Other popular models also include the DLM (diffuse layer model) and TLM (triple layer model). These models differ with their assumptions about the nature of the surface's charge balance, and the electrostatic layers or "planes" in the system. They are also 2pK models considering double protonation reactions. Unlike the CCM though, the DLM's calculations consider the diffuse sublayer containing counter-ions that fully neutralize the charge of the Stern layer (Goldberg, 1992). Still, this model also considers only inner-sphere complexation, and unlike other SCMs, it does not require capacitance as an input parameter. There are no previous studies modeling Ga adsorption on minerals using the DLM. However, because of its assumptions, the DLM is likely to be useful for Ga adsorption modeling and may be uniquely advantageous for new systems where capacitance is not yet available.

On the other hand, the TLM is a more grueling model, considering three charged planes. In the TLM, the Stern layer is split in two planes with different capacitance (inner and outer spheres), with the diffuse sublayer neutralizing the net surface charge. This model assumes metal cations to form outer-sphere complexes, while protons and hydroxyl groups form inner-sphere complexes (Goldberg, 1992). Due to the complexity of TLM models, they are more susceptible to mathematical convergence which results in model failure (Righetto et al., 1995). Their calculations also rely on outer capacitances which are often unavailable. In the past, TLM modeling of Ga adsorption on Al_2O_3 has concluded that the inclusion of outer-sphere complexation did not improve matching to experimental data (Lin et al., 1997). This also agrees with previous work suggesting that Ga complexation favors the inner-sphere. For this reason, the TLM is not a preferred approach for Ga adsorption modeling.

Chapter 3
Study Approaches

3.1 Laboratory Experiments

3.1.1 Starting Materials

All adsorption experiments were conducted at 21°C (± 1°C), except for low temperature experiments which were conducted at 5°C (± 0.5°C). Natural, poorly crystalized kaolinite clay (KGa-2) powder was obtained from the Clay Minerals Society (CMS) and was used for experiments testing the influence of pH, ionic strengths, and temperature. The KGa-2 kaolinite is highly pure (99% kaolinite) and not contaminated by quartz and mica (Belviso et al., 2013). The BET surface area of KGa-2 is 23.5 m^2/g (CMS). Ca-montmorillonite chunk (Saz-1) was also purchased from the CMS. Crystalline silica (S5631), aluminum oxide (199974) minerals were purchased from Sigma Aldrich whereas goethite mineral powder (Bayferrox 910) was generously provided by the Ecohydrology Research Group (University of Waterloo). The entire Ca-montmorillonite chunk was crushed using a mixer mill and analyzed for the BET surface area (84.9 m^2/g) using a Micromeritics Gemini VII Surface Area analyzer (Wojtczak, 2019). The BET surface area of the remaining mineral powder was retrieved from literature data reporting for the same mineral powder purchased from the same vendor (Sigma Aldrich) assuming that there is no difference between batches. The surface area of these minerals are as follow: 7.04 m^2/g (Shi et al., 2012); aluminum oxide: 155 m^2/g (Önnby et al., 2014); goethite (Bayferrox 910): 15.0 m^2/g (Bonnissel-Gissinger et al., 1999).

An in-house Ga stock solution was prepared by diluting a single element ICP-MS standard ($Ga(NO_3)_3$) in ultra-pure water (18.2 MΩ-cm^{-1}) for use in all experiments. All acids used in adsorption experiments and sample dilution (for concentration analysis) were either TraceMetal Grade, or double distilled using a Savillex DST Acid Purification System. All acids used in chromatographic Ga separation and dilution of those samples were ultra-pure (Optima Grade, Fisher Scientific). All centrifuge tubes, bottles, Teflon vials, pipette tips, resins and other labware were acid-washed prior to use in the experiments.

3.1.2 Kinetic Adsorptions

Time lapse experiments were first performed to determine the time for adsorption between Ga and KGa-2 to reach equilibrium. These experiments were conducted with high and low absorbate/adsorbent

(Ga/KGa-2) mass ratios: 400 and 10 µg/g, respectively. Two Ga stock solutions (1000 and 100 µg/L ($(GaNO_3)_3$) were prepared in 0.01M NaCl and adjusted to pH 7 using either 0.1N NaOH or 0.1N HCl. In these experiments, KGa-2 was not pre-rinsed, or pH re-adjusted. A series of 50 mL centrifuge tubes containing 20 mL of the stock and 0.05 or 0.1 g kaolinite (KGa-2) were rotated at 60 rpm at room temperature (21ºC). Samples were collected and processed at the following time increments (hour): 0.33, 0.66, 1, 2, 4, 8, 24, 50, 97, 172. Samples were centrifuged for 10 minutes at 4,500 rpm. The supernatants were then immediately measured for pH using a pH meter (Orion Star™ A111, Thermo Scientific). The supernatants were passed through a 0.2 µm membrane syringe filter into centrifuge tubes. Filtered samples were then acidified by adding 0.2 mL double distilled concentrate HNO_3 to prevent Ga precipitation during storage. Prior to elemental analysis, 1 mL sample aliquots were gravimetrically diluted in 2% double distilled HNO_3. In addition, for high Ga experiments, two control experiments were conducted simultaneously. The first control experiment contained 0.05 g KGa-2 and 0.01M NaCl to determine if Ga or other metals are released from KGa-2. The second control experiment contained only the Ga stock solution to determine if Ga is lost due to precipitation and/or adsorption to tube or filter.

3.1.3 Equilibrium Adsorptions

The equilibrium adsorption time for a Ga and kaolinite (KGa-2) solution at low ionic strength has been determined in kinetic experiments. A similar procedure was applied for equilibrium experiments with a 7-day contact time, where a series of experiments were designed with varying study parameters (Table 3.1) to evaluate the influence of pH, ionic strength, and temperature on the adsorption of Ga on the study minerals. Some experiments (Experiments A1, B, E) were conducted in 50 mL centrifuge tubes with a Ga/solid mass ratio of 3000 µg/g. The remaining experiments were conducted in 500 mL HDPE bottles with a Ga/solid mass ratio of 1500 µg/g, except for silica, where the ratio was 15 µg/g due to its low Brunauer, Emmett, and Teller (BET) specific surface area. The minerals used in experiments were rinsed in ultrapure water to remove soluble salts that affect pH or ionic strength prior to the start of the experiment. Low temperature adsorption was studied by conducting adsorption experiments in a temperature-controlled wine chiller set to 5°C. Temperature fluctuations were monitored regularly to ensure stability, and were mostly within 0.2°C. All experiments were adjusted to achieve the desired equilibrium pH values.

Table 3.1. Summary of equilibrium adsorption experiments.

Experiment	Studying parameter	Adsorbent	pH	Temperature (°C)	Ionic strength (M, NaCl)	[Ga] (μg/L)
A1	pH	Kaolinite	3 – 9	21	0.01	3000
A2	pH	Kaolinite	3 – 9	21	0.01	50
B	Ionic strength	Kaolinite	3	21	0.01, 0.1, 0.3, 0.5, 0.8, 1.0	3000
C	Adsorbent	Ca-montmorillonite, SiO_2, Al_2O_3, goethite	3 – 9	21	0.01	50
D	Ga/Al ratio	Kaolinite, Ca-montmorillonite, SiO_2, Al_2O_3, goethite	3, 5, 7	21	0.01	50
E	Temperature	Kaolinite	3 – 9	5	0.01	1000

3.2 Analytical Methods

3.2.1 Elemental Concentration Analysis by ICP-MS

The concentrations of Ga, major (Ca, K, Mg, Na), and minor (Fe, Ba, Cr, Cu, Mn, Mo, Ni, Zn) elements were analyzed by the Agilent 8800 QQQ-ICP-MS at the Metal Isotope Geochemistry Laboratory at the University of Waterloo. The kinetic energy discrimination mode (using He) was enabled to reduce double charge and polyatomic ion interferences (< 1.5%). An internal standard composed of Sc, Ge, and In was aspirated during analysis for signal drift correction. Four certified water reference standards (SLRS-6, T225, T227, TM 9.2) were analyzed in conjunction with unknown samples for data quality control. The elemental recoveries in the standards were calculated and compared with their certified concentrations (Equation 10) to estimate the accuracy of elemental concentration data. Based on repeated analysis of the reference standards, accuracy of Ga is within 5%. Accuracy of all other elements are within 10%.

$$R(\%) = \frac{C_{measured}}{C_{certified}} \cdot 100\% \quad (10)$$

where R = Recovery (%), $C_{measured}$ = measured concentration, $C_{certified}$ = certified concentration in reference material.

Due to significant interference of $^{138}Ba^{2+}$ on $^{69}Ga^{+}$ (m/z = 69) measurements even at low Ba/Ga, Ga concentration was monitored using ^{71}Ga. However, m/z = 71 is also interfered upon by $^{55}Mn^{16}O$, formed by the presence of Mn. Therefore, a series of samples containing a range of Mn/Ga was analyzed in each analytical batch to monitor this effect. The solutions were prepared by adding different amounts of single element Mn standard to TM 9.2 (Ga reference standard) such that different mass ratios of Mn/Ga are achieved. The Ga recovery increases to the increasing ratios of Mn/Ga indicating the threshold at which Mn poses a significant influence on Ga concentration data (recovery exceeding 110%). The Mn/Ga ratios in all experimental samples were much lower than these thresholds, suggesting that Mn interference was negligible.

3.2.2 Chromatographic Separation of Gallium Isotopes

Ga isotopes must be separated from the sample matrix to facilitate accurate and precise isotope ratio analysis. Several secondary standards (synthetic solutions) were prepared in-house to 1) evaluate whether the method can adequately purify Ga from a range of sample matrices, 2) monitor the method's consistency in Ga purification and isotope analysis between analytical sessions throughout this study. First, an in-house synthetic standard solution was prepared with an elemental composition resembling that of the certified basalt reference rock (BHVO-2; USGS). Three more standard solutions were also prepared to simulate varying levels (1x, 10x, 20x) of sample matrix that was typically observed from the kaolinite adsorption experiments. These secondary standards were diluted in 6M HCl to obtain [Ga] of approximately 1000 µg/L. In each analytical batch, aliquots containing 500 ng Ga were taken to process concurrently with unknown samples. For adsorption experiment samples, aliquots containing 300 ng Ga were taken if possible. In some samples with low Ga concentration, it was only possible to take an aliquot containing 200 ng Ga. All aliquots were taken into Teflon vials to be dried at 100°C and the remaining residues were dissolved in 1 mL 6M HCl, ready for loading to the column. Purification was conducted according to the method developed by Yuan et al., (2016).

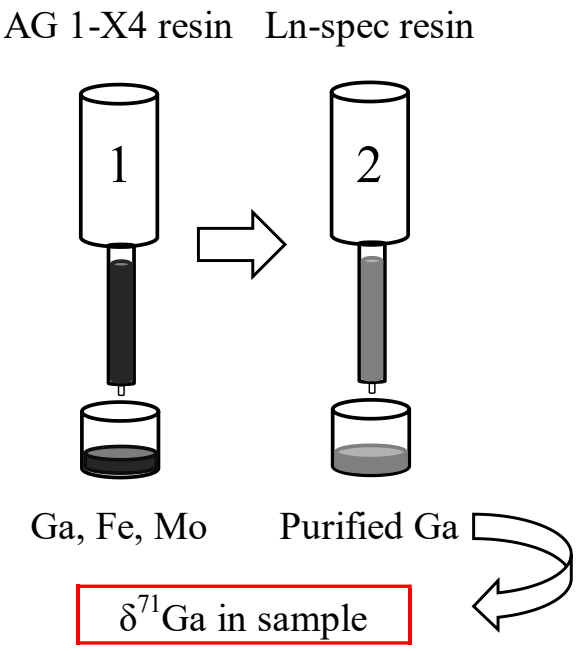

Figure 3.1. Schematic diagram of columns 1 and 2 (Yuan et al., 2016).

Two chromatographic columns charged with anion (AG 1-X4) and cation exchange (Ln-spec) resins, respectively, were used to separate Ga from other elements to minimize the influence of sample matrix on the accuracy of isotope ratio measurement (Figure 3.1). The procedure is summarized in Table 3.2 which was the procedure used to process all study samples. This is a slightly modified version of the procedure reported in Yuan et al., (2016). In this procedure, the AG 1-X4 resin in column 1 first underwent three cleaning and conditioning steps prior to sample loading (1 mL). The first column was used to remove most of the matrix elements in the sample except for Ga, Fe, and Mo. The final step in column 1 produces 5 mL of eluant that contains these elements. Subsequently, this 5 mL was then loaded into column 2 after one resin conditioning step. The remainder of the sequence for column 2 separates Ga, and later removes Fe and Mo so the Ln-spec resin can be reused. However, the Ln-spec was not reused to minimize cross contamination between samples. Pure Ga is present in volume interval 11 mL to 21 mL in column 2 which were evaporated to dryness in Teflon vials at 100°C. Residues were then dissolved in 0.5 mL concentrated HNO_3, and 0.5 mL concentrated H_2O_2 was added. The mixture was evaporated to dryness at 75°C and this step was repeated twice. Concentrated H_2O_2 was used to decompose any organic compounds originating from the ion exchange resins. The final residue was

dissolved in 2% HNO_3 to obtain Ga concentration of approximately 100 µg/L, the target concentration for isotope ratio analysis in this study. An aliquot was then taken for concentration analysis to determine purity and recovery of Ga in purified samples. Purification is satisfactory when all the matrix elements are effectively removed, and Ga recovery is ≥ 99%. Incomplete Ga recovery may cause Ga isotope fractionation during matrix separation. Further, insufficient removal of matrix elements or organics can cause matrix effects and polymeric interferences during analysis. For these reasons, it is crucial to process samples to high purity and maximum recovery of Ga.

Table 3.2. Summary of Ga purification steps, modified from Yuan et al., (2016) by increasing the volume of 6M HCl in step 6 in Column 1 to 18 mL (procedure A).

Step	Eluant	Volume (mL)	Purpose
	Column 1		
1	1.8mL AG1-X4 resin charged into column A		
2	H_2O	10	cleaning
3	0.1 M HCl	10	cleaning
4	6 M HCl	10	cleaning + conditioning
5	sample (in 6 M HCl)	1	loading
6	6 M HCl	18	matrix
7	0.5 M HCl	5	Ga (Fe and Mo)
	Column 2		
8	1.4 mL Ln-spec resin charged into column B		
9	0.5 M HCl	10	conditioning
10	0.5 M HCl sample solution	5	loading + Ga
11	1 M HCl	6	Ga
12	0.25 M oxalic acid + 3 M HCl	20	cleaning (Mo, Fe)
13	0.1 M HCl	20	cleaning
14	4 M HCl	20	Cleaning (Fe)

The dual-column method by Yuan et al. (2016) was chosen for this study. However, it was not previously tested for purifying samples with high matrix content such as those with high Na in this study. A high sample matrix may affect final Ga purity and recovery, so it is important to ensure that the method was adequately able to purify Ga from the sample matrix of the samples in this study. In this study, the original method by Yuan et al. (2016) was evaluated first in a trial run purifying of the secondary standards including several mixtures of synthetic BHVO-2 and a Ga isotope standard (SRM NIST-994) in different proportions. Two procedures were used to evaluate the precision and accuracy

of gallium isotope data, called procedure A and procedure B. Procedure A is as described above and summarized in Table 3.2 which was modified from the original procedure (Yuan et al., 2016) by increasing the volume of 6M HCl to 18 mL (Step 6 of Column 1), since some samples in this study had high matrix content. In procedure B, the same steps were followed as in procedure A except the purified Ga fraction was passed through column 2 a second time. This was done to evaluate whether a second run through column 2 improves the removal of interfering elements such as Fe, Zn, and Mo.

3.2.3 Isotope Ratio Analysis by MC-ICP-MS

Isotope ratio analysis of purified samples was performed using a Nu Plasma MC-ICP-MS at the Metal Isotope Geochemistry Laboratory at the University of Waterloo. The secondary standards mentioned in 3.2.2 were analyzed together with unknown samples for data quality control purposes. Standard sample bracketing (SSB) was used to correct for instrumental mass bias, where the certified isotope standard for Ga (NIST SRM 994) is utilized. SSB entails measuring the standard before and after the sample, with a blank in between (this is repeated for each sample). Figure 3.2 summarizes the SSB sequence.

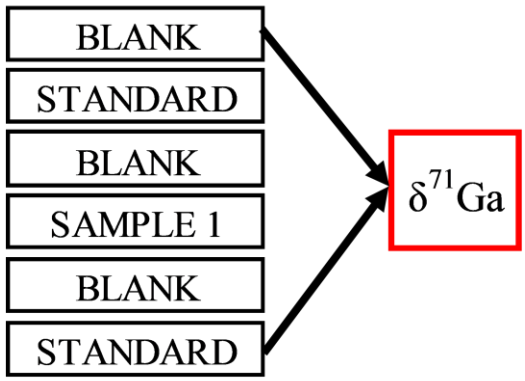

Figure 3.2. Diagram of standard-sample bracketing.

The measured $^{71}Ga/^{69}Ga$ was corrected for blank contribution by applying on-peak subtraction, then further corrected for ^{138}Ba interference on ^{71}Ga following the approach of (Kato et al., 2017; Zhang et al., 2016). There, the measured intensity (V) of $^{137}Ba^{2+}$ (m/z = 68.5) is multiplied by the natural ratio between $^{138}Ba^{2+}$ and $^{137}Ba^{2+}$, then subtracted from the measured intensity of $^{69}Ga^{+}$ (m/z = 69).

The corrected isotope ratio $^{71}Ga/^{69}Ga$ is reported using delta (δ) notation following Equation (11).

$$\delta^{71}\mathrm{Ga}\ (‰) = \left(\frac{(^{71}\mathrm{Ga}/^{69}\mathrm{Ga})_{\mathrm{sample}}}{(^{71}\mathrm{Ga}/^{69}\mathrm{Ga})_{\mathrm{NIST\ SRM\ 994,avg}}} - 1\right) \cdot 1000 \qquad (11)$$

where $^{71}Ga/^{69}Ga_{NIST\ SRM994,avg}$ is the average $^{71}Ga/^{69}Ga$ of the standard measured before and after the unknown sample.

To calculate fractionation magnitude ($\Delta_{solution\text{-}solid}$), the isotope ratio of the solid phase ($\delta^{71}Ga_{solid}$) is needed and calculated mathematically according to Equation (12), adapted from Barling & Anbar, (2004); Yuan et al. (2018). This mass balance equation is used to obtain the calculated solid phase for the measured $\delta^{71}Ga_{solution}$ values. The measured "initial $\delta^{71}Ga$" values of the Ga solution used in experiments were not reliable but are needed to calculate $\delta^{71}Ga_{solid}$. Thus, the highest confidence measured $\delta^{71}Ga_{solution}$ values from adsorption experiments were plotted (Ga fraction remaining vs $\delta^{71}Ga_{solution}$), and the intercept value (at F = 0) was used as $\delta^{71}Ga_{initial}$.

$$\delta^{71}\mathrm{Ga}_{\mathrm{solid}} = \frac{[100 \cdot \delta^{71}\mathrm{Ga}_{\mathrm{initial}} - (100 - \mathrm{F}) \cdot \delta^{71}\mathrm{Ga}_{\mathrm{solution}}]}{\mathrm{F}} \qquad (12)$$

where $\delta^{71}Ga_{initial}$ = isotope ratio of initial Ga standard used in experiments, F = fraction (%) Ga adsorbed.

The fractionation model (Rayleigh and equilibrium) $\delta^{71}Ga_{solution}$ values are calculated first by obtaining the fractionation factor (α) between phases, which is calculated using Equation (13). Average α values (of highest confidence $\delta^{71}Ga_{solution}$ points) were used for the fractionation models.

$$\alpha_{\text{solid/solution}} = \frac{1 + (\delta^{71}\text{Ga}_{\text{solid}})/1000}{1 + (\delta^{71}\text{Ga}_{\text{solution}})/1000} \quad (13)$$

$\delta^{71}Ga_{solution}$ of the Rayleigh model is then calculated using Equation (14).

$$\delta^{71}\text{Ga}_{\text{solution,Rayleigh}} = \left[(1000 + \delta^{71}\text{Ga}_{\text{initial}}) \cdot f^{(\alpha-1)}\right] - 1000 \quad (14)$$

where *f* is the mass fraction of Ga in solution phase.

The $\delta^{71}Ga_{solid}$ of the equilibrium fractionation model is calculated using Equation (15).

$$\delta^{71}\text{Ga}_{\text{solid,Equilibrium}} = \delta^{71}\text{Ga}_{\text{initial}} + 1000 \cdot f \cdot (\alpha - 1) \quad (15)$$

where *f* is the mass fraction of Ga in solution phase.

Then, the $\delta^{71}Ga_{solution}$ of the equilibrium fractionation model is calculated using Equation (16).

$$\delta^{71}\text{Ga}_{\text{solution,Equilibrium}} = \delta^{71}\text{Ga}_{\text{solid,Equilibrium}} - 1000 \cdot \ln(\alpha) \quad (16)$$

3.3 Geochemical Modeling of Gallium Speciation and Adsorption

3.3.1 Visual MINTEQ Modeling

Visual MINTEQ (J P Gustafsson, 2007) was used to model Ga speciation in experimental solutions and complexations with the study minerals. Visual MINTEQ code and databases are based on the older MINTEQA2 software and the default THERMO database was used in Visual MINTEQ. Although actual experiments were conducted at 21°C, all model calculations were conducted at 25°C due to lack of ΔH_r data for Ga hydrolysis reactions. It was assumed that Ga speciation at both temperatures is comparable. Consequently, adsorption modeling was not performed for the experiment at low temperature (5ºC) and experiments studying kinetic adsorption and Ga/Al ratios. Thermodynamic databases were updated manually in this study, with further details provided in each subsection.

3.3.2 Gallium Speciation in Experimental Solutions

The default thermodynamic database was updated with Ga hydrolysis constants from (Baes Jr & Mesmer, 1976; Bénézeth et al., 1997) and used to model Ga speciation (Table 3.3). With two documented Ga hydrolysis precipitates: ($Ga(OH)_{3,am}$ and $\alpha - GaOOH$), it is still unclear which one, or if a combination, is formed. Therefore, several models were constructed in this study considering all possibilities for Ga precipitation. Model outputs were then compared with concentration results of the control experiment (containing Ga only) to observe if Ga loss in the control experiments matched with the stability regime of the precipitate(s). Additionally, a new equilibrium constant for $\alpha - GaOOH$ was graphically extrapolated based on concentration data from the control experiments in this study and is also reported in Table 3.3.

Table 3.3. Ga hydrolysis reactions and constants.

Ga hydrolysis reactions	logK	logK (this study)
1) $Ga^{3+} + H_2O \leftrightarrow Ga(OH)^{2+} + H^+$	-2.85[a]	–
2) $Ga^{3+} + 2H_2O \leftrightarrow Ga(OH)_2^+ + 2H^+$	-7.28[a]	–
3) $Ga^{3+} + 4H_2O \leftrightarrow Ga(OH)_4^- + 4H^+$	-15.66[a]	–
4) $Ga^{3+} + 3H_2O \leftrightarrow Ga(OH)_3 + 3H^+$	-11.94[a]	–
5) $Ga^{3+} + 3H_2O \leftrightarrow Ga(OH)_{3,am} + 3H^+$	-5.64[b]	–
6) $Ga^{3+} + 2H_2O \leftrightarrow \alpha\text{-}GaOOH_{(s)} + 2H^+$	-3.54[b]	–
7) $Ga^{3+} + 2H_2O \leftrightarrow \alpha\text{-}GaOOH_{(s)} + 2H^+$	–	-4.14

[a] (Bénézeth et al., 1997)

[b] (Baes Jr & Mesmer, 1976)

Calculations were performed for 0.1 pH increments with Ga concentrations of 50 and 3000 µg/L, 0.01M NaCl, and various NO_3^- concentrations (calculated from mass of $Ga(NO_3)_3$ added in experimental solutions). Model parameters are shown in Table 3.4.

Table 3.4. Ga speciation modeling parameters.

[Ga]	[NaCl]	[NO_3^-]	pCO_2	T
µg/L	M	M	atm	°C
50	0.01	5.9E-05	0.00038	25
3000	0.01	3.5E-03	0.00038	25

Despite the low ionic strengths in these experiments, the Davies model in Equation (17) was used for activity correction. Generally 0.3 is used for the Davies coefficient (B), however, values as low as 0.2 have also been used (Liang et al., 2021). Therefore, in this study, calculations were done with both.

$$\log(\gamma_i) = -A_{z_i}\left(\frac{\sqrt{I}}{1+\sqrt{I}}\right) - B \cdot I \tag{17}$$

where $A = 0.5085 \cdot M^{-1/2}$, z_i = valence of ion i, I = ionic strength, B = Davies coefficient.

3.3.3 Surface Complexation Modeling of Gallium Adsorption under Varying pH values

The CCM was used to model all adsorption reactions. Model parameters are described in Table 3.5. At low Ga concentration, $Ga(OH)_{3,am}$ was considered as the only possible solid phase. At high Ga concentration (with KGa-2), both phases were considered. In this study, the surface complexation reactions and their equilibrium constants were manually (graphically) optimized to match experimental data, based on previous studies with the same or similar minerals. This approach was used for any reaction that the equilibrium constant is not available (Table 3.5). Models performed calculations at 0.1 pH increments for all adsorption experiments, from pH 1 – 14.

3.3.4 Surface Complexation Modeling of Gallium Adsorption on Kaolinite (KGa-2) at Variable Ionic Strengths

In Visual MINTEQ, the Davies equation presented in Equation (17) was used for activity correction, in SCMs. Models calculated Ga adsorption on KGa-2 with NaCl concentrations ranging from 0.01M to 1M, and a Ga concentration of 3000 µg/L at pH 3. The same parameters describing the Ga complexation reactions with KGa-2 in Table 3.5 (Part A) were used.

Table 3.5. Surface reactions and parameters used to model Ga adsorption.

A) Kaolinite (KGa-2) reactions			[KGa-2]	BET	C_1	ρ_{site} (SOH)	ρ_{site} (X^-)
	logK	$logK_{SEL}$	g/L	m^2/g	F/m^2	nm^{-2}	mmol/L
1. $SOH^0 + H^+ \leftrightarrow SOH_2^+$	4.80	N/A	0.034	23.50[i]	1.20[b]	2.31[a]	4E-4[y]
2. $SOH^0 - H^+ \leftrightarrow SO^-$	-3.80	N/A					
3.[v] $4SOH^0 + Ga^{3+} - 4H^+ \leftrightarrow (SO)_4Ga^-$	-4.30	N/A					
4.[b] $3XH^0 + Ga^{3+} - 3H^+ \leftrightarrow X_3Ga^0$	-14.00	1.00					
IS[b] $XH^0 + Na^+ - H^+ \leftrightarrow XNa^0$	-2.02[b]	1.00					
B) Montmorillonite (Saz-1)			[Saz-1]	BET	C_1	ρ_{site} (SOH)	ρ_{site} (X^-)
	logK	$logK_{SEL}$	g/L	m^2/g	F/m^2	nm^{-2}	mmol/L
5. $SOH^0 + H^+ \leftrightarrow SOH_2^+$	-4.80[c]	N/A	0.034	84.90[z]	1.06[a]	28.0[x]	22.0[x]
6. $SOH^0 - H^+ \leftrightarrow SO^-$	-12.0	N/A					
7.[c] $SOH^0 + Ga^{3+} - H^+ \leftrightarrow SOGa^{2+}$	5.40	N/A					
8.[c] $SOH^0 + Ga^{3+} + 3H_2O - 4H^+ \leftrightarrow SOGa(OH)_3^-$	-14.60	N/A					
9.[c] $SOH^0 + Ga^{3+} + 4H_2O - 3H^+ \leftrightarrow SOH_2Ga(OH)_4^0$	-7.80	N/A					
10.[b] $3XH^0 + Ga^{3+} - 3H^+ \leftrightarrow X_3Ga^0$	-6.70	1.00					
C) Silica (crystalline)			[SiO_2]	BET	C_1	ρ_{site} (SOH)	ρ_{site} (X^-)
	logK		g/L	m^2/g	F/m^2	nm^{-2}	mmol/L
11. $SOH^0 + H^+ \leftrightarrow SOH_2^+$	-7.50		3.4	7.04[ii]	1.40[d]	5.20[e]	N/A
12. $SOH^0 - H^+ \leftrightarrow SO^-$	6.50						
13. $SOH^0 + Ga^{3+} + 3H_2O - 4H+ \leftrightarrow SOGa(OH)_3^-$	3.15						
14.[v] $SOH^0 + 2Ga^{3+} + 8H_2O - 8H^+ \leftrightarrow SOH(Ga(OH)_4)_2^{2-}$	5.80						
D) Aluminum oxide			[Al_2O_3]	BET	C_1	ρ_{site} (SOH)	ρ_{site} (X^-)
	logK		g/L	m^2/g	F/m^2	nm^{-2}	mmol/L
15. $SOH^0 + H^+ \leftrightarrow SOH_2^+$	1.50		0.034	155.00[iii]	0.80[f]	8.00[f]	N/A
16. $SOH^0 - H^+ \leftrightarrow SO^-$	-9.10						
17.[f] $SOH^0 + Ga^{3+} - H^+ \leftrightarrow SOGa^{2+}$	2.00						
18.[f] $SOH^0 + Ga^{3+} + 3H_2O - 4H^+ \leftrightarrow SOGa(OH)_3^-$	-10.60						
E) Goethite			[α-FeOOH]	BET	C_1	ρ_{site} (SOH)	ρ_{site} (X^-)
	logK		g/L	m^2/g	F/m^2	nm^{-2}	mmol/L
19. $SOH^0 + H^+ \leftrightarrow SOH_2^+$	9.50		0.034	15.00[iv]	0.75[g]	1.68[g]	N/A
20. $SOH^0 - H^+ \leftrightarrow SO^-$	-11.50						
21.[g] $SOH^0 + Ga^{3+} + H_2O - 3H^+ \leftrightarrow SOGa(OH)_2^0$	-0.85						

Note: K_{SEL} = selectivity coefficient, BET = specific surface area, C_1 = inner capacitance, ρ_{site} = site density.

[a](Goldberg, 2002), [b](Gu & Evans, 2008b), [c](Benedicto et al., 2014; Missana et al., 2009),
[d](Phan et al., 2004), [e](Ernstsson et al., 1999), [f](Lin et al., 1997), [g](Yuan et al., 2018),
[h](Pokrovsky et al., 2004) [i](The Clay Minerals Society), [x](Wanner et al., 1994),
[y](Tombácz & Szekeres, 2006), [z](Wojtczak, 2019), [ii](Shi et al., 2012), [iii](Önnby et al., 2014),
[iv](Bonnissel-Gissinger et al., 1999), [v] **(this study)**. Part A, Reaction "IS" is only used for experiments testing ionic strength.

Chapter 4
Results

4.1 Gallium Adsorption Experiments

4.1.1 Kinetic Gallium Adsorption on Kaolinite (KGa-2)

Results of kinetic adsorption for the low Ga/KGa-2 ratio (Ga/KGa-2 = 10 µg/g, [Ga] = 100 µg/L) (Figure 4.1) show that approximately 99% of total Ga was adsorbed instantly; after 1 hour of contact with KGa-2. Similar results were observed for the kinetic experiments at high ratio (Ga/KGa-2 = 400 µg/g, [Ga] = 1000 µg/L). For the high Ga/KGa-2 ratio experiments, about 99% of Ga was adsorbed after 4 hours and the adsorption remained stable after 46 hours (Figure 4.1). Fluctuations in Ga adsorption beyond 4 hours of contact time were within mean analytical errors (2SD = 5%). Ga adsorption on KGa-2 was 0.41 ± 0.03 (2SD, n = 10) µg Ga/m^2 and 16.6 ± 0.54 (2SD, n = 6) µg Ga/m^2 for low and high Ga/KGa-2 ratio experiments, respectively. In the control experiment with only Ga stock solution, a 7.6% decrease of total Ga was observed after 172 hours (Appendix B, Table B1). In the control experiment without Ga, Ga released from kaolinite was negligible (0.04%; Appendix B, Table B2). Since pH was not re-adjusted, deviations from the initial pH adjustment (pH 7) were observed in all samples for kinetic adsorption experiments (Appendix B, Table B1). Specifically, pH decreased from the initial value (pH 7) of the stock solution to pH 5 and pH 6 in all samples of low and high Ga/KGa-2 ratio experiments, respectively.

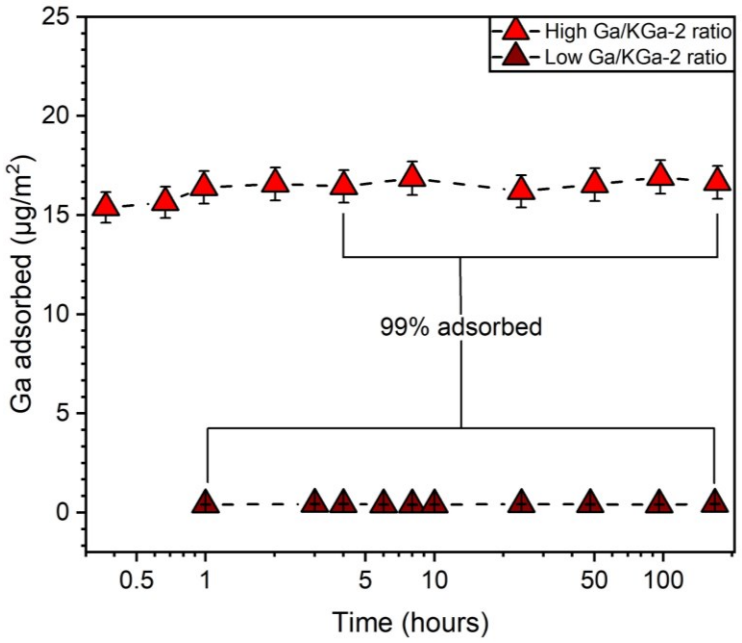

Figure 4.1. Kinetic Ga adsorption on kaolinite (KGa-2) at high and low Ga/KGa-2 ratios. Error bars represent a mean analytical uncertainty that was typically observed during this study (2SD = 5%).

4.1.2 Gallium Adsorption at Variable pH values at 21°C

4.1.2.1 Adsorption on Study Minerals with Low Gallium Concentration

The results of adsorption experiments conducted with 50 µg/L Ga concentration are illustrated in Figure 4.2 (A-E). In most control experiments containing Ga only, Ga precipitation was less than 5%, although 6% was lost at pH 5. Furthermore, in control experiments containing no Ga (mineral only), Ga release was also negligible (0%; Appendix B, Table B2), so initial Ga added was the only source of Ga in experiments. Thus, Ga lost in 50 µg/L Ga adsorption experiments was mainly due to adsorption, with small or negligible contribution from precipitation.

A) Kaolinite (KGa-2)

During adsorption on KGa-2, the highest amount of Ga was adsorbed at pH 4.8 (63%). Adsorption decreased when pH was more acidic or basic. At pH 3, around 20% Ga was adsorbed whereas no Ga adsorption was observed at pH 9. Overall, kaolinite did not adsorb Ga under highly basic conditions and only slightly adsorbed under highly acidic conditions. The highest adsorption occurred at mildly acidic conditions (pH 4.8).

B) Ca-Montmorillonite (Saz-1)

The highest adsorption of Ga (> 95%) occurred under acidic conditions (pH 3 – 5). Ga adsorption sharply decreased at pH values greater than 5. Roughly 20% of total Ga was adsorbed at pH 7.5, and < 5% was adsorbed at pH 9. Thus, Ca-Montmorillonite preferentially adsorbed Ga under acidic conditions, as low as at pH 3. Like kaolinite, Ca-montmorillonite did not adsorb Ga in highly basic environments (pH 9).

C) Silica

Gallium adsorption on silica followed a similar pattern of Ga adsorption on Ca-montmorillonite. Ga was preferentially adsorbed under acidic conditions with > 95% Ga adsorbed at pH 4 – 5. At pH > 5, adsorption decreased slightly though a moderate amount of Ga (55%) was adsorbed at pH 7. At pH > 7, a slight decrease in Ga adsorption was observed with 44% Ga adsorbed at pH 9. Thus, silica preferentially adsorbed Ga at mildly acidic conditions, as low as pH 4, the lowest pH investigated for the adsorption of Ga on silica in this study. Under highly basic conditions, moderate amount of Ga was adsorbed.

D) Aluminum Oxide

Gallium adsorption on aluminum oxide followed a similar pattern of Ga adsorption on silica. Most and relatively constant Ga adsorption (75%) occurred between pH 4 and 7. Ga adsorption decreased when pH was lower than 4, with ~20% adsorbed at pH 3. Ga adsorption also slightly decreased with pH > 7, with 40 % Ga adsorbed at pH 9. Thus, aluminum oxide preferentially adsorbed Ga on a wide pH range from mildly acidic to mildly basic (pH = 4 – 7.5). Moderate adsorption occurred under highly acidic (pH 3) or highly basic (pH 9) conditions.

E) Goethite

Like silica and aluminum oxide, most Ga adsorption (>95%) occurred between pH 4 and 7 and decreased slightly at pH 8 and abruptly at pH 9. Ga adsorption was less than 20% at pH 3, dropping significantly from 100% adsorption at pH 4. A slight decrease in Ga adsorption was observed when pH increased to slightly above 7. Moderate adsorption (50%) was observed at pH 9. Overall, goethite preferentially adsorbed Ga from mildly acidic to neutral pH values. Moderate adsorption occurred under highly basic (pH 9) conditions.

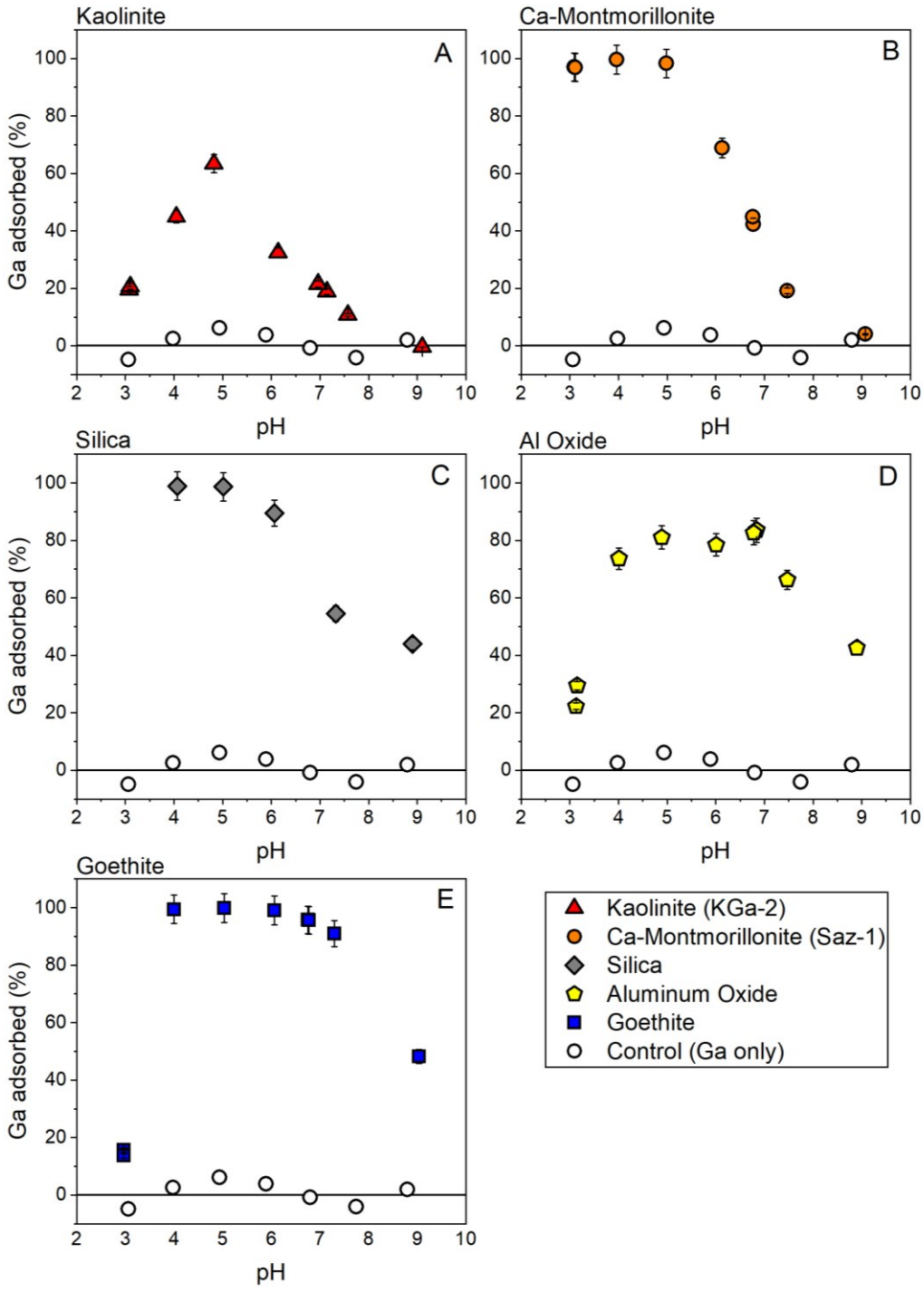

Figure 4.2. Ga adsorption experiments (50 µg/L) with all study minerals under variable pH values. Error bars represent a mean analytical uncertainty that was typically observed during this study. (2SD = 5%). Ga/silica mass ratio was 15 instead of 1500 µg/g due to its low BET surface area.

4.1.2.2 Adsorption on Kaolinite (KGa-2) With High Gallium Concentration

The results of adsorption experiments conducted with a Ga concentration of 3000 µg/L are illustrated in Figure 4.3. At pH 3, negligible Ga was lost/precipitated in the control experiment in which no adsorbent was present. In contrast, around 20% was adsorbed in the adsorption experiment. Between pH 4 and 6.8, over 90% of total Ga was lost/precipitated in both control and adsorption experiments. At pH 7.5, only 5% Ga was lost in the control in comparison to about 35% Ga lost in the adsorption experiment. At pH 9, negligible Ga was lost/precipitated in the control whereas around 20% of total Ga was adsorbed, which is identical to the observations of the experiment at pH 3. At all other pH values, similar amounts of Ga were lost in both adsorption experiments and the corresponding control experiments.

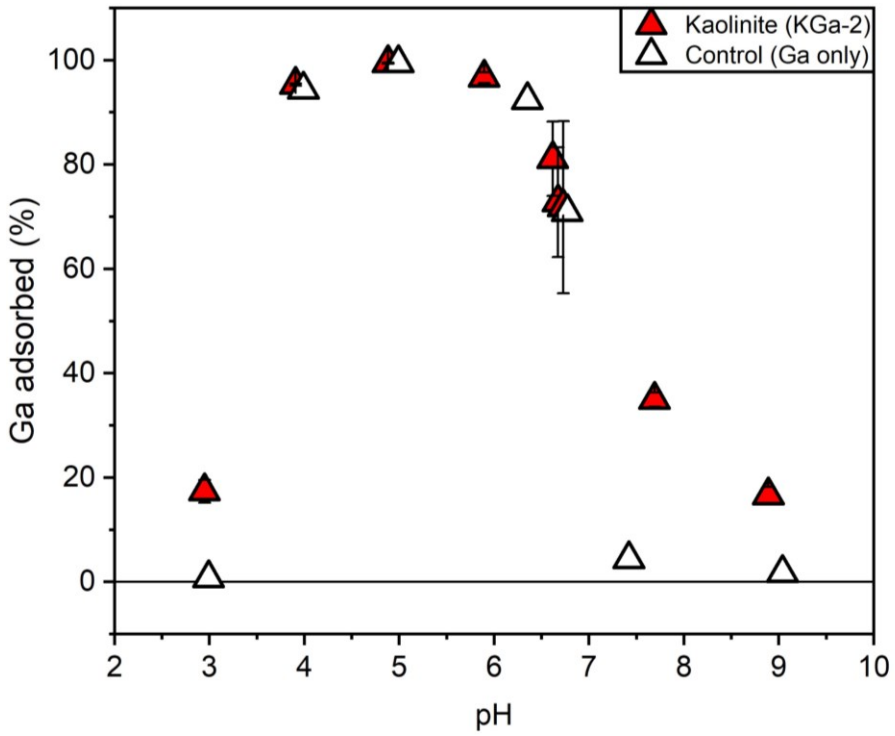

Figure 4.3. Ga adsorption experiments (3000 µg/L) with kaolinite (KGa-2) and variable pH. The experimental data points represent the mean value of triplicate experiments, and the error bars are two standard deviations. Note that similar amounts of Ga were lost in both adsorption experiments and the corresponding control experiments without the presence of adsorbents at pH 4 – 6.8.

4.1.3 Gallium Adsorption on Kaolinite (KGa-2) at Variable Ionic Strengths

The influence of ionic strength (IS) on the adsorption of Ga on kaolinite was investigated at pH 3. Under each ionic strength value, the experiments were conducted in triplicate. The results are shown in Figure 4.4. Negligible Ga was precipitated/lost in the control at all study ionic strength values. Ga adsorption generally decreased with increasing ionic strength. Ga adsorption at IS values ≥ 0.5M NaCl were within analytical error (2SD) and thus comparable. At 0.01M NaCl concentration, 17% Ga was adsorbed and slightly decreased to around 14% at 0.1M NaCl concentration. At 0.1M NaCl, one replicate experiment was significantly higher than the other two, resulting in the large observed deviation in Ga adsorption. At IS > 0.1M, a decrease by as many as 70% in Ga adsorption was observed.

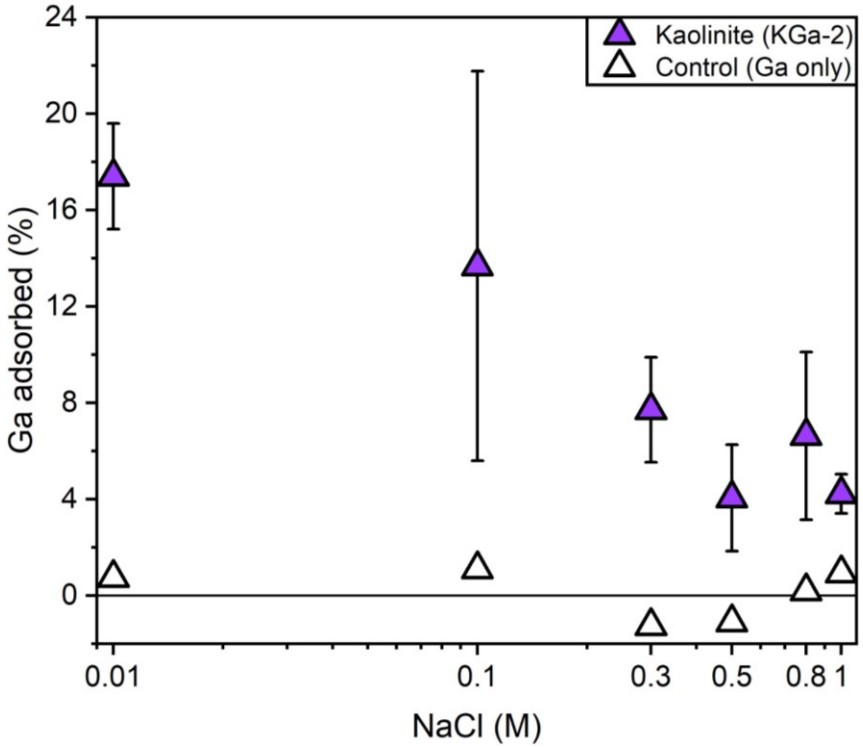

Figure 4.4. Ga adsorption experiments (3000 µg/L) with kaolinite (KGa-2) under variable ionic strength values. The experimental data points represent the mean value of triplicate experiments, and the error bars are two standard deviations (2SD, n = 3).

4.1.4 Influence of pH on the Ga/Al Ratio during Adsorption

The variation in Ga/Al ratios with pH for all adsorption experiments is illustrated in Figure 4.5 and the data are shown in Appendix B, Table B10.

A) Control Experiments (Gallium and aluminum only, no adsorbent)

The control experiments were conducted with the initial concentration of Ga and Al of 50 µg/L (Ga/Al wt. ratio = 1). An increasing loss of both metals was observed with increasing pH. At pH 3, the loss of Ga and Al were similar (2 – 3%). At pH 5, the loss of either metal was also similar, around 8%. At both pH values, the Ga/Al ratio was about 1.05, like the initial value. At pH 7 however, 13% of total Ga was lost whereas Al loss was significantly higher, around 86%. This resulted in an increase of the Ga/Al ratio due to a greater loss of Al (Ga/Al wt. ratio = 7).

B) Adsorption Experiments on Study Minerals

Following adsorption on kaolinite at pH ≈ 3, around 10% of total Ga was adsorbed and Al was measured around 10% higher than the added amount, and Ga/Al dropped from the initial value (Ga/Al = 1.05) to 0.86. Conversely, Ca-montmorillonite adsorbed 95% of total Ga and roughly 65% of total Al at the same pH, and the ratio decreased to 0.14. With silica, around 86% of total Ga was adsorbed, and roughly 21x of added Al was measured. Following adsorption on aluminum oxide, only 31% of total Ga was adsorbed, but 18x of total added Al was present in the sample. Following adsorption on both silica and aluminum oxide at pH 3, Ga/Al decreased to around 0. With goethite, only 23% of total Ga was adsorbed and 0% of total Al was adsorbed, and the ratio decreased to 0.78.

During adsorption on kaolinite at pH ≈ 5, Ga and Al adsorption increased to 66% and 36%, respectively, and Ga/Al remained at a similar value as the pH ≈ 3 experiment. With Ca-montmorillonite, Ga/Al increased to around 5 at the same pH (the highest ratio among all minerals at this pH) and both Ga and Al loss were >95% (Al loss was slightly more). Similar magnitudes of Ga and Al adsorption were observed following adsorption on silica (>90%), though in this case, that of Ga was greater compared with Al and Ga/Al remained low (around 0.3). During adsorption on aluminum oxide, Ga adsorbed was roughly 70%, Al adsorption was 4%, and Ga/Al also remained low (around 0.3). Following adsorption on goethite, adsorption of Ga and Al were 99% and 54%, respectively, and Ga/Al was around 0.

Following adsorption on all minerals, Al loss was >95% at pH 7 and though Ga adsorption was variable between the minerals, Ga/Al ratios ranged from 12 to 28. The lowest ratios were observed with goethite

and aluminum oxide which had Ga/Al ratios of 12 and 8, respectively. Conversely, kaolinite, Ca-montmorillonite, and silica all had Ga/Al ratios greater than 20. In summary, after adsorption on all study minerals under acidic conditions, Ga/Al ratios remained low and were significantly greater at pH 7 compared with the initial ratio ($p < 0.01$).

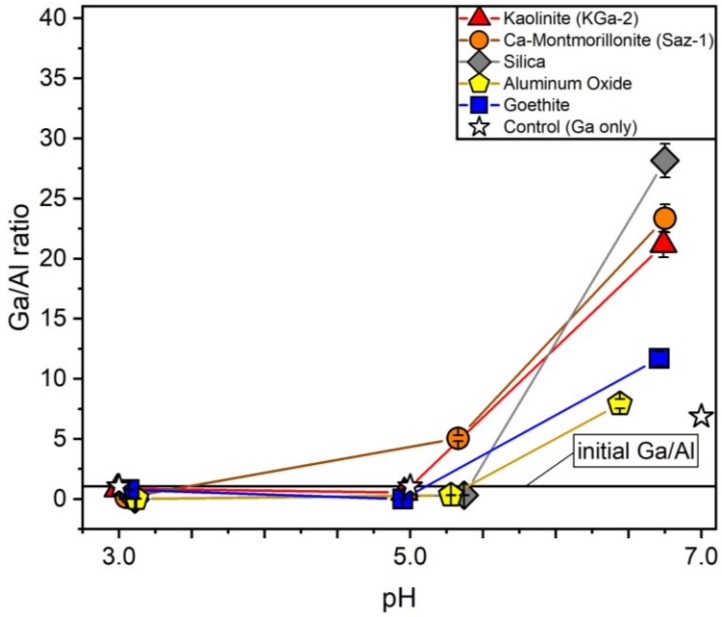

Figure 4.5. Ga adsorption experiments (50 µg/L) testing the influence of pH on Ga/Al ratios. Error bars represent a mean analytical uncertainty that was typically observed during this study (2SD = 5%). Ga/silica mass ratio was 15 instead of 1500 (µg/g).

4.1.5 Gallium Adsorption on Kaolinite (KGa-2) at 5°C

The influence of temperature on Ga adsorption on KGa-2 was investigated by conducting additional experiments under 5°C. The results are illustrated in Figure 4.6. For experiments with pH > 5, equilibrium pH dropped below the target pH, despite pH adjustment. As a result, the experimental pH values range from 3 to 6.8. At pH ≈ 3, negligible Ga was lost in the control experiment. At pH ≈ 4, around 30% Ga was lost in the control whereas about 70% lost was observed in the adsorption experiment on kaolinite (KGa-2). At pH ≈ 5, around 98% of Ga was lost in both control and adsorption experiment which was the highest among all study pH values. At pH ≈ 5.7, 90% of Ga was lost in both the control and adsorption experiment. At pH ≈ 6.5, around 14% of Ga was lost in the control whereas

50% of Ga was lost in the adsorption experiment. At pH ≈ 6.8, roughly 7% of Ga was lost in the control whereas 25% of Ga was lost in the adsorption experiment.

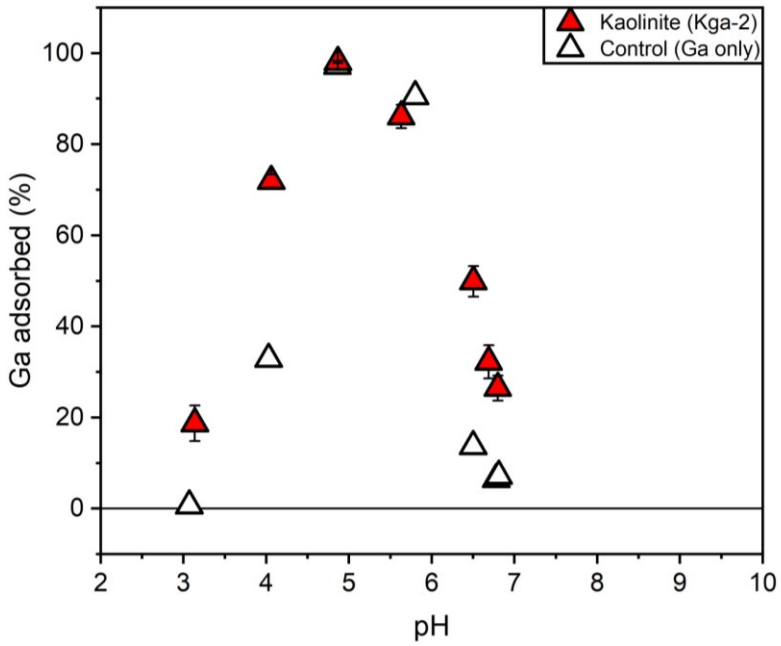

Figure 4.6. Ga adsorption experiments (1000 µg/L) with kaolinite (KGa-2) at 5°C under variable pH. The experimental data points represent the mean value of triplicate experiments, and the error bars are two standard deviations. Note that significant amounts of Ga were lost in the control experiments at pH 4 – 6.

4.2 Geochemical Modeling

4.2.1 Gallium Speciation and Precipitation in Experimental Solutions

4.2.1.1 Low Gallium Concentration (50 µg/L)

The Ga species in the experimental solution (50 µg/L) were predicted using Visual Minteq and the distribution of the predicted Ga species is illustrated in Figure 4.7 (A, B, and C). The model only considering $Ga(OH)_{3,am}$ as a possible solid phase (Figure 4.7-A) did not predict the occurrence of any precipitate. In the control experiments (Ga = 1000 µg/L and Ga = 3000 µg/L), significant Ga loss was observed at circumneutral pH values. Thus, $\alpha - GaOOH$ precipitation was also considered in addition to $Ga(OH)_{3,am}$ (Figure 4.7-B and C).

In the model considering $\alpha - GaOOH$ formation with a larger logK (Figure 4.7B), precipitation was predicted to occur within pH values 3.5 and 6, where 94% of total Ga precipitated at pH 4.5. Likewise, the model with smaller logK (Figure 4.7C) also predicted the formation of $\alpha - GaOOH$, but in lower proportion and under a narrower pH range (4 – 5.3). Remaining Ga species were distributed similarly in all models except for $Ga(OH)_3$, where 10% was formed in the models where only $Ga(OH)_{3,am}$ was considered (Figure 4.7A) and both precipitates were considered, using the smaller logK for $\alpha - GaOOH$ (Figure 4.7C). Otherwise, this species was predicted in low abundance (< 1%). At pH < 3, Ga^{3+} was dominant and only present up to pH 4. At pH 4, the presence of $Ga(OH)_4^{1-}$ began, and $GaOH^{2+}$ was dominant (70%). At neutral pH, 100% of Ga was in the form of $Ga(OH)_4^{1-}$. For the models predicting precipitation, the formation of $Ga(OH)_4^{1-}$ did not become dominant until precipitation sufficiently decreased. Otherwise, $Ga(OH)_4^{1-}$ became dominant at a comparably lower pH (Figure 4.7A).

4.2.1.2 High Gallium Concentration (3000 µg/L)

The models describing experimental solutions containing 3000 µg/L Ga are shown in Figure 4.7D, E, and F. The model only considering precipitation of $Ga(OH)_{3,am}$ (Figure 4.7D) predicted its formation between pH values 3.8 and 5.6, with peak precipitation of 87% at pH 4.5. Only in this model, $GaOH^{2+}$ was the dominant aqueous species (70%) at pH 3.7. In models that considered both precipitates (Figure 4.7E, F), $\alpha - GaOOH$ formation was predicted. In the model with the higher logK for this reaction (Figure 4.7E), the precipitation was around 100% between pH values 3 and 6, decreasing to 0 at pH 7.7. Comparatively, the model with smaller logK (Figure 4.7F) had a similar prediction, though precipitation was predicted on a slightly narrower pH range. Remaining Ga species were distributed similarly, except for $GaOH^{2+}$. In the model with the higher logK (Figure 4.7E), around 30% of $GaOH^{2+}$ was predicted at pH 2.8. For the lower logK model (Figure 4.7F), slightly more (44%) was formed at a slightly higher pH (pH 3). Otherwise, observations regarding $Ga(OH)_4^{1-}$ were consistent with 4.2.1.1.

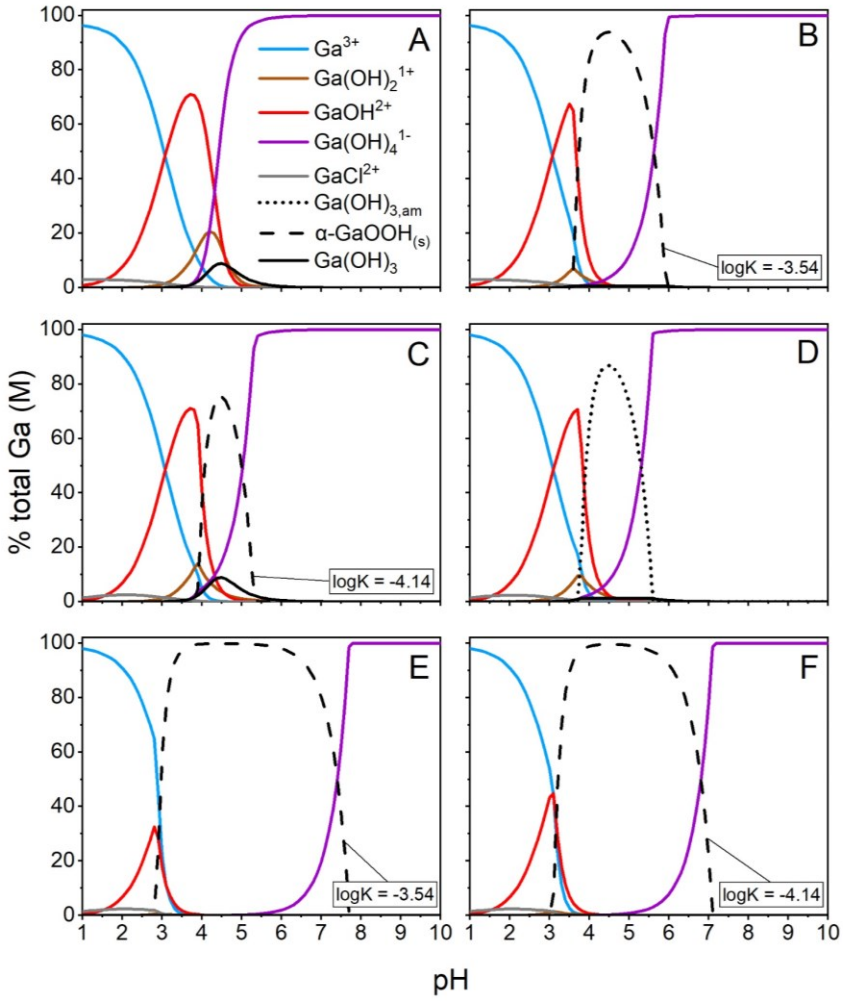

Figure 4.7. Ga speciation modeling of low (50 µg/L, A, B, and C) and high (3000 µg/L, D, E, and F) Ga concentration experiments. Only the formation of $Ga(OH)_{3,am}$ was considered in A and D whereas both $Ga(OH)_{3,am}$ and $\alpha - GaOOH$ were considered in B, C, E, F. Different logK values used to model $\alpha - GaOOH$ formation are indicated in each figure.

4.2.2 Surface Complexation Modeling of Gallium Adsorption

A) Kaolinite (KGa-2)

To describe adsorption experiments with KGa-2, the SCM calculation of SO_4Ga^{1-} predicted Ga adsorption at all pH values (Figure 4.8A). Although ionic exchange was included, its prediction by the SCM was around 0%. Compared with experimental results at pH 4, the model over-estimated the

abundance of SO_4Ga^{1-} by roughly 10%. At all other pH values, model results were within 5% of experimental results.

B) Ca-Montmorillonite (Saz-1)

To describe adsorption on Ca-montmorillonite, three surface species calculations and ionic exchange characterized adsorption at acidic, circumneutral, and basic pH conditions (Figure 4.8B). At pH < 4, $SOGa^{2+}$ was predicted as the dominant species. At pH 5 – 7, $SOH_2Ga(OH)_4$ and ionic exchange predicted adsorption, and $SOGa(OH)_3^{1-}$ mostly described the little adsorption occurring at pH > 8. Overall, the model described experiments within 1% of measured values.

C) Silica

Adsorption experiments with silica were described by the SCM using calculations of two surface species dominating acidic and basic pH (Figure 4.8C). The formation of $SOGa(OH)_3^{1-}$ was predicted to dominate pH ≤ 7, and $SOH(Ga(OH)_4^{1-})_2^{2-}$ dominated Ga adsorption under highly basic conditions. Compared with experimental data at pH 7, the model over-estimated the abundance of $SOH(Ga(OH)_4^{1-})_2^{2-}$ by roughly 19%. Otherwise, model calculations were within 5% of experimental results.

D) Aluminum Oxide

To simulate adsorption on aluminum oxide, the SCM considered two surface species (Figure 4.8D). The first, $SOGa^{2+}$, dominated the adsorption at pH values 3 – 4, and $SOGa(OH)_3^{1-}$ dominated adsorption at pH > 4. Compared with experimental results, the model over-estimated adsorption at pH 7.5 by roughly 10%, and under-estimated adsorption at pH 9 by around 28%. Otherwise, the model predicted experimental results within 5% of measured values.

E) Goethite

Adsorption experiments with goethite at all pH values were described by the SCM considering a single surface species; $SOGa(OH)_2$ (Figure 4.8E). Compared with experimental results at pH values 3 and 9, the model underestimated adsorption by 50% and 29%, respectively. At all other pH values, model calculations were within 5% of experimental results.

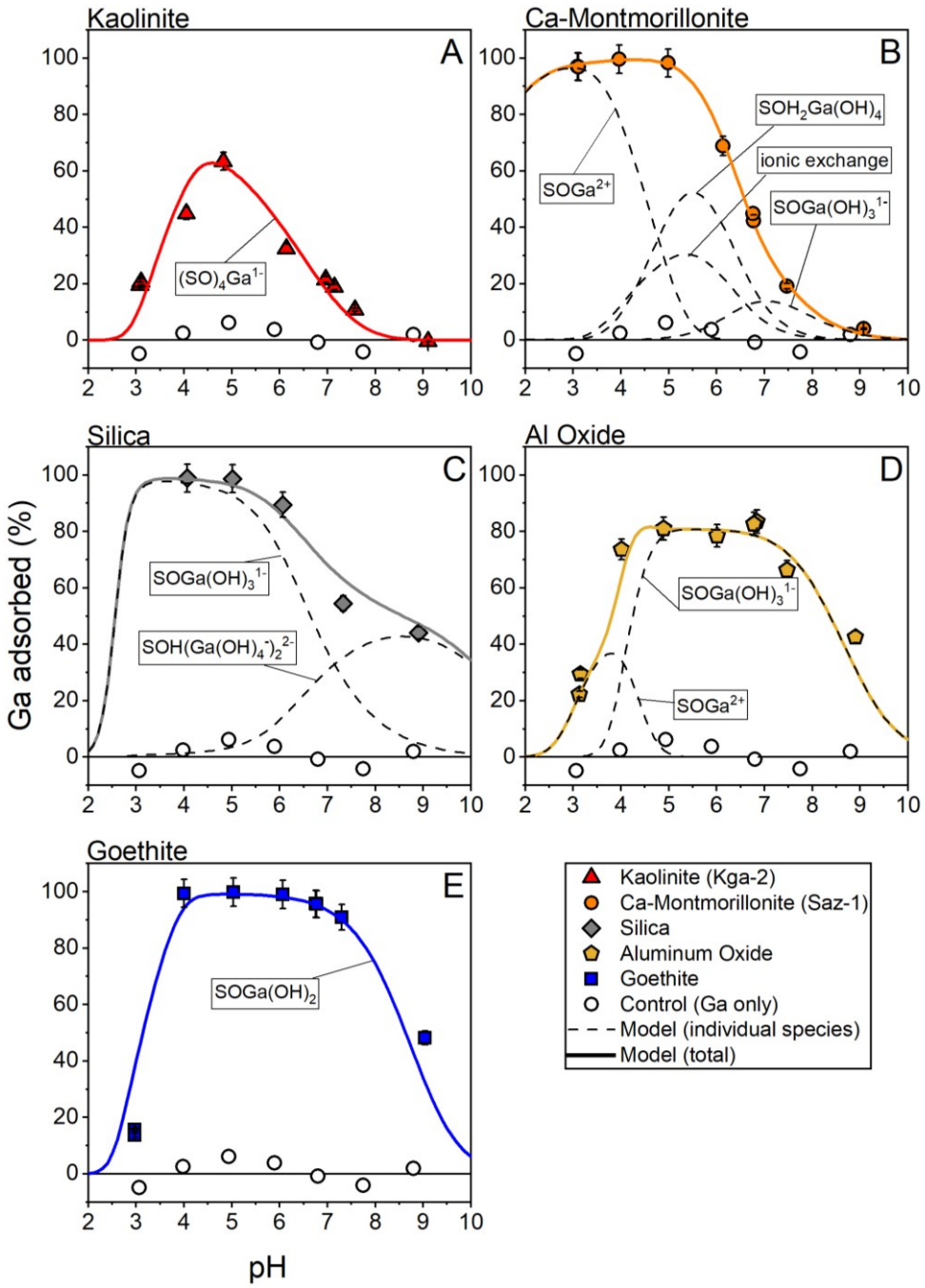

Figure 4.8. SCMs of 50 µg/L Ga adsorption experiments testing pH dependence with experimental results. Error bars represent a mean analytical uncertainty that was typically observed during this study (2SD= 5%). Horizontal dashed line indicates 0% adsorption line. Ga/silica mass ratio was 15 instead of 1500 (µg/g) due to its low BET area.

4.2.2.1 Adsorption on Kaolinite (KGa-2) with High Gallium Concentration

The surface complexation model (SCM) describing the adsorption on KGa-2 (Ga = 3000 µg/L) is shown in Figure 4.9. At pH 3, the model predicted no precipitation and all Ga lost due to the formation of the SO_4Ga^{1-} surface complex. At pH values 4 – 6, around 70% of total Ga was predicted to precipitate as $\alpha - GaOOH$ and the remaining species was SO_4Ga^{1-}. At pH 7, α-GaOOH precipitate was predicted to sharply decrease, however, as much as 30% of Ga was in the form of SO_4Ga^{1-}. At all pH values, the SCM predicted species were within 5% of all experimental results except for those at pH 7.5 and 9, where the predicted SO_4Ga^{1-} was lower than the experimental values by 38% and 64%, respectively. The predicted $Ga(OH)_{3,am}$ in the speciation modeling did not adequately explain the loss of Ga in the control experiments. In contrast, the model predicting $\alpha - GaOOH$ precipitation closely resembled all results from the control experiments.

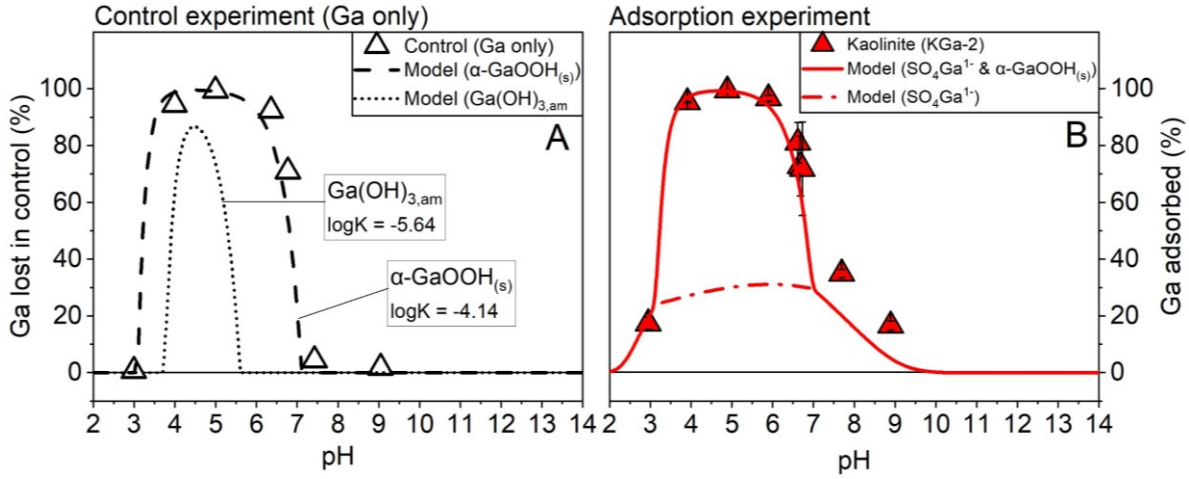

Figure 4.9. SCM of 3000 µg/L Ga adsorption experiments with KGa-2 testing pH dependence (red), experimental results and speciation of possible Ga precipitates in the control (black). The experimental data points represent the mean value of triplicate experiments, and the error bars are two standard deviations. LogK = -4.14 was also used for $\alpha - GaOOH$ in the SCM (B).

4.2.2.2 Gallium Adsorption on Kaolinite (KGa-2) at Variable Ionic Strengths

The SCM describing adsorption (Ga = 3000 µg/L) on kaolinite (KGa-2) under variable ionic strength values (IS) is illustrated in Figure 4.10. The SO_4Ga^{1-}surface complex predictions were slightly higher than the results for the experiments with the concentration of NaCl ranging from 0.01M to 0.1M (10 – 15%). However, a greater difference was observed for the experiments with the concentration of NaCl greater than 0.1M (up to 300%). Two models using different Davies "B" values (0.2 vs. 0.3) exhibited negligible differences in predicted SO_4Ga^{1-} for IS ≤ 0.1M NaCl. In contrast, the difference was more significant with increasing IS. Overall, the model using lower "B" value (B = 0.2) yielded slightly closer predictions to experimental data. In both models (B = 0.2 and B = 0.3), increasing $GaCl^{2+}$ complex was predicted with increasing ionic strengths. The model with higher "B" value (B = 0.3) predicts slightly higher SO_4Ga^{1-} complex at any ionic strength values that are greater than 0.1M.

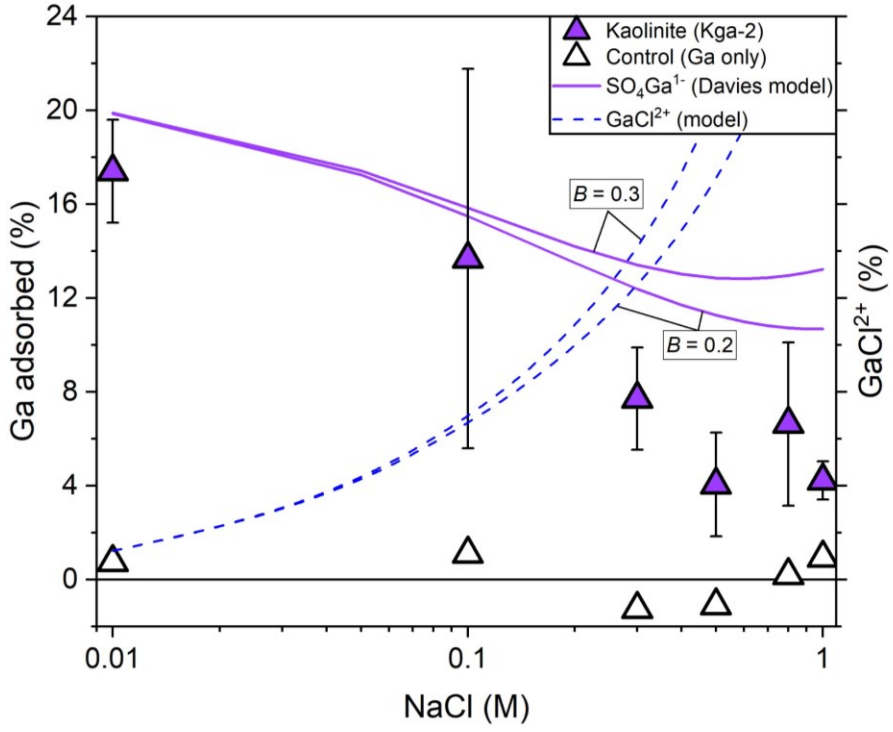

Figure 4.10. Ga adsorption experiments (3000 µg/L) with kaolinite (KGa-2) under variable ionic strength values. Both y-axes use the same scale. The solid lines are SCM using two different "B" constant values used in the Davies equation for calculating the ion activity co-efficient. Dashed lines show the predicted $GaCl^{2+}$ species. The experimental data points represent the mean value of triplicate experiments, and the error bars are two standard deviations.

4.3 Gallium Isotopes

4.3.1 Gallium Isotope Data Quality Control/Method Validation

The anion exchange column (column 1) was sufficiently able to purify major matrix elements from the samples, evident from their elution curves (Appendix A, Figure A2). Furthermore, the elution curves of column 1 show the elution of Ga with high recovery along with Fe and Mo (Appendix A, Figure A3). In the cation exchange column (column 2), Fe and Mo were retained, and Ga was collected with high recovery (Appendix A, Figure A4). The modified methods in this study called procedures A and B; discussed in Section 3.2.2. In short, the difference between the procedures entails a second elution through the cation exchange (Ln-spec) column in Procedure B. Procedure A mostly achieved Ga recoveries of 95% or greater, and sufficiently low element/Ga mass ratios shown in Appendix B, Table B5.

Ga isotopes must not fractionate during purification for the method to be successful. This was tested by analyzing the Ga isotope ratio of several samples that were previously purified using both procedures. These samples include: a pure Ga isotope standard (SRM NIST-994), an in-house solution (synthetic BHVO-2) prepared by mixing pure ICP standards to simulate the composition of BHVO-2 (basalt; USGS), three samples which are mixtures with varying proportions of SRM NIST-994 and synthetic BHVO-2 (Figure 4.11). For simplicity, this group of samples is also referred to as "mixing fraction" samples. Since SRM NIST-994 is used as a bracketing standard, its δ^{71}Ga should be around 0‰ if no fractionation occurred during chromatographic separation. Using the mass-balance calculation, the δ^{71}Ga values of the mixtures are expected to increase linearly based on the mixing fraction with synthetic BHVO-2, which was prepared using the Ga ICP stock δ^{71}Ga = 1.44 ± 0.09‰, 2SD; n = 21; Figure 4.11). However, after being processed by Procedure A, the δ^{71}Ga values of these samples were all shifted by around 0.3‰ (Figure 4.11). Possible reasons of this shift could be a combination between insufficient Ga recoveries, insufficient Ga purity, or Ga fractionation by the chromatographic column.

The pure Ga ICP solution that was not processed through the columns yielded consistent δ^{71}Ga values through multiple analytical sessions (δ^{71}Ga = 1.44 ± 0.09‰, 2SD; n = 21), ruling out instrumental instability as a source of inconsistency. After chromatographic separation using procedure A, the mixture samples had high Ga recoveries (98 to 107%). Although Ga recovery was not consistently ≥ 99%, Ga recovery was still adequate such that isotope fractionation is still not expected to be

observable. This is illustrated by the same shift (+0.3‰) in SRM NIST-994 (Ga recovery = 93%), and synthetic BHVO-2 (Ga recovery = 107%). Therefore, insufficient Ga recovery is unlikely to induce the observed shift in δ^{71}Ga values. This leaves the final possibility which is most likely an effect caused by the incomplete purification and/or effects of matrix element presence. The mixing fraction samples (Figure 4.11) with increasing proportions of synthetic BHVO contain interfering matrix elements (e.g. Fe) in the purified Ga fraction, shown in Appendix B, Table B5. These elements have been documented by previous works (Feng et al., 2019; Yuan et al., 2016; Zhang et al., 2016) for creating polyatomic or mass bias interferences during analysis, and thus, their removal to within acceptable ratios with Ga is prioritized (Feng et al., 2019; Yuan et al., 2016). However, in this study, their presence doesn't fully explain the uniform shift in δ^{71}Ga across mixing fraction samples (especially SRM NIST-994), because they are removed relatively the same and within acceptable limits (Appendix B, Table B5). The uniform shift in δ^{71}Ga (and linear trend; Figure 4.11) also suggests that any differences in removal of those elements did not induce observable effects on Ga isotope analysis. However, the presence of many matrix elements abundant in natural samples (including Al, Si, P) can also produce polyatomic interferences during Ga isotope analysis, also making their removal important (Zhang et al., 2016). Thus, in order to eliminate possible matrix effects, Ga isotope studies reporting reproducible results (Feng et al., 2019; Kato et al., 2017; Wimpenny et al., 2020; Yuan et al., 2018; Zhang et al., 2016) purified their unknown samples extensively, and well below recommended limits (where applicable). In all experiment samples of this study, substantially high element/Ga ratios were measured for several matrix elements (Al, Si, P, K, Ca) (Appendix B, Table B9). Although there are no recommended ratios for these elements, purified samples are still not expected to have consistently high element/Ga ratios (e.g., P/Ga > 3 in all samples, Appendix B, Table B9). Moreover, it is still unclear which of those elements, if not all, can induce polyatomic interferences during Ga isotope analysis. Nonetheless, among mixing fraction samples (Appendix B, Table B9), similar mass ratios of Si/Ga (0.82 ± 0.21, 2SD; n = 5) and P/Ga (2.74 ± 0.47, 2SD; n = 5) were observed. This may be suggestive that similar matrix content among purified samples may cause similar deviations in their δ^{71}Ga values.

This suggests that during purification of these unknown samples, the resins may not effectively separate Ga from matrix elements. A series of secondary standards were processed using both procedures A and B. Compared with procedure A, procedure B produced similar Ga recovery and removal of critical interfering elements (Cu, Zn, Fe, Mo, Ba, Mn), shown in Appendix B, Table B5. In general, most of those elements were removed to within recommended element/Ga ratios for both procedures. In two

samples, Fe removal from synthetic BHVO-2 samples (with high Fe content) processed by procedure A was insufficient, but acceptable after being processed by procedure B. However, compared with procedure A, procedure B had higher ratios for several elements (Si, P, K, Ca), shown in Appendix B, Table B6. This suggests that during the second pass through the cation exchange column, additional masses of those elements are released into samples, likely from the Ln-spec resin. In terms of δ^{71}Ga values, samples processed using procedure B were also analyzed to determine if there were differences in the δ^{71}Ga values obtained by these procedures. Both methods produced similar δ^{71}Ga values (Figure 4.12), indicating that the second cation exchange column did not fractionate Ga isotopes. In summary, processing the sample through the cation exchange column a second time did not produce any improvements to the method's efficacy in terms of Ga purity and recovery.

The similar content of elements such as Al, Si, P, K and Ca among samples is likely to induce the uniform shift observed in Ga isotope values observed in mixing fraction samples. Moreover, among samples from the same adsorption experiment (pH/kaolinite, pH/Ca-montmorillonite, ionic strength/kaolinite), ratios of certain elements (Al, Si, P) were also similar, and as high as 9.7 (kaolinite; Appendix B, Table B9). Thus, Ga isotope shift due to matrix content is likely also similar in those samples. Conversely, the matrix content was more scattered in experiments conducted with aluminum oxide (e.g., P/Ga ranges from 9 – 14.1; Appendix B, Table B9). Several matrix elements were present in purified samples, however, the effect of specific elements on Ga isotope measurement remains unclear. Still, the Ln-spec (cation exchange) resin used in this study (second column) contains acidic alkyl-phosphorus extractants (Eichrom Technologies, 2022). Judging by increased P levels after purifying through the Ln-spec resin a second time, it is likely that P originates from the resin itself. The source of other elements remains unclear, but they may also originate from the resin. Since newly manufactured resins contain impurities, they must be cleaned thoroughly. To remove them, both resins were repeatedly treated with various molarities of ultrapure hydrochloric acid to leach a wide spectrum of elements. It is possible that the resin cleaning protocol was excessive and partially damaged/decomposed the resin, releasing high levels of P and moderate levels of other elements into samples. This effect is expected to induce similar shifts in the isotope values among samples which have comparable levels of those matrix elements.

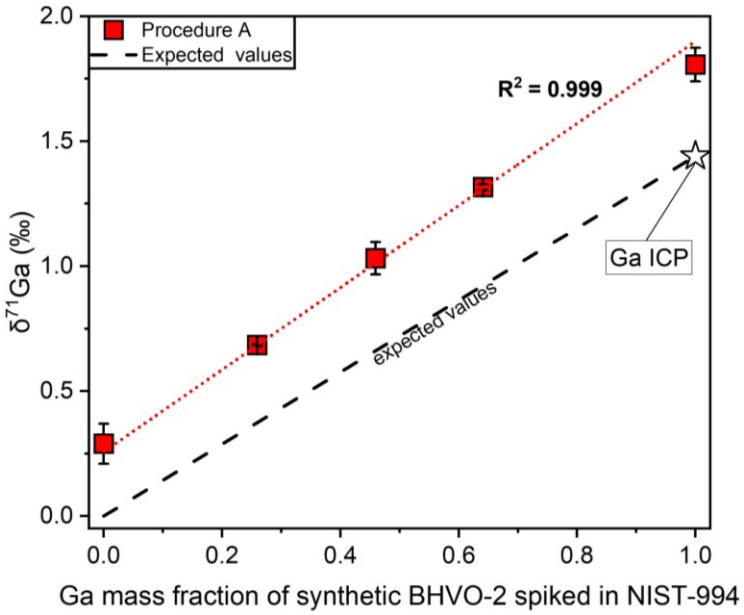

Figure 4.11. δ^{71}Ga of SRM NIST-994 mixed with varying proportions of synthetic BHVO-2. The experimental data points represent the mean value of duplicate measurements, and the error bars are two standard errors (2SE, n = 2).

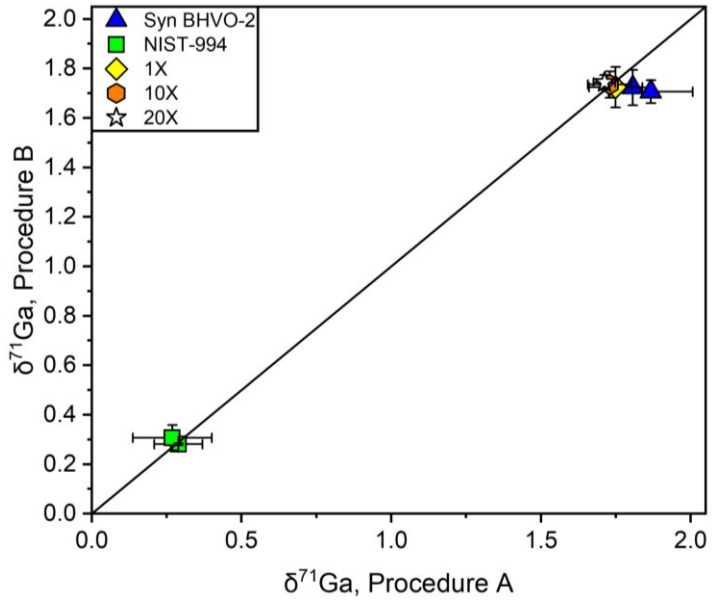

Figure 4.12. δ^{71}Ga of secondary standards purified with procedure A and procedure B. The experimental data points represent the mean value of duplicate measurements, and the error bars are two standard errors (2SE, n = 2).

4.3.2 Gallium Adsorption at Variable pH values at 21°C (Low Gallium Concentration)

A) Gallium Isotopes of the Experimental Stocks

The experimental stock solutions (prepared using the Ga ICP, $\delta^{71}Ga$ = 1.44 ± 0.09‰, 2SD; n = 21) were also purified and analyzed for $\delta^{71}Ga$ value. The mean $\delta^{71}Ga$ value of the stock was 2.04 ± 0.09‰ (2SD, n = 6) (Figure 4.13). In all experiments, the measured $\delta^{71}Ga_{solution}$ values of the experimental samples were higher than $\delta^{71}Ga$ in the stock solutions. Ideally, the $\delta^{71}Ga$ of the stock must be the same as $\delta^{71}Ga_{initial}$ value where the fractionation models intercepting the Y-axis ($f_{solution}$ = 1). However, in kaolinite and Ca-montmorillonite experiments (Figure 4.13-A, B) the $\delta^{71}Ga_{initial}$ calculated following the approach discussed in Section 3.2.3 was more adequate in modelling the fractionation of Ga by both models: equilibrium and Rayleigh distillation models. The $\delta^{71}Ga_{initial}$ values for Ga adsorption on kaolinite and Ca-montmorillonite were 2.374‰ and 2.480‰, respectively.

B) Kaolinite (KGa-2)

The $\delta^{71}Ga_{solution}$ is the $\delta^{71}Ga$ value of the experimental solution after adsorption. The $\delta^{71}Ga_{solution}$ of all Ga adsorption experiments with kaolinite under a wide range of pH values (5 – 9) increased linearly with the adsorbed Ga fraction, excluding the outliers at pH values 3 and 4 (Figure 4.13-A). These data points were treated as outliers because when used to calculate the theoretical $\delta^{71}Ga_{solid}$, the results were over-estimated to be even greater than their $\delta^{71}Ga_{solution}$ values. The highest $\delta^{71}Ga_{solution}$ (2.93‰) was observed in the experiment at pH 4.8 in which 63% of Ga was adsorbed; shown in Table 4.1. The lowest $\delta^{71}Ga_{solution}$ value (2.37‰) was observed in the experiment at pH 9 in which 0% of Ga was adsorbed. Fractionation model plots compared with measured $\delta^{71}Ga_{solution}$ values show that Ga adsorption on KGa-2 follows closed-system equilibrium fractionation, as opposed to Rayleigh distillation. The Ga isotope fractionation between the solution and calculated solid phase ($\Delta_{sol'n\text{-}solid}$) was 0.94 ± 0.37‰ (2SD, n = 5) where n is the number of experiments under different pH values (5 – 9).

B) Ca-montmorillonite (Saz-1)

Similar to the adsorption on kaolinite, the $\delta^{71}Ga_{solution}$ values of Ga adsorption experiments (pH = 6 – 9) with Ca-montmorillonite also increased linearly with the adsorbed Ga fraction (Figure 4.13B). Experimental solutions at pH lower than 6 were not analyzed because Ga was not enough for isotope analysis. Adsorption at pH 6 yielded the highest $\delta^{71}Ga_{solution}$ measurement (3.74‰) in which 69% of Ga was adsorbed (Table 4.1). The lowest value was observed at pH 9 (2.56‰) where 4% of Ga was

adsorbed. Ga adsorption on Ca-montmorillonite closely followed a closed-system equilibrium fractionation model as observed for kaolinite. The Ga isotope fractionation between the solution and calculated solid phase ($\Delta_{sol'n\text{-}solid}$) was 1.70 ± 0.63‰ (2SD, n = 4).

C) Aluminum Oxide

The $\delta^{71}Ga_{solution}$ values of Ga adsorption experiments with aluminum oxide (pH = 3 – 9) are poorly correlated with the Ga adsorbed fraction, however, there was still a slight linear relationship between the $\delta^{71}Ga_{solution}$ and the Ga adsorbed fraction (Figure 4.13-C). Thus, Ga adsorption on aluminum oxide likely followed the equilibrium fractionation model as also observed for kaolinite and Ca-montmorillonite. The highest $\delta^{71}Ga_{solution}$ value was at pH 9 ($\delta^{71}Ga_{solution}$ = 2.63‰) and the lowest values at pH 3 and 4 ($\delta^{71}Ga_{solution}$ = 2.06‰). The Ga isotope fractionation between the solution and calculated solid phase ($\Delta_{sol'n\text{-}solid}$) was 0.62 ± 0.97‰ (2SD, n = 6).

Table 4.1. Ga adsorption experiments (50 µg/L) with all study minerals under variable pH values.

Experiment	[NaCl]	Mineral	BET	pH	Mineral	$[Ga]_{loaded}$	$[Ga]_{ads}$	% Ga_{ads}		$\delta^{71}Ga$	2σ	n
	M		m^2/g		g	µg/m^2	µg/m^2	meas.	model	‰		
3KG-A50	0.01	Kaolinite (KGa-2)	23.5	3.1	0.02	57.38	11.26	19.63	12.73	2.4	—	1
3KG-B50				3.1	0.02	57.72	11.93	20.67	12.73	—	—	—
4KG-50				4.1	0.02	45.55	20.48	44.97	56.25	2.2	—	1
5KG-50				4.8	0.02	52.10	33.04	63.42	61.90	2.9	—	1
6KG-50				6.1	0.02	54.45	17.67	32.46	39.03	2.8	—	1
7KG-A50				7.1	0.02	53.99	10.20	18.90	15.19	2.5	—	1
7KG-B50				7.0	0.02	54.09	11.65	21.53	17.34	2.5	—	1
8KG-50				7.6	0.02	52.86	5.69	10.77	6.60	2.4	—	1
9KG-50				9.1	0.02	55.55	-0.21	-0.37	0.15	3.7	—	1
3SA-A50		Montmorillonite (Saz-1)	84.9	3.1	0.02	15.45	14.99	97.08	0.99	—	—	—
3SA-B50				3.1	0.02	14.95	14.47	96.79	0.99	—	—	—
4SA-50				4.0	0.02	12.88	12.83	99.65	12.54	—	—	—
5SA-50				5.0	0.02	14.00	13.76	98.27	28.67	—	—	—
6SA-50				6.1	0.02	14.56	10.02	68.85	22.75	3.7	—	1
7SA-A50				6.8	0.02	14.89	6.29	42.28	9.55	3.1	—	1
7SA-B50				6.8	0.02	14.38	6.45	44.89	9.55	—	—	—
8SA-50				7.5	0.02	14.76	2.84	19.24	2.56	2.7	—	1
9SA-50				9.1	0.02	15.35	0.62	4.05	0.07	2.6	—	1
4SI-50		Crystalline Silica	7.0	4.1	1.71	2.02	2.00	98.94	98.50	—	—	—
5SI-50				5.0	1.70	2.00	1.97	98.71	96.36	—	—	—
6SI-50				6.1	1.70	2.05	1.83	89.47	84.94	—	—	—
8SI-50				7.3	1.71	1.96	1.07	54.52	63.48	2.6	0.2	2
9SI-50				8.9	1.72	2.02	0.89	44.05	47.29	2.5	0.2	2
3AL-A50		Aluminum Oxide	155.0	3.1	0.02	8.13	1.81	22.30	20.93	2.1	0.2	2
3AL-B50				3.2	0.02	7.85	2.31	29.45	24.78	—	—	—
4AL-50				4.0	0.02	6.88	5.07	73.63	63.25	2.1	0.01	2
5AL-50				4.9	0.02	7.60	6.16	81.04	81.01	2.5	0.01	2
6AL-50				6.0	0.02	8.89	6.97	78.46	80.56	—	—	—
7AL-A50				6.8	0.02	8.73	7.29	83.52	78.61	2.4	0.00	2
7AL-B50				6.8	0.02	8.20	6.78	82.69	78.61	—	—	—
8AL-50				7.5	0.02	8.18	5.42	66.33	71.91	2.5	0.1	2
9AL-50				8.9	0.02	8.34	3.56	42.62	31.40	2.6	0.1	2
3GT-A50		Goethite	15.0	3.0	0.02	87.74	13.76	15.69	39.90	—	—	—
3GT-B50				3.0	0.02	87.58	12.00	13.70	39.90	2.1	0.1	2
4GT-50				4.0	0.02	64.79	64.40	99.39	94.20	—	—	—
5GT-50				5.0	0.02	68.08	67.94	99.80	99.14	—	—	—
6GT-50				6.1	0.02	72.89	72.18	99.03	98.03	—	—	—
7GT-A50				6.8	0.02	87.85	84.11	95.74	95.07	—	—	—
7GT-B50				6.8	0.02	88.27	84.41	95.63	95.07	—	—	—
8GT-50				7.3	0.02	72.04	65.49	90.92	89.97	—	—	—
9GT-50				9.0	0.02	77.89	37.61	48.28	34.00	3.0	0.0	2
3STK50		N/A (Ga stock)		3.0	N/A					2.0	0.1	2
4STK-50				4.1						2.1	0.1	2
5STK-50				5.0						2.2	0.2	2
7STK50				7.0						2.0	0.1	2
8STK-50				8.4						2.1	0.3	2
9STK-50				9.3						2.1	0.1	2

Dashes indicate samples which were not analyzed for isotopes. The first character in the experiment name indicates experimental pH.

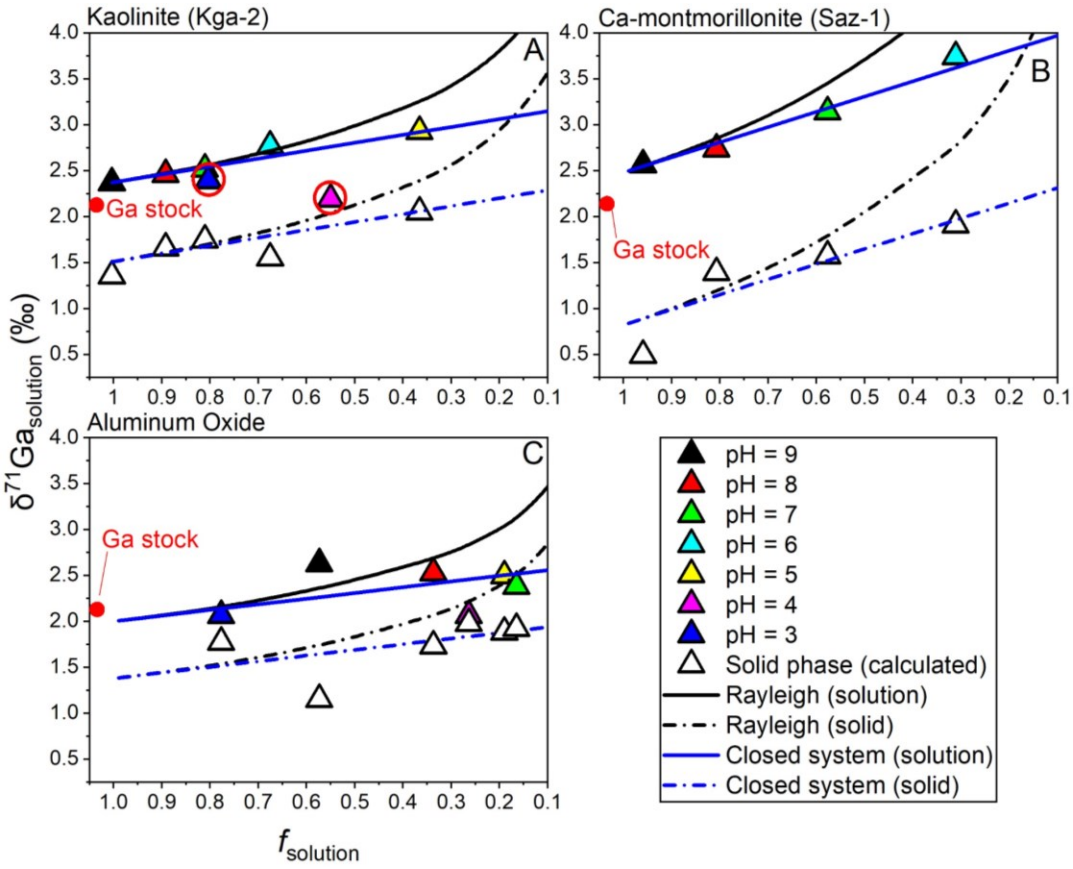

Figure 4.13. $\delta^{71}Ga_{solution}$ of Ga adsorption experiments (50 µg/L) with kaolinite, Ca-montmorillonite, and aluminum oxide. Experimental data points in A & B represent single measurements. Data points in C represent duplicate measurements for which error bars are two standard errors (2SE, n = 2), but are within the size of the symbol and not shown.

Red dots denote the mean $\delta^{71}Ga$ of the experimental Ga stock = 2.04 ± 0.09‰ (2SD, n = 6). Outliers circled in red and their solid phases are omitted because they resulted in an unreasonable (high) $\delta^{71}Ga_{solid}$ calculation due to their large deviation from the equilibrium (solid blue) line. The fractionation factors for each experiment: A) α = 0.99914, B) α = 0.99834, C) α = 0.99938. Aluminum oxide: no isotope measurement of pH 6 sample.

4.3.3 Adsorption of Gallium on Kaolinite at Variable Ionic Strengths

The Ga isotopes ($\delta^{71}Ga_{solution}$) of the Ga adsorption experiments (3000 µg/L) with kaolinite under variable ionic strength values are illustrated in Figure 4.14. Within the range of the study ionic strength (0.01M to 1M NaCl), the solution ionic strength did not exhibit observable influence on $\delta^{71}Ga_{solution}$

values which varied within ± 0.06‰ (2SD, n = 6), similar to typical long-term analytical uncertainty observed by repeated measurement of an in-house standard Ga-ICP (1.44 ± 0.09‰, 2SD; n = 21). The mean $\delta^{71}Ga_{solution}$ value was 1.78 ± 0.06‰ (2SD, n = 6). The Ga stocks used in ionic strength experiments were purified and analyzed for Ga isotope ratios, and their mean $\delta^{71}Ga_{solution}$ value (excluding the stock of 1M NaCl experiments which was an outlier) was 2.01 ± 0.09‰ (2SD, n = 4) (Figure 4.14). Therefore, $\delta^{71}Ga_{solution}$ values of the adsorption experiments with varying ionic strengths were lower than the Ga stock solutions by around 0.2‰. The control experiments (Ga only) corresponding to these experiments did not experience any precipitation (Appendix B, Table B4), and had similar isotope values with the stocks and adsorption experiments, (mean $\delta^{71}Ga_{solution}$ = 1.89 ± 0.16‰,2SD; n = 5).

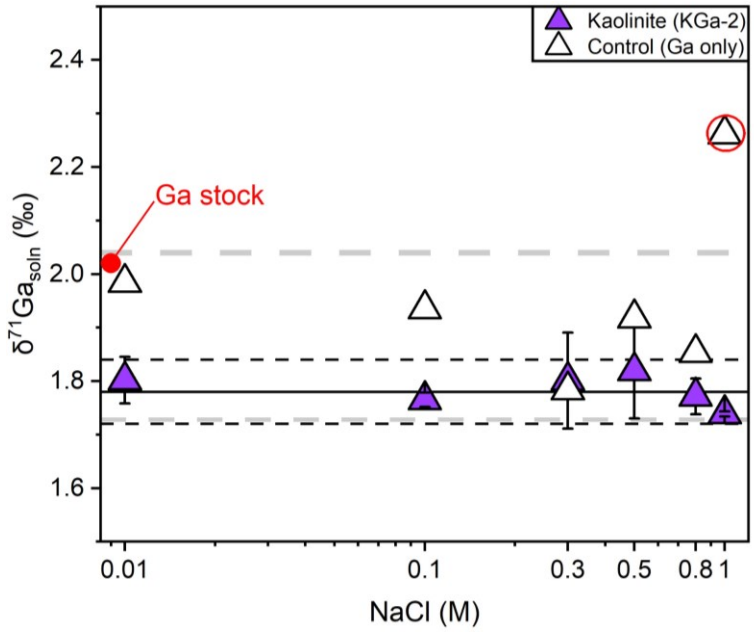

Figure 4.14. $\delta^{71}Ga_{solution}$ Ga adsorption experiments (3000 µg/L) with kaolinite under variable ionic strengths (0.01M – 1M NaCl). The purple experimental data points represent the mean value of triplicate experiments, and the error bars are two standard deviations (2SD, n = 3). The solid black line indicates their mean $\delta^{71}Ga_{solution}$, and the dashed black lines indicate two standard deviations. The white data points represent single measurements of control experiment samples. Dashed gray lines indicate their upper and lower bounds (± 2SD) from the mean (1.89 ± 0.16). Solid and dashed lines represent the mean $\delta^{71}Ga_{solution}$ and 2SD, respectively. Red circle indicates the outlier point which was significantly deviated (higher) and not plausible.

Chapter 5
Discussion

5.1 Kinetic Gallium Adsorption on Kaolinite (KGa-2)

The objective of the kinetic adsorption experiments was to determine the time it takes for the adsorption to reach the equilibrium under which both gallium concentration and isotope composition remained constant. Based on the results from kinetic Ga adsorption experiments at low and high Ga/kaolinite ratio (10μg/g and 400 μg/g, respectively), a contact time of seven days was chosen to conduct all equilibrium adsorption experiments in this study. As adsorption stabilized after a few hours of contact time (Figure 4.1), it was clear that 7-day length was long enough to achieve adsorption equilibrium. Ga adsorption on similar minerals (illite, montmorillonite) also reached adsorption equilibrium within this contact time (Benedicto et al., 2014). In the kinetic adsorption experiments with kaolinite, consistent pH decreases were observed in all samples regardless of the contact time (Appendix B, Table B1). This fluctuation in the solution pH is likely caused by the dissolution of soluble salt impurities from the mineral or changes in the carbonate equilibriums or a combination of both (Loeppert, 1986). An instant drop in pH (from 7 to 5.9) was observed after KGa-2 was suspended in the solution (Appendix B, Table B1) whereas pH in the control experiment (Ga only) after 7 days only decreased slightly. This observation suggests that equilibration of CO_2 from the test tube headspace induced a minor effect on the change in the solution pH (Appendix B, Table B1). Since soluble salts in kaolinite affect the solution pH, adsorbents used in all equilibrium experiments in this study were rinsed with the NaCl solution (0.01M or higher) which has shown to effectively remove soluble salts (Anderson et al., 1991).

Although adsorption equilibrium was attained in 7 days based on Ga concentration, isotopic equilibrium was of great importance to ensure meaningful insights from Ga isotope fractionation by equilibrium adsorptions. Unfortunately, Ga isotope ratios of the kinetic adsorption experiments were not obtained. However, previous works have shown that isotopic equilibrium during adsorption can be reached in shorter contact times than those imposed in this study. For example, Zn adsorption on kaolinite (KGa-2) reaches isotopic equilibrium within 48 hours (Guinoiseau et al., 2016). Likewise, Ga adsorption on calcite and goethite did not exhibit detectable changes in δ^{71}Ga after three days (Yuan et al., 2018). Therefore, the 7-day duration of the equilibrium adsorption experiments in this study was assumed to be adequate for reaching isotopic equilibrium.

5.2 Effects of pH on Gallium Adsorption and Isotope Fractionation at 21°C

5.2.1 Aqueous Gallium Speciation

Negligible Ga was lost in the control experiments (Ga only, no adsorbent; Figure 4.2 (A – E) and thus, the Ga lost in all adsorption experiments (50 µg/L) with the study minerals is attributed to adsorption. So, the Ga speciation model (50 µg/L; Figure 4.7A), which only considers $Ga(OH)_{3,am}$ as a possible precipitate, is consistent with the results of the control experiments. This model predicts that all gallium species are soluble. In contrast, the models that also considered the precipitation of $\alpha - GaOOH$ (with larger and smaller logK, respectively, Figure 4.7B and C) are ruled out, as they predict significant Ga precipitation on a wide pH range. Therefore, both $\alpha - GaOOH$ and $Ga(OH)_{3,am}$ are not expected to precipitate in the adsorption experiments with the initial Ga stock solution of 50 µg/L.

In contrast, significant loss of Ga was observed under a wide range of circumneutral pH (4 – 7) in the control experiments conducted at higher Ga concentration (3000 µg/L) (Figure 4.9A). The loss of gallium is likely due to the formation of gallium precipitates. However, to date, it is unclear whether the precipitates are in the form of $\alpha - GaOOH$ or $Ga(OH)_{3,am}$ or both. The speciation models considering the precipitation of only $Ga(OH)_{3,am}$ (Figure 4.7D) and both $\alpha - GaOOH$ or $Ga(OH)_{3,am}$ (Figure 4.7E) did not adequately described the significant Ga precipitation observed in the control experiments (3000 µg/L; Figure 4.3). In the model considering only $Ga(OH)_{3,am}$, the predicted narrow stability regime of this species does not capture the experimental observation, implying that that $Ga(OH)_{3,am}$ precipitate could not fully explain the loss of Ga in the control experiments (Figure 4.9). When considering both species, the model predicted $\alpha - GaOOH$ formation under a wide pH range that did not closely resemble the Ga precipitation observed in the control experiments. Therefore, the equilibrium constant for the formation of $\alpha - GaOOH$ was adjusted (proposed in Table 3.3, Reaction 7) which resulted in a prediction that accurately described the Ga loss in the control experiments (Figure 4.9). The equilibrium constant proposed in this study (-4.14) was lower than -3.54 which has been used in literature (Baes Jr & Mesmer, 1976; Persson et al., 2006). Nonetheless, based on the control experiments in this study, the Ga loss in adsorption experiments under similar conditions (Benedicto et al. 2014) might not be entirely attributed to adsorption, but partially due to the precipitation of Ga.

In summary, control experiments exhibit no evidence of Ga precipitation at low Ga concentration (50 µg/L). In contrast, in control experiments with high Ga concentration solutions (1000 µg/L and 3000

μg/L), significant Ga precipitation occurred under a wide pH range, possibly in the $\alpha - GaOOH$ form as predicted by the speciation model. Therefore, Ga lost in all equilibrium adsorption experiments with the study minerals (50 μg/L) is attributed to adsorption.

5.2.2 Effects of pH on Gallium Adsorption

A) Kaolinite (KGa-2)

For experiments conducted at low (50 μg/L) Ga concentration, the data showed that the highest adsorption occurred at mildly acidic conditions (pH 4.8) whereas kaolinite did not adsorb Ga under highly basic conditions (pH 9) and only slightly adsorbed Ga under highly acidic conditions (pH 3). Since there was no previous study of Ga adsorption on kaolinite, the surface complex SO_4Ga^{1-} was proposed for the first time in this study. A previous study showed that formation of a neutrally charged surface complex (SO_3M) of a trivalent metal "M^{3+}" was predicted to be responsible for Al^{3+} and Fe^{3+} adsorption on kaolinite (Doi et al., 2020). This approach was unsuccessful in predicting the adsorption observed in the experiments conducted with 50 μg/L Ga concentrations (Appendix A, Figure A1). The model predicted a maximum adsorption at a slightly lower pH (4.4), but in the experiments, maximum adsorption occurred at pH 4.8. Otherwise, the stability curve of SO_3Ga was similar with experiments that it peaked in mildly acidic conditions, though it still failed to capture adsorption at the extreme pH values (highly acidic and highly basic). The charge of a surface complex can be indicative of the pH where the complex is dominant, which is supported by point of zero charge (pzc) theory. The pzc of kaolinite is around 4, meaning the surface is more negatively charged at higher pH values (Leong et al., 2021). Since maximum adsorption was observed at pH 4.8 in the experiments, a negatively charged surface complex could be expected in these conditions. This hypothesis was tested by including the SO_4Ga^{1-} surface complex in the model, where Ga^{3+} bonds to four surface functional groups (SO^{1-}) forming a negatively charged complex. The model considering the formation of this complex accurately simulated the adsorption of Ga on kaolinite which is a result of SO_4Ga^{1-} surface complexation under all study pH values (Figure 4.8-A).

Cation exchange could also contribute to the Ga adsorption on clay minerals as observed for other cations where the cation replaces protons or a central cation on/within permanently (negatively) charged sites (Gu & Evans, 2008b; Ikhsan et al., 1999). The inclusion of the Ga^{3+} ionic exchange reaction (Table 3.5, Part A, Reaction 4) predicted negligible contribution to sorption. Kaolinite has a

low density of permanently charged sites due to its low charge density and cation exchange capacity (Boeva et al., 2016; Tombácz & Szekeres, 2006). This was simulated in the model, using a similar ratio of the variable charge and permanent charge sites as in Gu & Evans, (2008), however, the SCM predicted a negligible ionic exchange at all pH values when a low logK was used (Table 3.5, Part A, Reaction 4). When a higher logK was substituted to the model, ionic exchange at pH 3 was still negligible and was predicted instead at much higher pH (4.5), where Ga complexation would occur. However, since Ga^{3+} is more abundant in acidic conditions (pH 3) and negligible even at slightly higher pH (4.5) (Figure 4.7-A), the exchange reaction with permanent charge sites is expected most around pH 3. Ga was shown to partially sorb on kaolinite via ionic exchange with Al in the octahedral sheets (Bénézeth et al., 1997). Therefore, ionic exchange likely contributes greater Ga sorption than the SCM's prediction of negligible ionic exchange during adsorption on kaolinite in this study. Since the CCM is a purely electrostatic model, a nonspecific ion exchange reaction (with protons) is used to simulate cation exchange (Gu & Evans, 2008a). This reaction is shown in Table 3.5, Part A, Reaction 4. Furthermore, cation exchange is an outer-sphere process as opposed with surface complexation, which occurs in the inner-sphere (Bradbury et al., 2005). The CCM's limitation to inner-sphere sorption likely explains its inability to accurately predict Ga exchange with Al in the kaolinite structure. As protons in acidic environments induce a positive charge on a greater proportion of the variable-charged sites, less surface complexation was observed on kaolinite due to repulsion of Ga^{3+} ions. Similarly, the positively charged goethite surface was shown to repel positively charged Ga hydroxides in acidic conditions (Yuan et al., 2018). Therefore, under acidic conditions, since ionic exchange on kaolinite is limited by low permanent charged sites and adsorption is limited by the presence of negatively charged variable-charged sites, kaolinite has low adsorption capacity in acidic solutions. Under basic conditions where the surface is more negatively charged, the dominant Ga hydroxide ($Ga(OH)_4^{1-}$) is likely also repelled, which explains the decrease in adsorption under these conditions. This was also observed during Ga adsorption on birnessite at high pH (Pokrovsky et al., 2004). For these reasons, kaolinite has low adsorption capacity at extremely basic or acidic pH values.

For experiments conducted at high (3000 µg/L) Ga concentration, the SCM model predicted that SO_4Ga^{1-} and $\alpha - GaOOH$ are accounted for Ga losses for all pH values less than 7 (Figure 4.9B). At pH 3, adsorbed Ga (20%) was identical with the experiments conducted at low (50 µg/L) Ga concentrations. The Ga lost in the adsorption experiments between pH 4 and 7 was comparable with their respective control experiments which is very likely due to the precipitation, as demonstrated by

the SCM and Ga speciation modeling results (Figure 4.9). At pH > 7, Ga lost in the controls was negligible whereas Ga lost in the adsorption experiments was much higher (up to 35%; Figure 4.9-B). The adsorbed Ga under these basic pH values were slightly higher than those observed in the experiments conducted with low Ga concentration (up to 11%; Figure 4.8-A). Overall, Ga adsorption increased with increasing Ga/kaolinite ratio, which was around double in the experiments conducted with high Ga concentrations.

According to EXAFS analysis of Ga adsorbed to calcite, magnesite, and birnessite at low and high Ga concentrations, surface Ga polymerization or precipitation was attributed to the difference in the spectra observed at Ga high concentration in comparison to those at low Ga concentrations (Pokrovsky et al., 2004). Thus, these processes may also contribute to the Ga loss in experiments conducted with high Ga concentrations in this study. At pH values 4 – 7, the SCM predicted roughly two thirds of total Ga lost by α-phase precipitation and the remaining by the formation of SO_4Ga^{1-} surface complex (Figure 4.9B). However, in the control (and its speciation model), almost 100% Ga is predicted to precipitate as $\alpha - GaOOH$, which suggests that in the presence of kaolinite, less Ga precipitation occurs due to the preferential adsorption. Previous studies have suggested that the precipitation of Ga is prevented or minimized by the presence of colloids (Benedicto et al., 2014; Pokrovski et al., 2002; Pokrovsky et al., 2004). Consistently, the SCM results in this study suggests that the presence of colloids suppresses Ga precipitation but doesn't prevent it. Regardless, methods such as EXAFS spectroscopy are required to confirm Ga speciation on the kaolinite surface after adsorption. In summary, the negatively charged surface complex (SO_4Ga^{1-}) described Ga adsorption on kaolinite at low Ga concentrations, where Ga is adsorbed most in mildly acidic conditions (pH 4.8), and adsorption decreases towards lower and higher pH values. Despite kaolinite's capacity for some ionic exchange in acidic conditions, the simplicity of the SCM (CCM) in this study limited its ability to accurately predict ionic exchange processes. At high Ga concentrations, Ga lost in experiments appears to be due to a combination of $\alpha - GaOOH$ precipitation and the SO_4Ga^{1-} surface complex. At high Ga concentrations, prevention of Ga precipitation by the presence of colloids is unlikely (as previous studies suggested), however, their presence may cause less Ga precipitation as suggested by the SCM.

B) Ca-Montmorillonite (Saz-1)

The SCM in this study described adsorption on Ca-montmorillonite with similar surface reactions modeled by Benedicto et al. (2014). However, in that study, the CD-MUSIC (Charge Distribution

Multi-Site Complexation) model was used. CD-MUSIC considers varying charges on the ligands of adsorbing ions, and a more detailed electrostatic solid surface (Hiemstra & Van Riemsdijk, 2006). Those surface complexation features were used by Benedicto et al. (2014) to classify montmorillonite's adsorption sites as "strong" and "weak" sites, and also to consider two Ga sorption processes: surface complexation and ionic exchange. This description of metal adsorption on montmorillonite has been also reported in previous works (Bradbury & Baeyens, 2005; Kraepiel et al., 1999; Tournassat et al., 2013). Like kaolinite, the Ga ionic exchange mechanism in montmorillonite is also via exchange with Al, but can also occur with montmorillonite's counter ions (Na or Ca) (Benedicto et al., 2014; Schaller, 2022). In nonspecific (proton exchange) form, the Ga ionic exchange reaction with Al and Ca on montmorillonite is approximated by a single reaction (Table 3.5, Part B, Reaction 10), though, in more complex models (such as CD-MUSIC) each process is treated separately. In this study, at pH < 4 where Ga loss is greatest (100%), $SOGa^{2+}$ was predicted to dominate Ga adsorption, with minor contribution from ionic exchange (Figure 4.8-B), conflicting with the finding by Benedicto et al. (2014), suggesting that ionic exchange dominates sorption up to pH 5. Conversely, in this study, predicted ionic exchange was very minor in highly acidic conditions and peaked at around pH 5.5, regardless of optimization efforts in the SCM equilibrium constant values. In contrast, cation exchange dominates sorption on montmorillonite in highly acidic conditions (Kraepiel et al., 1999). In the SCM, only the complexation reaction of $SOGa^{2+}$ was able to capture acidic adsorption, which requires Ga^{3+} to bond with the SO^{1-} ions on variable charged sites. With a pzc at pH 8.4, the variable charged sites of Ca-montmorillonite are overwhelmingly positive at in those conditions (Chang et al., 2015). Furthermore, a lesser abundance of variable charge sites exists on the montmorillonite surface (Tombácz & Szekeres, 2006). Therefore, this surface complexation reaction is unlikely in acidic conditions as Ga^{3+} would be repelled by any variable (positive) charge sites. The significant adsorption at acidic conditions can thus only be explained by ionic exchange of Ga^{3+} with the permanently charged sites, which was missed by the SCM prediction.

Despite including ionic exchange in the calculation, the SCM was likely unable to accurately predict its dominance because it assumes that all adsorption sites are uniformly charged, and all sorption occurs at the inner-sphere. However, the charge magnitudes of variable charged and permanently charged sites are heterogeneous, and both processes are spatially separated (Tombácz & Szekeres, 2006). These differences clearly impact the nature of montmorillonite's electric double layer and must be considered to accurately quantify the contribution of each process. Therefore, the simplified approach by the CCM

appears prone to inaccurate predictions when attempting multi-surface, multi-process sorption modeling. The similarity between the SCM prediction of $SOGa^{2+}$ dominance in this study and ionic exchange dominance in previous studies and can be explained by the similarity of their chemical reactions due to the nonspecific proton exchange reaction to simulate ion exchange (Table 3.5, Reactions 7, 10). Both involve the replacement of proton(s) or a cation by a Ga^{3+} ion, which results in an identical charge balance and as a result, similar predictions. Compared with kaolinite, at acidic conditions, Ca-montmorillonite adsorbs Ga much more due to ionic exchange. This is due to its high permanent charge site density, where the opposite is true of kaolinite. With increasing pH, adsorption decreases with both minerals because of the increasingly negatively charged surface, repelling $Ga(OH)_4^{1-}$; the dominant Ga species at pH > 5. In either case, both minerals have very low adsorption capacity in highly basic solutions. In summary, contrary with kaolinite, Ga sorption on Ca-montmorillonite is greatest in acidic conditions, but like kaolinite, also decreases with increasing pH. The high adsorption capacity of Ca-montmorillonite at low pH is due to ionic exchange on its abundance of permanently charged sites. Despite this, the nonspecific ionic exchange reaction used by the SCM (CCM) was unable to accurately predict ionic exchange, whose dominance during adsorption in acidic conditions is well documented. Instead, the SCM (CCM) predicted surface complexation as the dominant process and predicted ionic exchange occurrence at higher pH values where ionic exchange is not dominant. These predictions are due to the CCM's limitations and assumptions, designed to predict inner-sphere surface complexation reactions only.

C) Oxide Minerals

In this study, Ga adsorption on crystalline silica was observed greatest at pH 4 – 5, and gradually decreased with increasing pH. In contrast, Ga adsorption on amorphous silica was observed to remain at its maximum value from pH values 3 – 10 (Pokrovsky et al., 2004). The CCM modeling Ga adsorption on amorphous silica predicted that surface complexation of $SOGa(OH)_3^{1-}$ was responsible for adsorption at all pH values (Pokrovsky et al., 2004). When applied to model adsorption on crystalline silica, however, this approach predicted little Ga adsorption under basic conditions, contradicting experimental observations (Figure 4.8C). Compared with amorphous silica, the BET area (and subsequent site density) of crystalline silica is significantly less (Shi et al., 2012). Furthermore, the pzc of crystalline silica is less than 1 whereas pzc was around 3.9 for the amorphous form (Kobayashi et al., 2020; Sverjensky, 1994). Therefore, compared with amorphous silica, the negative

surface charge of crystalline silica is greater in highly basic solutions. Repulsive forces thus likely play a role in the comparatively less Ga adsorption on crystalline silica, however, its substantially lower BET area and subsequent lower site density are also contributing factors to its lesser adsorption. Despite this, moderate Ga adsorption was still observed with crystalline silica at high pH values. In basic solutions, it is hypothesized that $Ga(OH)_4^{1-}$ is more stable in the presence of Si ions (positively charged), facilitating Ga complexation with the silica surface (Pokrovski et al., 2002; Pokrovsky et al., 2004). The dissolution of silica increases with pH, where more positively charged Si ions are released in basic aqueous environments (Brady & Walther, 1990). Based on this, $Ga(OH)_4^{1-}$ can bond with one or two surface silicate groups, which was used to explain the high Ga adsorption on amorphous silica in the form of $SOGa(OH)_3^{1-}$ (Pokrovsky et al., 2004). It is possible that Si ions facilitate this reaction by attracting anionic species such as $Ga(OH)_4^{1-}$, keeping them close to the surface where silica dissolution occurs. Since SCM calculations of $SOGa(OH)_3^{1-}$ alone were unable to capture basic adsorption on crystalline silica observed in experiments, an additional complexation reaction was required to explain the adsorption at high pH. There, two $Ga(OH)_4^{1-}$ ions bond to one sorption site, forming $SOH(Ga(OH)_4^{1-})_2^{2-}$, described in Table 3.5, Part D, Reaction 14. Inclusion of this reaction in the SCM produced a result that accounts for the adsorption peak observed at basic pH, which was indicative of an additional Ga complex (Figure 4.8C). This is a possible extension of the hypothesis by Pokrovsky et al. (2004) where the tetrahedral Ga species is stabilized by dissolved Si ions such that two $Ga(OH)_4^{1-}$ ions can be held near one surface site, approximated by $SOH(Ga(OH)_4^{1-})_2^{2-}$ at high pH values. Nonetheless, silica dissolution also likely releases adsorbed Ga as well, and although dissolved Si may stabilize some Ga adsorption, silica dissolution at basic pH likely also mobilizes previously sorbed Ga as well.

Of the three oxides studied in this study, Ga adsorption on aluminum oxide and goethite were closest in resemblance, highest adsorption occurring at pH 4 – 7.5. The main difference being the magnitude of Ga adsorption, which was lower with aluminum oxide (Figure 4.8-D, E). Previously, Ga adsorption on γ-aluminum oxide (cubic structure) under acidic conditions was modeled with the TLM, which predicted neutral and positively charged surface complexes. However, surface species at basic pH values were not studied (Lin et al., 1997). The octahedral structure of aluminum oxide in this study resembles the octahedral aluminol sheets present in Ca-montmorillonite, where $SOGa(OH)_3^{1-}$ was a dominant Ga surface complex at circumneutral pH (Figure 4.8-B) (Benedicto et al., 2014). Therefore, $SOGa(OH)_3^{1-}$ formation on the octahedral aluminol sheets can also explain the SCM prediction of its

dominance during adsorption on the aluminum oxide used in this study (Figure 4.8-D). Lin et al. (1997) included $SOGa^{2+}$ in the TLM model to account for Ga complexation in acidic conditions but concluded that other species ($SOGaOH^{+}$ and SO_2Ga^{+}) were more likely to form. This approach was followed in the CCM but did not produce results that described experimental data. Instead, the inclusion of $SOGa^{2+}$ in SCM calculations of this study produced an accurate prediction of Ga adsorption on aluminum oxide at acidic pH (Figure 4.8-D). The $SOGa^{2+}$ complex was also included in the CCM model describing aluminum adsorption on kaolinite, which has the same octahedral aluminol sheet in montmorillonite (Lützenkirchen et al., 2014). Thus, it is possible that formation of this surface complex is favorable on the octahedral aluminum oxide surface, and not on the cubic lattice of γ-aluminum oxide. Of the oxide minerals in this study (Figure 4.8-C, D, E), aluminum oxide had the largest BET area, however, it adsorbed the least Ga at circumneutral pH values. The dissolution of aluminum oxide increases with acidic conditions (Franke et al., 1987), as observed increase in the dissolved Al concentration in the control experiments containing aluminum oxide only, as pH decreases (Appendix B, Table B2). Thus, the adsorption of Ga hydroxides occurs concurrently with aluminum oxide dissolution. This likely results in Ga desorption and subsequent release back into the solution, determined by the fraction of aluminum oxide that dissolves. This feedback would likely lower net Ga adsorption compared with the oxides that are resistant to acidic dissolution, as observed with goethite. Furthermore, the hydrolysis of Ga and Al are similar and they have similar interactions with ligands in aqueous environments (Pokrovsky et al., 2004). As a result, another possible explanation is the competitive effect of Al on Ga adsorption, where increasing Al presence in the solution may significantly interfere with Ga adsorption (Benedicto et al., 2014).

Although Ga adsorption behavior with goethite is similar with that of aluminum oxide, goethite was still able to adsorb more Ga on a wider pH range (Figure 4.8-E). Fe oxides/hydroxides such as goethite are known to scavenge Ga from aqueous solutions, where Ga is immobilized in surface complexes (Hieronymus et al., 2001; Schier et al., 2021; Schmidt et al., 2014; Zhang et al., 2021). Goethite also remains insoluble in highly acidic environments, allowing adsorbed Ga to remain in the surface complex (Yuan et al., 2018). Furthermore, the Ga complex formed on the goethite surface is more hydrolysis-resilient, where liberation of the Ga hydroxide back into solution is less likely (Persson et al., 2006). These factors are likely contributors to the high Ga adsorption by goethite compared to aluminum oxide, which shows no evidence of Ga scavenging, nor insolubility on the same pH range. Ga adsorption on goethite has been attributed to the neutrally charged surface complex; $SOGa(OH)_2$,

modeled with the CCM (Yuan et al., 2018). This approach was applied in this study, with a comparable fit to experimental results (Figure 4.8-E). Goethite and aluminum oxide have similar pzc (pzc ≈ 9), indicating comparable net surface charge at a given pH (Appelo & Postma, 2005). This is supported by their inner capacitances, which are also close in magnitude (Lin et al., 1997; Yuan et al., 2018). Furthermore, the Ga surface complexation reactions describing their circumneutral pH adsorption are stoichiometrically similar, described in Table 3.5, Part D, Reaction 18 (aluminum oxide) and Table 3.5, Part E, Reaction 21 (goethite).

Ga adsorption on oxide minerals was generally similar, and most adsorption occurred at circumneutral pH values (Figure 4.8-C, D, E). Moderate Ga adsorption on crystalline silica at basic pH can be explained by a stabilizing effect by dissolved Si, allowing two Ga hydroxide ions to immobilize on one adsorption site. Similar stability regimes of the aluminum oxide and goethite Ga complexes can be explained by the minerals' comparably high pzc, similar inner capacitances, and similar complexation stoichiometries. Due to their high pzc, acidic Ga adsorption is less due to the positively charged surface at low pH values, repelling the cationic Ga species. Conversely, the extremely low pzc of crystalline silica allows it to adsorb the positively charged Ga species more in acidic conditions. In all cases, at extremely high pH values, the negatively charged surface repels the anionic Ga hydroxide. This may be offset in minerals such as amorphous silica, where its significantly larger BET area and site density appears to compensate since its adsorption is unaffected in basic solutions. In contrast with clays, Ga adsorption on oxide minerals occurs via inner-sphere surface complexation only, and not ionic exchange (Persson et al., 2006; Pokrovsky et al., 2004; Yuan et al., 2018). This is because oxide minerals are considered variable charge minerals and their structures/properties do not facilitate cation exchange, but rather, anion complexation (Violante, 2013). Overall, based on experimental results, oxide minerals constitute more robust Ga adsorbents, due to their higher Ga adsorption at most pH values. Among them, goethite adsorbs Ga most efficiently due to its scavenging properties and its insolubility even in strong acids.

5.2.3 Gallium Isotope Fractionation During Adsorption

A) Clay Minerals

The experimental data showed that $\delta^{71}Ga_{solution}$ increased with increasing adsorbed Ga fractions (Figure 4.13-A, B). However, because the $\delta^{71}Ga_{solution}$ values for this experiment were obtained from a single

measurement, higher uncertainty is expected. Also, since similar matrix content (Al, Si, P, Ca) relative to Ga within samples from the same groups (kaolinite, Ca-montmorillonite) were observed (Appendix B, Table B9), their effect on Ga isotope fractionation was likely similar. Regardless, although the influence of specific elements on Ga isotope measurement remains unclear, it appears to be the same among purified samples with similar matrix load (Section 4.3.1). Preferential adsorption of ^{69}Ga results in the remaining solutions that are enriched in ^{71}Ga, thus higher in $\delta^{71}Ga_{solution}$. Their fractionation factors (α) did not vary with pH, suggesting that Ga isotope fractionation during adsorption is not pH dependent. Since Ga isotope fractionation during adsorption on kaolinite and Ca-montmorillonite are closed-system equilibrium processes, Ga adsorption on these minerals is reversible. During equilibrium fractionation, the $Ga(OH)_4^{1-}$ molecules with heavier isotope ^{71}Ga form stiffer and shorter bonds that are more difficult to break. Thus, the forward and backward reaction (e.g., adsorption and desorption) rates are greater for the lighter isotope ^{69}Ga because of lower zero-point vibrational energy (Criss, 1999; Schauble, 2004; Yuan et al., 2018). With an increasing Ga adsorption on kaolinite, these stronger bonds of ^{71}Ga in $Ga(OH)_4^{1-}$ are progressively concentrated in the solution whereas ^{69}Ga is more concentrated in the kaolinite surface complex, SO_4Ga^{1-}. Some studies demonstrated that hydration plays a significant role in metal isotope fractionation during adsorption such as Mg^{2+} (Huang et al., 2012) and Zn^{2+} (Bryan et al., 2015). However, this process does not likely control Ga isotope fractionation because Ga is predominantly present as $Ga(OH)_4^{1-}$. The similar magnitude of Ga isotope fractionation (0.94 ± 0.37‰, 2SD; n = 5; Figure 4.15) observed between pH values 5 and 9 (Figure 4.13-A) is consistent with the SCM prediction that a single Ga complexation reaction (forming SO_4Ga^{1-}) was responsible for Ga adsorption on kaolinite.

During adsorption on Ca-montmorillonite, Ga isotope fractionation followed the same direction as observed with kaolinite in which the lighter isotope ^{69}Ga was preferentially adsorbed on the mineral surface. Likewise, similar isotope fractionation factors were observed in a range of the pH values (pH 6 – 9) (Figure 4.13-B). Thus, the complexation reactions responsible for adsorption on Ca-montmorillonite under these pH values appear to fractionate the isotopes in similar magnitude and mechanism. Compared with the kaolinite Ga surface complex (SO_4Ga^{1-}, coordination = 4) the surface complexes of Ca-montmorillonite at the same pH values ($SOH_2Ga(OH)_4$, $SOGa(OH)_3^{1-}$) have a coordination of 6. Ga isotope fractionation during adsorption has been attributed to an increase in coordination from 4 (aqueous Ga species) to 6 (Ga surface complexes), and longer Ga-O bond lengths of Ga surface complexes (Yuan et al., 2018). Ga-O bond lengths of kaolinite and Ca-montmorillonite

surface complexes were not determined in this study. However, increases in M-O (metal-oxygen) bond lengths were reported for 11 transition metals, accompanying an increase in coordination number (Mayer, 1988). Thus, the relative difference in coordination between surface complex(es) of kaolinite (4) and Ca-montmorillonite (6) are also likely accompanied by longer Ga-O bond lengths in the Ca-montmorillonite complexes. This explains the comparably greater extent of Ga isotope fractionation following adsorption on Ca-montmorillonite.

Though both Ga adsorption on kaolinite and Ca-montmorillonite follows the equilibrium fractionation mechanism, adsorption on Ca-montmorillonite induced a greater Ga isotope fractionation (1.70 ± 0.63‰, 2SD; n = 4; Figure 4.15). The main difference between the two clay minerals is that kaolinite is a 1:1 clay with lower permanent charge sites, and Ca-montmorillonite is a 2:1 clay with higher permanent charge sites (Tombácz & Szekeres, 2006). Previously, greater fractionations of stable isotopes ($^{2}H/^{1}H$ and $^{18}O/^{16}O$) were observed in soil samples that contained larger proportions of 2:1 clays in comparison with those containing less (Gaj et al., 2017). This has been attributed to either ion exchange or dehydration processes that occur in the octahedral Al-O sheet during sorption (Gaj et al., 2017). Thus, minerals with significant permanent charge site density such as montmorillonite can be expected to induce a greater isotope fractionation, as seen with Ca-montmorillonite.

For both kaolinite and Ca-montmorillonite, the average $\delta^{71}Ga$ value of the Ga stock solutions (2.04 ± 0.09‰, 2SD; n = 6) was lower than the y-intercept of the trend predicted for closed system equilibrium (Figure 4.13A, B). This y-intercept represents the $\delta^{71}Ga$ of the initial solutions (adsorbed Ga = 0%) for each experiment since both follow closed-system equilibrium. However, the theoretical $\delta^{71}Ga_{initial}$ values were also similar in magnitude for both minerals, 2.37‰ and 2.48‰, respectively (Section 4.3.1, Part D). This may be indicative of inconsistent performance of the purification method due to the differences in sample matrices loaded from kaolinite and Ca-montmorillonite (Appendix B, Table B2) during adsorption. For example, for all samples but one, Fe/Ga ratios in purified samples (5.3 to 8.5) were above the recommended value (Fe/Ga = 5, (Feng et al., 2019); Appendix B,

Table B7). The variable matrix loading between samples coupled with above acceptable Fe/Ga ratios, as well as any shift from elements such as Al, Si, P and Ca may contribute to isotope fractionation during purification, as well as interference during isotope ratio analysis. As discussed in Section 4.3.1, a 0.3‰ shift in δ^{71}Ga was observed in the purified bracketing standard (SRM NIST-994) and other mixing fraction samples, indicating that Ga isotopes fractionated during purification likely from the uniform presence of those matrix elements. Also, δ^{71}Ga in purified experimental stocks (2.04 ± 0.09‰, 2SD; n = 6) were higher (0.6‰) than that of the δ^{71}Ga of pure Ga ICP (1.44 ± 0.09‰, 2SD; n = 21, no chromatographic separation). These observations might also reiterate other fractionation process(es) occurring during purification such as incomplete removal of organics derived from the resin. However, two treatments of purified samples with hydrogen peroxide are considered sufficient which is widely used for other isotope systems (Phan et al., 2018). Regardless, the causes of purification induced Ga isotope fractionation process requires further investigation.

Nonetheless, considering the linear trend of measured $\delta^{71}Ga_{solution}$ of the mixing fraction samples (discussed in Section 4.3.1), column induced isotope fractionations are uniform for unknown samples, given that their matrix contents are similar. Therefore, the results still provide valuable insight about

Ga isotope behavior during adsorption on the study minerals. Also, despite measured $\delta^{71}Ga_{solution}$ values being shifted, since the difference between measured $\delta^{71}Ga_{solution}$ and $\delta^{71}Ga_{solid}$ ($\Delta_{solution\text{-}solid}$) is calculated according to mass balance, this presumably constant shift does not change the magnitude of $\Delta_{solution\text{-}solid}$. Thus, the reported Ga isotope fractionations in this study could still be reliable regardless of the observed shifts in $\delta^{71}Ga_{solution}$ measurements.

B) Aluminum Oxide

The uptake of ^{69}Ga into the surface complex during adsorption on aluminum oxide is favored which is the same as observed in clay minerals. Overall, the $\delta^{71}Ga_{solution}$ values also increase with the adsorbed Ga fraction during adsorption on aluminum oxide. However, Ga isotope fractionation magnitude is lower than those induced by clay minerals (Figure 4.15), suggesting that clays preferentially adsorb ^{69}Ga with greater affinity. Since the $\delta^{71}Ga_{solution}$ values moderately follow a linear trend predicted for closed system equilibrium, this suggests that isotope fractionation is likely pH independent. Still, the linear relationship observed in clay minerals was much stronger than with aluminum oxide, whose data was more scattered and less obvious. As previously mentioned, this was likely due to issues with purification. Fe/Ga ratios (5.4 to 8.5) were above recommended value (5) in purified samples of adsorption experiments with aluminum oxide (Appendix B,

Table B7). Furthermore, unlike kaolinite and Ca-montmorillonite experiments which had similar matrix element/Ga ratios among their samples, this was not true with aluminum oxide (Appendix B, Table B9), which had P/Ga as high as 14, and as low as 9. Moreover, purified samples from aluminum oxide adsorption experiments had the highest P/Ga ratios among all adsorption experiments (Appendix B, Table B9). This may explain the more scattered distribution of the data, unlike kaolinite and Ca-montmorillonite which were more linear (and had generally less, and more uniform matrix element content). Regardless, adsorption on aluminum oxide follows closed-system equilibrium, which is a reversible process.

C) Comparison with previous work

This laboratory study demonstrates the largest magnitude ($\Delta = 1.70 \pm 0.63$‰, 2SD; n = 4) of Ga isotope fractionation during adsorption on Ga on Ca-montmorillonite (Figure 4.15), likely due to the significant contribution of ionic exchange reaction resulting from high permanent charge site density in 2:1 clays. A similar degree of Ga isotope fractionation ($\Delta = 0.94 \pm 0.37$, 2SD; n = 5) was observed for Ga adsorption on kaolinite (this study) and goethite (Yuan et al., 2018; Figure 4.15). Adsorption on oxides generally induce lower fractionations; differences between δ^{71}Ga in solution and δ^{71}Ga in solid phases. For example, adsorption on aluminum oxide at various pH values induced $\Delta = 0.62 \pm 0.97$‰ (2SD, n = 6) which is also lower than the fractionation factor caused by adsorption on goethite (0.89 ± 0.28‰, n = 3, Yuan et al., 2018). Overall, Ga isotope fractionation during adsorption on a variety of minerals (clays, calcite, and oxides) follow a similar direction where lighter isotope is preferentially adsorbed, leaving the solution enriched in the heavier isotope. Adsorption on clay minerals, particularly 2:1 clays, induces a larger fractionation magnitude than adsorption on oxides.

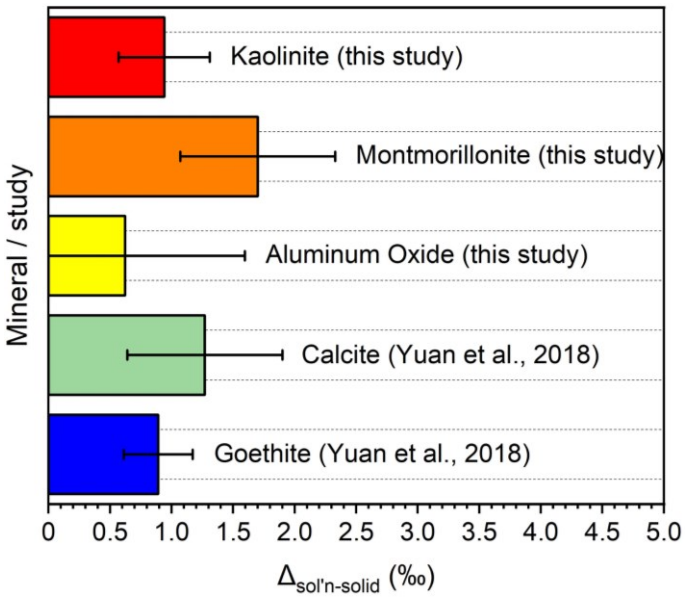

Figure 4.15. Ga isotope fractionation during adsorption on kaolinite, Ca-montmorillonite, aluminum oxide (this study), calcite, and goethite (Yuan et al. 2018).

5.3 Effects of Ionic Strengths on Gallium Adsorption and Gallium Isotope Fractionation

Ga adsorption on kaolinite in acidic solutions is hindered by increasing ionic strengths up to 1M NaCl (Figure 4.4). This was also observed during Ga adsorption on illite and montmorillonite, though reported for ionic strengths (< 0.2M NaCl; (Benedicto et al., 2014) that are lower than those in this study. Under acidic conditions, the competitive effects of Na^+ decreases cation adsorption on kaolinite (Puls et al., 1991). This explains the decrease in Ga adsorption with ionic strengths up to 1M in this study. Also, the Ga adsorption SCM did not fit the experimental data well at higher ionic strength values (Figure 4.10). This is likely because the Davies' activity model does not include the ion fit parameter needed for accurate calculations of ion activity coefficients at high ionic strengths. Thus, the model is best for predicting the adsorption with ionic strength less than 0.5M (Aqion, 2022). However, the SCM model still failed to accurately predict the adsorption up to 0.5M, which is likely due to the default equilibrium constant for the Ga-Cl complex ($GaCl^{2+}$) which does not adequately represent the Ga-Cl complexation. Regardless, it is apparent that the abundance of $GaCl^{2+}$ increases with increasing ionic

strength (Figure 4.10). This is likely to hinder Ga complexation with the mineral surface since the reactions rely on ionic Ga^{3+} or its hydroxide complexes.

Since $\delta^{71}Ga_{solution}$ did not vary with ionic strength (Figure 4.14), the potential competitive effects of Na^+ likely did not affect the preferential adsorption of ^{69}Ga during the complexation of SO_4Ga^{1-} in the experiments. During Zn adsorption on kaolinite, isotope fractionations at low ionic strengths were much smaller than adsorption at high ionic strengths (Guinoiseau et al., 2016). Similarly, larger isotope fractionations at higher ionic strengths compared with lower ionic strengths were observed during Cu adsorption on kaolinite. Na^+ presence facilitates outer-sphere Cu complex formation, which were presumed to fractionate Cu isotopes at a higher degree by inducing an isotopically lighter solid phase (Li et al., 2015). Outer-sphere complexation is likely irrelevant to Ga adsorption on kaolinite because Ga adsorption on variable charge dominant minerals occurs via inner-sphere complexation (Persson et al., 2006; Pokrovsky et al., 2004), consistent with SCM results in this study. Thus, since $\delta^{71}Ga_{solution}$ remained relatively constant between all samples, ionic strength did not influence Ga isotopes in this study.

Interestingly, only the $\delta^{71}Ga_{solution}$ values of the experiments testing the influence of ionic strength were slightly lower than those of Ga stocks, whereas $\delta^{71}Ga_{solution}$ in the adsorption experiments testing the influence of pH were higher than the $\delta^{71}Ga$ of the initial stock solution (discussed in Section 4.3.2, Part D). Initially, this suggests that Ga isotopes fractionate in opposite directions between the experiments. However, control experiments (Ga only) with varying ionic strengths had similar $\delta^{71}Ga_{solution}$ values (1.89 ± 0.16‰, 2SD; n = 5) with the adsorption experiments (1.78 ± 0.06‰, 2SD; n = 6), despite observing no adsorption or precipitation. Further, the $\delta^{71}Ga$ values of purified Ga stocks from all experiments were similar in magnitude (2.04 ± 0.09‰, 2SD; n = 10). Although ionic strengths have induced greater isotope fractionations, they have not changed isotope fractionation direction (Guinoiseau et al., 2016; Li et al., 2015), so this is highly unlikely for this study. Instead, the presence of matrix elements (Al, Si, P) in similar Ga ratios as mixing fraction samples (Appendix B, Table B9) introduces an uncertainty to the measurements due to polyatomic interferences during isotope analysis. Furthermore, Fe/Ga ratios in these experiments were lower (0.2) than acceptable (5) (Appendix B, Table B8). This contrasts with the Fe/Ga ratios observed in experiments testing the influence of pH which had ratios as high as 8.5 (Appendix B,

Table B7). Thus, the observed opposing directions of Ga isotope fractionation in experiments testing pH and ionic strength is likely related to purification induced isotope fractionation which may vary among purified samples having different matrix contents.

5.4 Changes in Ga/Al Ratio During Adsorption on Study Minerals

At pH 3, Ga/Al at equilibrium slightly decreased to 0.84 from the initial value of 1.05. The percentage of Ga adsorbed on kaolinite in the presence of Al (Ga/Al = 1) was around half of the value observed in the same experiments without Al added (Figure 5.1-A). This suggests that in the presence of Al, Ga adsorption on kaolinite was suppressed under highly acidic conditions. Under this pH, kaolinite dissolution releases Al ions into solution (Sutheimer et al., 1999) as observed in the experiments (Appendix B, Table B10). As a result, the extent of Al adsorption (if any) is unclear because dissolution of kaolinite released Al into the solution. At 5 and 7, Ga adsorption was comparable with the

experiments without Al added (Figure 5.1-A), and Al loss increased to almost 100% at pH 7 (Appendix B, Table B10). This is likely due to the precipitation of gibbsite which is stable under a wide pH range from 6 to 8 (Gensemer & Playle, 1999). In the control experiments, similar Ga and Al behavior was observed in the experimental solutions at pH 3 and 5, as Ga and Al loss were comparable (3% and 8% at 3 and 5, respectively) Appendix B, Table B10). However, at pH 7, the majority of Al precipitated in the control (~86%) whereas most Ga remained dissolved, resulting in a slightly increase in Ga/Al ratio (Figure 4.5). Therefore, at pH 7, Ga loss in the adsorption experiments is primarily due to adsorption whereas Al loss at a much higher magnitude is due to gibbsite precipitation. Thus, these two processes induced a significant increase in Ga/Al from 1.05 to 7 when the experimental solution reaches equilibrium.

During adsorption on Ca-montmorillonite at pH 3 and 5, Ga adsorptions were near 100% which is consistent with the experiments without Al added (Appendix B, Table B10). This indicates the Al did not inhibit Ga adsorption at the study ratio (1.05) under these pH values. Likewise, Al adsorption under these two pH values were almost 100% (Figure 5.1-B). Thus, Ga/Al remained unchanged at pH 3 whereas a slight increase in the Ga/Al ratio at pH 5 was due to higher degree of adsorption of Al. Similar to kaolinite, at pH 7, preferential adsorption of Ga and precipitation of Al as gibbsite explain the increase in Ga/Al.

During adsorption on oxides (silica, aluminum oxide, and goethite) at pH 3, Ga adsorption was similar in magnitude to experiments without Al added under the same pH value (Figure 5.1-C, D, E). Thus, Al competition had little or no effects. Al concentrations in the experiments conducted with silica at pH 3 were greater than the total Al added (Appendix B, Table B10), suggesting that impurities in silica released Al into the solution. Thus, the extent of Al adsorption on the silica surface remains unclear. Higher Al concentration in the experimental solution was also observed for aluminum oxide at pH 3, where in this case, Al was released by the dissolution of the aluminum oxide. Overall, at pH 5, negligible effect of Al on the adsorption of Ga was observed. Thus, the Ga/Al remained relatively unchanged.

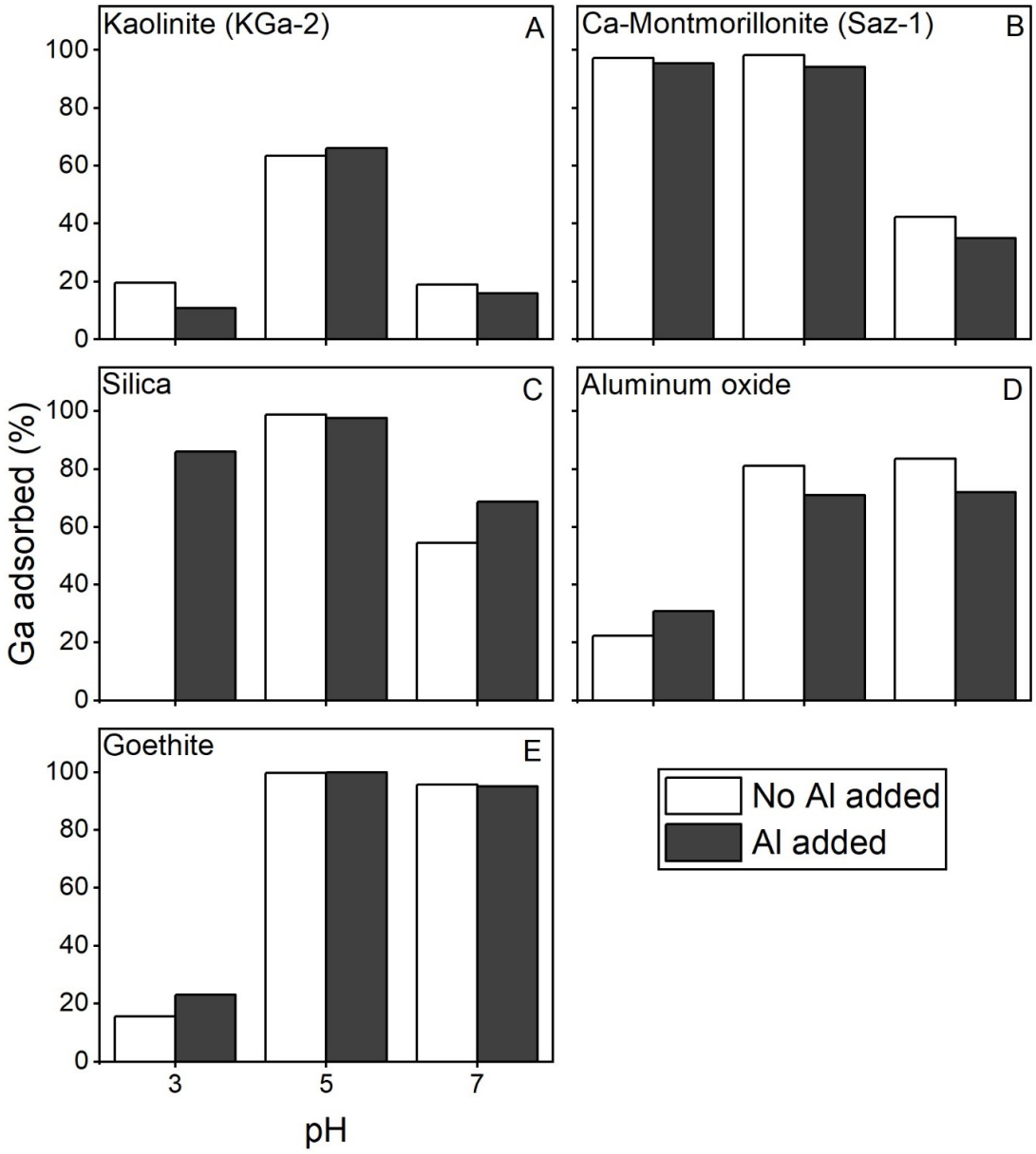

Figure 5.1. Comparison of Ga adsorbed in experiments with all study minerals conducted with Ga only, and Ga + Al (1:1 ratio). There was no data for pH experiments with silica at pH 3.

In summary, competitive effects of Al had overall negligible effects on Ga adsorption on clay and oxide minerals. Also, despite small differences in Ga adsorption with or without Al presence observed at certain pH values (such as aluminum oxide at all pH values, and silica at pH 7; Figure 5.1), Ga/Al ratios remained the same under acidic pH but increased at pH 7. This was likely due to moderate-high Ga adsorption coupled with significant gibbsite precipitation which increases the ratio despite the extent of Ga adsorption. In neutral pH solutions, the highest (and comparable) Ga/Al ratios are observed following adsorption on silica and clay minerals, suggesting that these minerals have strong potential to raise Ga/Al of water under neutral pH. Lower and comparable ratios are observed following adsorption on goethite and aluminum oxide, because those minerals can adsorb more Ga than clays in neutral solutions.

5.5 Effects of Temperature on Gallium Adsorption

In the adsorption experiments with kaolinite under low temperature (5°C), Ga did not precipitate in the control experiment at pH 3 which is consistent with the experiments conducted at 21°C (Appendix A, Figure A5). Furthermore, at this pH, the same amount of Ga was lost in both sets of experiments, despite being conducted at different initial Ga concentrations (but Ga/kaolinite ratio was the same). Therefore, the temperature difference between 21ºC and 5°C did not exhibit any difference in the percentage of Ga adsorbed at pH 3. In the control experiments conducted at pH 4, Ga precipitation at 5°C (65%) was less than the precipitation at 21°C (97%) (Appendix A, Figure A5). Lower Ga precipitation at 5°C is likely due to limited precipitation of $\alpha - GaOOH$ because the initial concentration of Ga (1000 μg/L) was lower than the Ga concentration in the experiments at 21°C (3000 μg/L). Under this pH, Ga lost in the adsorption experiment is about two times higher than the Ga lost in the control, suggesting that adsorption and Ga precipitation equally contribute to the Ga loss. However, it is not possible to differentiate the percentage of Ga adsorbed at pH values between 4 and 7 in the experiments at 21°C. Moreover, SCM modeling for the experiments at 5°C was not possible due to the lack of ΔH data for the Ga hydrolysis reactions. Thus, the effect of temperature on the adsorption under these pH values cannot be reliably evaluated. Regardless, Ga adsorption is favored under lower temperature which is also a generally accepted phenomenon regarding adsorption (Chegrouche & Bensmaili, 2002). However, this study shows that Ga adsorption at 5°C and 21°C did not exhibit any observable difference in the percentage of Ga adsorbed on kaolinite.

Chapter 6
Environmental Implications and Future Studies

This study expands the state of knowledge regarding gallium mobility and isotope fractionation through conducting laboratory experiments on the adsorption of gallium on common aquifer minerals. The results are relevant to natural systems where gallium is released and immobilized by chemical weathering processes and water-rock/sediment interactions. The control experiments and SCM modeling demonstrated that of possible Ga precipitates ($Ga(OH)_{3,am}$ or $\alpha - GaOOH$), the latter is formed at high Ga concentrations. Also, Ga remains dissolved as Ga^{3+} under acidic pH values, and $Ga(OH)_4^{1-}$ under basic pH values. During chemical weathering of sulfides or hydrothermal water fluxes, Ga concentration in hot spring water can be up to 15 µg/L which is still relatively low (Ogawa et al., 2012). In this study, even at a much higher Ga concentration (50 µg/L), Ga remains dissolved. Furthermore, at the same concentration, most Al precipitates as gibbsite in neutral to basic pH conditions. Therefore, despite variable Ga adsorption efficiencies between minerals, Ga/Al ratios increase in transport dominated (weathering limited) environments at neutral pH due to Al precipitation. Ga/Al ratios are even higher following adsorption on clay minerals since they adsorb less Ga under those conditions. This explains the higher Ga/Al ratios in geothermal waters compared with their basaltic source rocks (Elmi, 2009), where clay minerals are among the hydrothermal sediments, and Al concentrations were up to 742 µg/L. There, most Al was likely precipitated, and due to the limited Ga adsorption capacity of clays, Ga/Al ratios were much higher in those waters.

Due to precipitation of Al, lack of Al competition on Ga adsorption, and Ga's higher solubility, Ga/Al ratios tend to increase in natural waters even when Ga adsorption is less. Therefore, precipitation of gallium is not likely the primary process controlling the mobility of gallium in aqueous environments. In contrast, gallium adsorption on clay and oxide minerals is highly pH-dependent, which is governed by mineral crystal structures and electrical surface properties. Particularly, oxides such as goethite adsorb gallium greatly at circumneutral pH values which are commonly observed in natural waters. Clay minerals tend to sorb Ga through two processes: ionic exchange and surface complexation. However, ionic exchange is more dominant in 2:1 clays, explaining their high adsorption capacities in acidic conditions. Conversely, ionic exchange capacity is less in 1:1 clays, which thus have low Ga adsorption in acidic conditions. Clays are weak Ga adsorbents in alkaline waters, due to their highly negatively charged surface in those conditions. For these reasons, clay minerals can be effective Ga

removal agents in some acidic aqueous environments but have lower Ga adsorption efficiency in most natural water conditions. Higher Ga/Al ratios in surface waters compared with their source rocks (Schier, 2021; Shiller & Frilot, 1996) can be explained by this as clays are abundant in sediments. Furthermore, most organic particles (also abundant in natural waters) bind Al more easily than Ga (Schier, 2021), which also contributes to higher Ga/Al ratios in transport dominated systems.

During adsorption on clay and oxide minerals, ^{69}Ga is preferentially adsorbed and thus, Ga adsorption tends to induce higher $\delta^{71}Ga$ in the aqueous phase. Furthermore, Ga adsorption on clays is a reversible, pH independent process, and because of ionic exchange effects, adsorption on 2:1 clays results in greater Ga isotope fractionations compared with 1:1 clays. High ionic strengths decrease Ga adsorption on clays in acidic environments but do not appear to affect the magnitude or direction of Ga isotope fractionation. Also, independent of pH and ionic strength, Ga isotope fractionations were in the same direction which is not true for some other metals (Cu, Zn), making this an important finding for Ga. Contrasting with clays, oxide minerals adsorb Ga via surface complexation only, and tend to significantly adsorb Ga at circumneutral pH. Oxides also constitute more robust adsorbents due to their Ga adsorption abilities at acidic and basic pH conditions. Goethite is a highly effective Ga removal agent due to its Ga scavenging properties and insolubility in highly acidic environments. Ga isotope fractionation during Ga adsorption on oxides remains unclear, though adsorption on goethite is also pH independent and reversible (Yuan et al., 2018), inducing similar $\Delta_{solution\text{-}solid}$ (0.89 ± 0.28‰, 2SD; n = 3), as the kaolinite in this study ($\Delta_{solution\text{-}solid}$ = 0.94 ± 0.37, 2SD; n = 5). However, Ga isotope fractionation during adsorption on aluminum oxide was minimal and the isotope fractionation between the aqueous and solid phase was lower ($\Delta_{solution\text{-}solid}$ = 0.62 ± 0.97, 2SD; n = 6) than those observed during adsorption on clay minerals. The greatest extent of Ga isotope fractionation following adsorption was observed with Ca-montmorillonite in this study, with $\Delta_{solution\text{-}solid}$ = 1.70 ± 0.63, 2SD; n = 4. Lastly, adsorption on most minerals in natural waters can be expected to raise Ga/Al ratios, largely due to formation of Al precipitates, and thus, adsorption drives Ga/Al ratios upwards, which mimic weathering limited areas.

This study's observations regarding adsorption induced Ga isotope fractionations shed light on Ga mobility in many aqueous environments. However, processes such as precipitation and dissolution also affect Ga mobility (in more extreme settings) but are poorly understood. In addition to adsorption, these mechanisms are active controls on Ga mobility in systems such as semiconductor waste and acid mine drainage effluents containing high Ga concentrations in harsh environments. With increasing Ga

consumption and rising global warming, Ga mobility in that context is becoming more relevant. Thus, future study about Ga fractionation caused by its precipitation and dissolution will complement the current state of knowledge regarding Ga adsorption, making it a more useful and robust tracer.

This study reports Ga isotope fractionation mechanisms during adsorption by combining laboratory experiments, SCM modeling, and Ga isotope analysis. In the future, SCM modeling with more considerations (such as CD-MUSIC) will allow for improved accuracy of multi-process sorption predictions which is especially relevant for clay minerals. Supplementing this with EXAFS spectroscopy will confirm the accuracy of Ga complex predictions as well as Ga precipitate(s). In the future, Ga isotopes should be coupled with the Ga/Al ratio to trace Al (which is monoisotopic), and to investigate the Ga isotope trends for weathering/transport dominant environments. Further work should also be conducted to understand the Ga isotope signatures from industrial activity such as semiconductor manufacturing. Furthermore, testing the Ga purification method with a wider variety of matrix loads will help pinpoint the method's purification limits. Also, future attention must be given to producing a universal resin cleaning procedure that prepares resins adequately without the risk of damaging the resin. Lastly, a relatively uniform shift has been identified, likely due to the consistent presence of a select few matrix elements (Al, Si, P) in purified samples, though their relative effects remain unknown. In the future, analyses of samples containing various proportions of those (and other) matrix elements can help identify the mechanism of polyatomic interference on Ga isotope analysis. Subsequently, it may be possible to apply a correction to Ga isotope data even when those elements are present in purified samples. With these future study directions, the potential of the Ga isotope system as a geochemical tracer will be magnified by improving the purification reproducibility, as well as identifying the isotope effects induced by other natural processes.

References

Akcil, A., & Koldas, S. (2006). Acid Mine Drainage (AMD): causes, treatment and case studies. In *Journal of Cleaner Production*. https://doi.org/10.1016/j.jclepro.2004.09.006

Anderson, M. A., Zelazny, L. W., & Bertsch, P. M. (1991). Fluoro-Aluminum Complexes on Model and Soil Exchangers. *Soil Science Society of America Journal*, *55*(1), 71–75.

Ando, A., Mita, N., & Terashima, S. (1987). 1986 Values for Fifteen GSJ Rock Reference Samples, "Igneous Rock Series." *Geostandards Newsletter*. https://doi.org/10.1111/j.1751-908X.1987.tb00023.x

Appelo, C. A. J., & Postma, D. (2005). Geochemistry. *Groundwater and Pollution*, *536*.

Aqion. (2022). *Activity Coefficients (Activity Models)*. 2022. https://www.aqion.de/site/101

Baes Jr, C. F., & Mesmer, R. E. (1976). The Hydrolysis of Cations: Wiley Interscience. *New York*.

Ball, P. J., & Gilkes, R. J. (1987). The mount saddleback bauxite deposit, southwestern Australia. *Chemical Geology*, *60*(1–4), 215–225.

Barling, J., & Anbar, A. D. (2004). Molybdenum isotope fractionation during adsorption by manganese oxides. *Earth and Planetary Science Letters*, *217*(3–4), 315–329.

Belviso, C., Cavalcante, F., Lettino, A., & Fiore, S. (2013). A and X-type zeolites synthesised from kaolinite at low temperature. *Applied Clay Science*, *80–81*, 162–168. https://doi.org/https://doi.org/10.1016/j.clay.2013.02.003

Benedicto, A., Degueldre, C., & Missana, T. (2014). Gallium sorption on montmorillonite and illite colloids: Experimental study and modelling by ionic exchange and surface complexation. *Applied Geochemistry*, *40*, 43–50. https://doi.org/10.1016/J.APGEOCHEM.2013.10.015

Bénézeth, P., Diakonov, I. I., Pokrovski, G. S., Dandurand, J. L., Schott, J., & Khodakovsky, I. L. (1997). Gallium speciation in aqueous solution. Experimental study and modelling: Part 2.

Solubility of α-GaOOH in acidic solutions from 150 to 250°C and hydrolysis constants of gallium (III) to 300°C. *Geochimica et Cosmochimica Acta*, *61*(7), 1345–1357. https://doi.org/10.1016/S0016-7037(97)00012-4

Boeva, N. M., Bocharnikova, Y. I., Belousov, P. E., & Zhigarev, V. V. (2016). Determining the cation exchange capacity of montmorillonite by simultaneous thermal analysis method. *Russian Journal of Physical Chemistry A*, *90*(8), 1525–1529.

Bonnissel-Gissinger, P., Alnot, M., Lickes, J.-P., Ehrhardt, J.-J., & Behra, P. (1999). Modeling the Adsorption of Mercury(II) on (Hydr)oxides II: α-FeOOH (Goethite) and Amorphous Silica. *Journal of Colloid and Interface Science*, *215*(2), 313–322. https://doi.org/https://doi.org/10.1006/jcis.1999.6263

BP. (2015). Statistical Review of World Energy June 2015. *British Petroleum*. https://doi.org/bp.com/statisticalreview

Bradbury, Baeyens, B., Geckeis, H., & Rabung, T. (2005). Sorption of Eu(III)/Cm(III) on Ca-montmorillonite and Na-illite. Part 2: Surface complexation modelling. *Geochimica et Cosmochimica Acta*, *69*(23), 5403–5412. https://doi.org/https://doi.org/10.1016/j.gca.2005.06.031

Bradbury, M. H., & Baeyens, B. (2005). Experimental measurements and modeling of sorption competition on montmorillonite. *Geochimica et Cosmochimica Acta*, *69*(17), 4187–4197. https://doi.org/https://doi.org/10.1016/j.gca.2005.04.014

Brady, P. V, & Walther, J. V. (1990). Kinetics of quartz dissolution at low temperatures. *Chemical Geology*, *82*, 253–264.

Bryan, A. L., Dong, S., Wilkes, E. B., & Wasylenki, L. E. (2015). Zinc isotope fractionation during adsorption onto Mn oxyhydroxide at low and high ionic strength. *Geochimica et Cosmochimica Acta*, *157*, 182–197. https://doi.org/https://doi.org/10.1016/j.gca.2015.01.026

Burton, J. ., Culkin, F., & Riley, J. . (1959). The abundances of gallium and germanium in terrestrial materials. *Geochimica et Cosmochimica Acta*, *16*(1–3), 151–180. https://doi.org/10.1016/0016-7037(59)90052-3

Chang, P.-H., Li, Z., Jiang, W.-T., Kuo, C.-Y., & Jean, J.-S. (2015). Adsorption of tetracycline on montmorillonite: influence of solution pH, temperature, and ionic strength. *Desalination and*

Water Treatment, *55*(5), 1380–1392.

Chegrouche, S., & Bensmaili, A. (2002). Removal of Ga(III) from aqueous solution by adsorption on activated bentonite using a factorial design. *Water Research*. https://doi.org/10.1016/S0043-1354(01)00498-5

Chen, H. W. (2006). Gallium, indium, and arsenic pollution of groundwater from a semiconductor manufacturing area of Taiwan. *Bulletin of Environmental Contamination and Toxicology*. https://doi.org/10.1007/s00128-006-1062-3

Criss, R. E. (1999). *Principles of stable isotope distribution*. Oxford University Press on Demand.

De Argollo, R. M., & Schilling, J. G. (1978). Ge/Si and Ga/Al variations along the Reykjanes Ridge and Iceland. *Nature*. https://doi.org/10.1038/276024a0

Derry, L. (2017). *Development of gallium-aluminum ratios as a tracer of the Critical Zone behavior of Al*.

Diakonov, I. (1995). *Etude expérimentale de la complexation de l'aluminium avec l'ion sodium et de la spéciation du gallium et du fer (III) dans les solutions naturelles*.

Doi, A., Khosravi, M., Ejtemaei, M., Nguyen, T. A. H., & Nguyen, A. V. (2020). Specificity and affinity of multivalent ions adsorption to kaolinite surface. *Applied Clay Science*, *190*, 105557.

Eichrom Technologies. (2022). *Ln Resins*. 2022. https://www.eichrom.com/eichrom/products/ln-resins/

Elmi, S. A. (2009). Gallium and germanium distribution in geothermal water. *Geothermal Training Programme, Reports*, *2009*(5), 1–13.

Erdmann, L., & Graedel, T. E. (2011). Criticality of non-fuel minerals: A review of major approaches and analyses. In *Environmental Science and Technology*. https://doi.org/10.1021/es200563g

Ernstsson, M., Claesson, P. M., & Shao, S. Y. (1999). Characterization of adsorption sites on a quartz powder from ESCA analysis of an adsorbed fatty diamine. *Surface and Interface Analysis: An International Journal Devoted to the Development and Application of Techniques for the Analysis of Surfaces, Interfaces and Thin Films*, *27*(10), 915–929.

European Commission, & Ad-hoc Working Group. (2014). Critical raw materials for the EU. In *Eucom*.

Feng, L. ping, Zhou, L., Liu, J., Hu, Z. chu, & Liu, Y. sheng. (2019). Determination of Gallium Isotopic Compositions in Reference Materials. *Geostandards and Geoanalytical Research*. https://doi.org/10.1111/ggr.12294

Fleischer, M. (1955). Minor elements in some sulfide minerals. *Econ. Geol*, *50*(970), 1024.

Franke, M. D., Ernst, W. R., & Myerson, A. S. (1987). Kinetics of dissolution of alumina in acidic solution. *AIChE Journal*, *33*(2), 267–273.

Frenzel, M., Ketris, M. P., Seifert, T., & Gutzmer, J. (2016). On the current and future availability of gallium. *Resources Policy*. https://doi.org/10.1016/j.resourpol.2015.11.005

Frings, P. J., & Buss, H. L. (2019). The Central Role of Weathering in the Geosciences. *Elements*. https://doi.org/10.2138/gselements.15.4.229

Gaj, M., Kaufhold, S., Koeniger, P., Beyer, M., Weiler, M., & Himmelsbach, T. (2017). Mineral mediated isotope fractionation of soil water. *Rapid Communications in Mass Spectrometry*, *31*(3), 269–280.

Gensemer, R. W., & Playle, R. C. (1999). The bioavailability and toxicity of aluminum in aquatic environments. *Critical Reviews in Environmental Science and Technology*, *29*(4), 315–450.

Gladyshev, S. V., Akcil, A., Abdulvaliyev, R. A., Tastanov, E. A., Beisembekova, K. O., Temirova, S. S., & Deveci, H. (2015). Recovery of vanadium and gallium from solid waste by-products of Bayer process. *Minerals Engineering*. https://doi.org/10.1016/j.mineng.2015.01.011

Goldberg, S. (1992). Use of surface complexation models in soil chemical systems. *Advances in Agronomy*, *47*(C), 233–329. https://doi.org/10.1016/S0065-2113(08)60492-7

Goldberg, S. (2002). Competitive adsorption of arsenate and arsenite on oxides and clay minerals. *Soil Science Society of America Journal*, *66*(2), 413–421.

Gray, F., Kramer, D. A., & Bliss, J. D. (2013). Gallium and Gallium Compounds. In *Kirk-Othmer Encyclopedia of Chemical Technology* (pp. 1–26). https://doi.org/doi:10.1002/0471238961.0701121219010215.a01.pub3

Gu, X., & Evans, L. J. (2008a). Surface complexation modelling of Cd (II), Cu (II), Ni (II), Pb (II) and Zn (II) adsorption onto kaolinite. *Geochimica et Cosmochimica Acta*, *72*(2), 267–276.

Gu, X., & Evans, L. J. (2008b). Surface complexation modelling of Cd(II), Cu(II), Ni(II), Pb(II) and

Zn(II) adsorption onto kaolinite. *Geochimica et Cosmochimica Acta*, *72*(2), 267–276. https://doi.org/10.1016/J.GCA.2007.09.032

Guinoiseau, D., Gelabert, A., Moureau, J., Louvat, P., & Benedetti, M. F. (2016). Zn isotope fractionation during sorption onto kaolinite. *Environmental Science & Technology*, *50*(4), 1844–1852.

Gustafsson, J P. (2007). A Windows version of MINTEQA2 version 4.0, MINTEQA2 was released by the US Environmental Protection Agency in 1999. *Visual MINTEQ Version*, *2*.

Gustafsson, Jon Petter. (2011). Visual MINTEQ 3.0 user guide. *KTH, Department of Land and Water Recources, Stockholm, Sweden*.

Hacht, B. (2008). Gallium(III) ion hydrolysis under physiological conditions. *Bulletin of the Korean Chemical Society*. https://doi.org/10.5012/bkcs.2008.29.2.372

Hiemstra, T., & Van Riemsdijk, W. H. (2006). On the relationship between charge distribution, surface hydration, and the structure of the interface of metal hydroxides. *Journal of Colloid and Interface Science*, *301*(1), 1–18. https://doi.org/https://doi.org/10.1016/j.jcis.2006.05.008

Hieronymus, B., Kotschoubey, B., & Boulègue, J. (2001). Gallium behaviour in some contrasting lateritic profiles from Cameroon and Brazil. *Journal of Geochemical Exploration*, *72*(2), 147–163. https://doi.org/https://doi.org/10.1016/S0375-6742(01)00160-1

Ho, P., Resing, J. A., & Shiller, A. M. (2019). Processes controlling the distribution of dissolved Al and Ga along the U.S. GEOTRACES East Pacific Zonal Transect (GP16). *Deep Sea Research Part I: Oceanographic Research Papers*, *147*, 128–145. https://doi.org/https://doi.org/10.1016/j.dsr.2019.04.009

Hohl, H., Sigg, L., & Stumm, W. (1980). *Characterization of surface chemical properties of oxides in natural waters: the role of specific adsorption in determining the surface charge*. ACS Publications.

Horbe, A. M. C., & Anand, R. R. (2011). Bauxite on igneous rocks from Amazonia and Southwestern of Australia: Implication for weathering process. *Journal of Geochemical Exploration*, *111*(1–2), 1–12.

Huang, K.-J., Teng, F.-Z., Wei, G.-J., Ma, J.-L., & Bao, Z.-Y. (2012). Adsorption- and desorption-

controlled magnesium isotope fractionation during extreme weathering of basalt in Hainan Island, China. *Earth and Planetary Science Letters*, *359–360*, 73–83. https://doi.org/https://doi.org/10.1016/j.epsl.2012.10.007

Ikhsan, J., Johnson, B. B., & Wells, J. D. (1999). A Comparative Study of the Adsorption of Transition Metals on Kaolinite. *Journal of Colloid and Interface Science*, *217*(2), 403–410. https://doi.org/https://doi.org/10.1006/jcis.1999.6377

Jaskula, B. W. (2017). Gallium. *US Geological Survey Mineral Commodity Summaries; US Geological Survey: Reston, VA, USA*, 64–65.

Jennings, S. R., Dollhopf, D. J., & Inskeep, W. P. (2000). Acid production from sulfide minerals using hydrogen peroxide weathering. *Applied Geochemistry*, *15*(2), 235–243. https://doi.org/https://doi.org/10.1016/S0883-2927(99)00041-4

Jensen, H., Gaw, S., Lehto, N. J., Hassall, L., & Robinson, B. H. (2018). The mobility and plant uptake of gallium and indium, two emerging contaminants associated with electronic waste and other sources. *Chemosphere*. https://doi.org/10.1016/j.chemosphere.2018.06.111

Kato, C., & Moynier, F. (2017). Gallium isotopic evidence for extensive volatile loss from the Moon during its formation. *Science Advances*, *3*(7), e1700571.

Kato, C., Moynier, F., Foriel, J., Teng, F. Z., & Puchtel, I. S. (2017). The gallium isotopic composition of the bulk silicate Earth. *Chemical Geology*. https://doi.org/10.1016/j.chemgeo.2016.11.020

Kloo, L., Rosdahl, J., & Taylor, M. J. (2002). The nature of subvalent gallium and indium in aqueous media. *Polyhedron*, *21*(5–6), 519–524. https://doi.org/10.1016/S0277-5387(01)01030-0

Kobayashi, T., Tsubokura, Y., Oshima, Y., Sasaki, T., Kawaguchi, K., Koga, K., Uchida, K., Shinohara, N., Ajimi, S., & Kayashima, T. (2020). *Time-course Analysis of Pulmonary Inflammation Induced by Intratracheal Instillation of Fine Crystalline Silica Particles*.

Kraepiel, A. M. L., Keller, K., & Morel, F. M. M. (1999). A model for metal adsorption on montmorillonite. *Journal of Colloid and Interface Science*, *210*(1), 43–54.

Leong, Y.-K., Liu, P., Au, P.-I., & Clode, P. (2021). Microstructure of KGa-1b and KGa-2 kaolin suspensions revisited. *Colloids and Surfaces A: Physicochemical and Engineering Aspects*, *617*,

126354. https://doi.org/https://doi.org/10.1016/j.colsurfa.2021.126354

Li, D., Liu, S.-A., & Li, S. (2015). Copper isotope fractionation during adsorption onto kaolinite: Experimental approach and applications. *Chemical Geology*, *396*, 74–82. https://doi.org/https://doi.org/10.1016/j.chemgeo.2014.12.020

Liang, S.-Y., Lin, W.-S., Chen, C.-P., Liu, C.-W., & Fan, C. (2021). A review of geochemical modeling for the performance assessment of radioactive waste disposal in a subsurface system. *Applied Sciences*, *11*(13), 5879.

Lin, C. F., Chang, K. Sen, Tsay, C. W., Lee, D. Y., Lo, S. L., & Yasunaga, T. (1997). Adsorption Mechanism of Gallium(III) and Indium(III) onto γ-Al2O3. *Journal of Colloid and Interface Science*, *188*(1), 201–208. https://doi.org/10.1006/JCIS.1996.4739

Loeppert, R. H. (1986). Reactions of iron and carbonates in calcareous soils. *Journal of Plant Nutrition*, *9*(3–7), 195–214.

Lourakis, M. I. A. (2005). A brief description of the Levenberg-Marquardt algorithm implemented by levmar. *Foundation of Research and Technology*, *4*(1), 1–6.

Lu, F., Xiao, T., Lin, J., Ning, Z., Long, Q., Xiao, L., Huang, F., Wang, W., Xiao, Q., Lan, X., & Chen, H. (2017). Resources and extraction of gallium: A review. *Hydrometallurgy*. https://doi.org/10.1016/j.hydromet.2017.10.010

Lützenkirchen, J., Abdelmonem, A., Weerasooriya, R., Heberling, F., Metz, V., & Marsac, R. (2014). Adsorption of dissolved aluminum on sapphire-c and kaolinite: implications for points of zero charge of clay minerals. *Geochemical Transactions*, *15*(1), 1–14.

Marchuk, S. (2016). *The dynamics of potassium in some Australian soils*.

Mayer, J. M. (1988). Metal-oxygen multiple bond lengths: a statistical study. *Inorganic Chemistry*, *27*(22), 3899–3903.

McDonough, W. F. (2003). Compositional Model for the Earth's Core. In *Treatise on Geochemistry*. https://doi.org/10.1016/B0-08-043751-6/02015-6

Meija, J., Coplen, T. B., Berglund, M., Brand, W. A., De Bièvre, P., Gröning, M., Holden, N. E., Irrgeher, J., Loss, R. D., Walczyk, T., & Prohaska, T. (2016). Isotopic compositions of the elements 2013 (IUPAC Technical Report). In *Pure and Applied Chemistry*.

https://doi.org/10.1515/pac-2015-0503

Missana, T., Alonso, U., & García-Gutiérrez, M. (2009). Experimental study and modelling of selenite sorption onto illite and smectite clays. *Journal of Colloid and Interface Science*, *334*(2), 132–138. https://doi.org/10.1016/J.JCIS.2009.02.059

Mojid, M. A. (2011). Diffuse double layer (DDL). In *Encyclopedia of agrophysics* (pp. 213–214). Springer Dordrecht, Netherlands.

Moskalyk, R. R. (2003). Gallium: the backbone of the electronics industry. *Minerals Engineering*, *16*(10), 921–929. https://doi.org/10.1016/J.MINENG.2003.08.003

O'Neill, S., & C., H. (1998). Composition of the silicate Earth : Implications for accretion and core formation. *The Earth's Mantle : Composition, Structure, and Evolution*, 3–126. http://ci.nii.ac.jp/naid/10025676323/en/

Ogawa, Y., Ishiyama, D., Shikazono, N., Iwane, K., Kajiwara, M., & Tsuchiya, N. (2012). The role of hydrous ferric oxide precipitation in the fractionation of arsenic, gallium, and indium during the neutralization of acidic hot spring water by river water in the Tama River watershed, Japan. *Geochimica et Cosmochimica Acta*. https://doi.org/10.1016/j.gca.2012.03.009

Önnby, L., Kumar, P. S., Sigfridsson, K. G. V, Wendt, O. F., Carlson, S., & Kirsebom, H. (2014). Improved arsenic(III) adsorption by Al2O3 nanoparticles and H2O2: Evidence of oxidation to arsenic(V) from X-ray absorption spectroscopy. *Chemosphere*, *113*, 151–157. https://doi.org/https://doi.org/10.1016/j.chemosphere.2014.04.097

Payne, C. E. (2016). *Isotope geochemistry of gallium in hydrothermal systems*.

Persson, P., Zivkovic, K., & Sjöberg, S. (2006). Quantitative adsorption and local structures of gallium(III) at the water-α-FeOOH interface. *Langmuir*. https://doi.org/10.1021/la052555j

Phan, Gardiner, J. B., Capo, R. C., & Stewart, B. W. (2018). Geochemical and multi-isotopic (87Sr/86Sr, 143Nd/144Nd, 238U/235U) perspectives of sediment sources, depositional conditions, and diagenesis of the Marcellus Shale, Appalachian Basin, USA. *Geochimica et Cosmochimica Acta*, *222*, 187–211. https://doi.org/https://doi.org/10.1016/j.gca.2017.10.021

Phan, T. N. T., Louvard, N., Bachiri, S. A., Persello, J., & Foissy, A. (2004). Adsorption of zinc on colloidal silica, triple layer modelization and aggregation data. *Colloids and Surfaces A:*

Physicochemical and Engineering Aspects, *244*(1–3), 131–140. https://doi.org/10.1016/J.COLSURFA.2004.06.012

Pokrovski, G. S., Schott, J., Hazemann, J. L., Farges, F., & Pokrovsky, O. S. (2002). An X-ray absorption fine structure and nuclear magnetic resonance spectroscopy study of gallium - silica complexes in aqueous solution. *Geochimica et Cosmochimica Acta*. https://doi.org/10.1016/S0016-7037(02)00973-0

Pokrovsky, Pokrovski, & Schott. (2004). Gallium(III) adsorption on carbonates and oxides: X-ray absorption fine structure spectroscopy study and surface complexation modeling. *Journal of Colloid and Interface Science*, *279*(2), 314–325. https://doi.org/10.1016/j.jcis.2004.06.095

Połedniok, J. (2008). Speciation of scandium and gallium in soil. *Chemosphere*, *73*(4), 572–579. https://doi.org/10.1016/J.CHEMOSPHERE.2008.06.012

Puls, R. W., Powell, R. M., Clark, D., & Eldred, C. J. (1991). Effects of pH, solid/solution ratio, ionic strength, and organic acids on Pb and Cd sorption on kaolinite. *Water, Air, and Soil Pollution*, *57*(1), 423–430.

Righetto, L., Azimonti, G., Missana, T., & Bidoglio, G. (1995). The triple layer model revised. *Colloids and Surfaces A: Physicochemical and Engineering Aspects*, *95*(2–3), 141–157. https://doi.org/10.1016/0927-7757(94)02990-A

Ringering, K., Kouhail, Y., Yecheskel, Y., Dror, I., & Berkowitz, B. (2019). Mobility and retention of indium and gallium in saturated porous media. *Journal of Hazardous Materials*. https://doi.org/10.1016/j.jhazmat.2018.09.079

Root, R. A., Hayes, S. M., Hammond, C. M., Maier, R. M., & Chorover, J. (2015). Toxic metal(loid) speciation during weathering of iron sulfide mine tailings under semi-arid climate. *Applied Geochemistry*, *62*, 131–149. https://doi.org/https://doi.org/10.1016/j.apgeochem.2015.01.005

Sahlström, F., Arribas, A., Dirks, P., Corral, I., & Chang, Z. (2017). Mineralogical distribution of germanium, gallium and indium at the Mt arlton high-sulfidation epithermal deposit, NE Australia, and comparison with similar deposits worldwide. *Minerals*. https://doi.org/10.3390/min7110213

Savenko, A. V., & Savenko, V. S. (2010). Gallium (III) Speciation in Seawater. *Geochemistry International*. https://doi.org/10.1134/S0016702910090090

Schaller, C. (2022). *Structure & Reactivity in Organic, Biological and Inorganic Chemistry*. https://employees.csbsju.edu/cschaller/Principles Chem/network/NWalumina.htm

Schauble, E. A. (2004). Applying stable isotope fractionation theory to new systems. *Reviews in Mineralogy and Geochemistry*, *55*(1), 65–111.

Schier, K. (2021). *Trace elements and their application as geochemical proxies in marine chemical sediments*. Jacobs University Bremen.

Schier, K., Ernst, D. M., de Sousa, I. M. C., Garbe-Schönberg, D., Kuhn, T., Hein, J. R., & Bau, M. (2021). Gallium-aluminum systematics of marine hydrogenetic ferromanganese crusts: Inter-oceanic differences and fractionation during scavenging. *Geochimica et Cosmochimica Acta*, *310*, 187–204. https://doi.org/https://doi.org/10.1016/j.gca.2021.05.019

Schmidt, K., Bau, M., Hein, J. R., & Koschinsky, A. (2014). Fractionation of the geochemical twins Zr–Hf and Nb–Ta during scavenging from seawater by hydrogenetic ferromanganese crusts. *Geochimica et Cosmochimica Acta*, *140*, 468–487.

Schulte, R. F., & Foley, N. K. (2014). Compilation of gallium resource data for bauxite deposits. In *Open-File Report*. https://doi.org/10.3133/ofr20131272

Shaw, D. M. (1957). The geochemistry of gallium, indium, thallium—a review. *Physics and Chemistry of the Earth*, *2*, 164–211. https://doi.org/10.1016/0079-1946(57)90009-5

Shi, J., Hedberg, Y., Lundin, M., Odnevall Wallinder, I., Karlsson, H. L., & Möller, L. (2012). Hemolytic properties of synthetic nano- and porous silica particles: The effect of surface properties and the protection by the plasma corona. *Acta Biomaterialia*, *8*(9), 3478–3490. https://doi.org/10.1016/J.ACTBIO.2012.04.024

Shiller, A. M. (1988). Enrichment of dissolved gallium relative to aluminum in natural waters. *Geochimica et Cosmochimica Acta*, *52*(7), 1879–1882. https://doi.org/https://doi.org/10.1016/0016-7037(88)90011-7

Shiller, A. M., & Frilot, D. M. (1996). The geochemistry of gallium relative to aluminum in Californian streams. *Geochimica et Cosmochimica Acta*. https://doi.org/10.1016/0016-7037(96)00002-6

Spence, J., & Telmer, K. (2005). The role of sulfur in chemical weathering and atmospheric CO2

fluxes: Evidence from major ions, δ13CDIC, and δ34SSO4 in rivers of the Canadian Cordillera. *Geochimica et Cosmochimica Acta*, *69*(23), 5441–5458. https://doi.org/https://doi.org/10.1016/j.gca.2005.07.011

Sposito, G. (1984). *The surface chemistry of soils.* Oxford university press.

Stumm, W. (1995). *The inner-sphere surface complex: A key to understanding surface reactivity*.

Stumm, W., & Morgan, J. J. (1996). Aquatic chemistry: chemical equilibria and rates in natural waters. *Choice Reviews Online*, *33*(11), 33-6312-33–6312. https://doi.org/10.5860/choice.33-6312

Stumm, W., & Morgan, J. J. (2012). *Aquatic chemistry: chemical equilibria and rates in natural waters* (Vol. 126). John Wiley & Sons.

Sutheimer, S. H., Maurice, P. A., & Zhou, Q. (1999). Dissolution of well and poorly crystallized kaolinites: Al speciation and effects of surface characteristics. *American Mineralogist*, *84*(4), 620–628.

Sverjensky, D. A. (1994). Zero-point-of-charge prediction from crystal chemistry and solvation theory. *Geochimica et Cosmochimica Acta*, *58*(14), 3123–3129. https://doi.org/https://doi.org/10.1016/0016-7037(94)90184-8

Syu, C.-H., Chen, P.-W., Huang, C.-C., & Lee, D.-Y. (2020). Accumulation of gallium (Ga) and indium (In) in rice grains in Ga- and In-contaminated paddy soils. *Environmental Pollution*, *261*, 114189. https://doi.org/https://doi.org/10.1016/j.envpol.2020.114189

Takahashi, Y., Minai, Y., Ambe, S., Makide, Y., & Ambe, F. (1999). Comparison of adsorption behavior of multiple inorganic ions on kaolinite and silica in the presence of humic acid using the multitracer technique. *Geochimica et Cosmochimica Acta*. https://doi.org/10.1016/S0016-7037(99)00065-4

Tamura, H., Mita, K., Tanaka, A., & Ito, M. (2001). Mechanism of Hydroxylation of Metal Oxide Surfaces. *Journal of Colloid and Interface Science*, *243*(1), 202–207. https://doi.org/https://doi.org/10.1006/jcis.2001.7864

Thakur, P. (2017). Global Reserves of Coal Bed Methane and Prominent Coal Basins. In *Advanced Reservoir and Production Engineering for Coal Bed Methane*. https://doi.org/10.1016/b978-0-

12-803095-0.00001-6

Tombácz, E., & Szekeres, M. (2006). Surface charge heterogeneity of kaolinite in aqueous suspension in comparison with montmorillonite. *Applied Clay Science*, *34*(1), 105–124. https://doi.org/https://doi.org/10.1016/j.clay.2006.05.009

Torrance, K. W., Keenan, H. E., Hursthouse, A. S., & Stirling, D. (2010). Measurement of arsenic and gallium content of gallium arsenide semiconductor waste streams by ICP-MS. *Journal of Environmental Science and Health Part A*, *45*(4), 471–475.

Tournassat, C., Grangeon, S., Leroy, P., & Giffaut, E. (2013). Modeling specific pH dependent sorption of divalent metals on montmorillonite surfaces. A review of pitfalls, recent achievements and current challenges. *American Journal of Science*, *313*(5), 395–451.

US. EPA. (1999). *Understanding variation in partition coefficient, Kd, values*.

Violante, A. (2013). Elucidating mechanisms of competitive sorption at the mineral/water interface. In *Advances in agronomy* (Vol. 118, pp. 111–176). Elsevier.

Wanner, H., Albinsson, Y., Karnland, O., Wieland, E., Charlet, L., & Wersin, P. (1994). The acid/base chemistry of montmorillonite. *Radiochimica Acta*, *66*(s1), 157–162.

Wimpenny, J., Marks, N., Knight, K., Borg, L., Badro, J., & Ryerson, F. (2020). Constraining the behavior of gallium isotopes during evaporation at extreme temperatures. *Geochimica et Cosmochimica Acta*, *286*, 54–71. https://doi.org/https://doi.org/10.1016/j.gca.2020.07.006

Wojtczak, A. (2019). *Gallium leaching during acidic dissolution of silicate minerals: implications for silicate weathering*.

Wood, S. A., & Samson, I. M. (2006). The aqueous geochemistry of gallium, germanium, indium and scandium. *Ore Geology Reviews*. https://doi.org/10.1016/j.oregeorev.2003.06.002

Yu, H.-S., & Liao, W.-T. (2011). *Gallium: Environmental Pollution and Health Effects* (J. O. B. T.-E. of E. H. Nriagu (ed.); pp. 829–833). Elsevier. https://doi.org/https://doi.org/10.1016/B978-0-444-52272-6.00474-8

Yuan, W., Chen, J. Bin, Birck, J. L., Yin, Z. Y., Yuan, S. L., Cai, H. M., Wang, Z. W., Huang, Q., & Wang, Z. H. (2016). Precise Analysis of Gallium Isotopic Composition by MC-ICP-MS. *Analytical Chemistry*. https://doi.org/10.1021/acs.analchem.6b02317

Yuan, W., Saldi, G. D., Chen, J. Bin, Vetuschi Zuccolini, M., Birck, J. L., Liu, Y., & Schott, J. (2018). Gallium isotope fractionation during Ga adsorption on calcite and goethite. *Geochimica et Cosmochimica Acta*. https://doi.org/10.1016/j.gca.2017.12.008

Zhang, L., Zhu, Y., Li, H., Liu, N., Liu, X., & Guo, X. (2010). Kinetic and thermodynamic studies of adsorption of gallium (III) on nano-TiO 2. *Rare Metals*, *29*(1), 16–20.

Zhang, Liao, S., Tao, C., Wen, H., Fan, H., Wen, J., Yang, W., & Li, W. (2021). Ga isotopic fractionation in sulfides from the Yuhuang and Duanqiao hydrothermal fields on the Southwest Indian Ridge. *Geoscience Frontiers*, *12*(4), 101137.

Zhang, Zhou, L., Yang, L., Wang, Q., Feng, L., & Liu, Y. (2016). High precision measurements of gallium isotopic compositions in geological materials by MC-ICP-MS. *Journal of Analytical Atomic Spectrometry*, *31*(8), 1673–1679.

Zhong, S.-L., Dang, Z.-M., Zhou, W.-Y., & Cai, H.-W. (2018). Past and future on nanodielectrics. *IET Nanodielectrics*, *1*(1), 41–47.

Appendix A

Figures

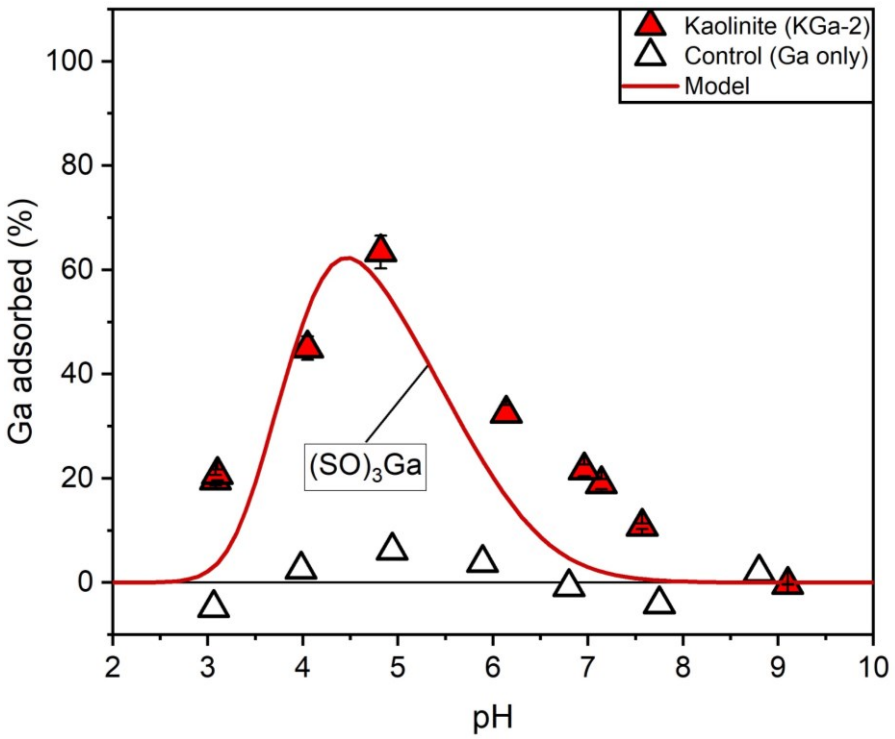

Figure A1. SCM of 50 µg/L Ga adsorption experiments with kaolinite (KGa-2) testing the influence of pH. The SCM predicts the neutral complex (SO_3Ga) as per the approach outlined by Doi et al. (2020), which did not describe adsorption in this study's experiments. The experimental data points represent single measurements. Error bars represent a mean analytical uncertainty that was typically observed during this study (2SD = 5%). testing pH dependence with experimental results. Error bars represent a mean analytical uncertainty that was typically observed during this study (2SD= 5%).

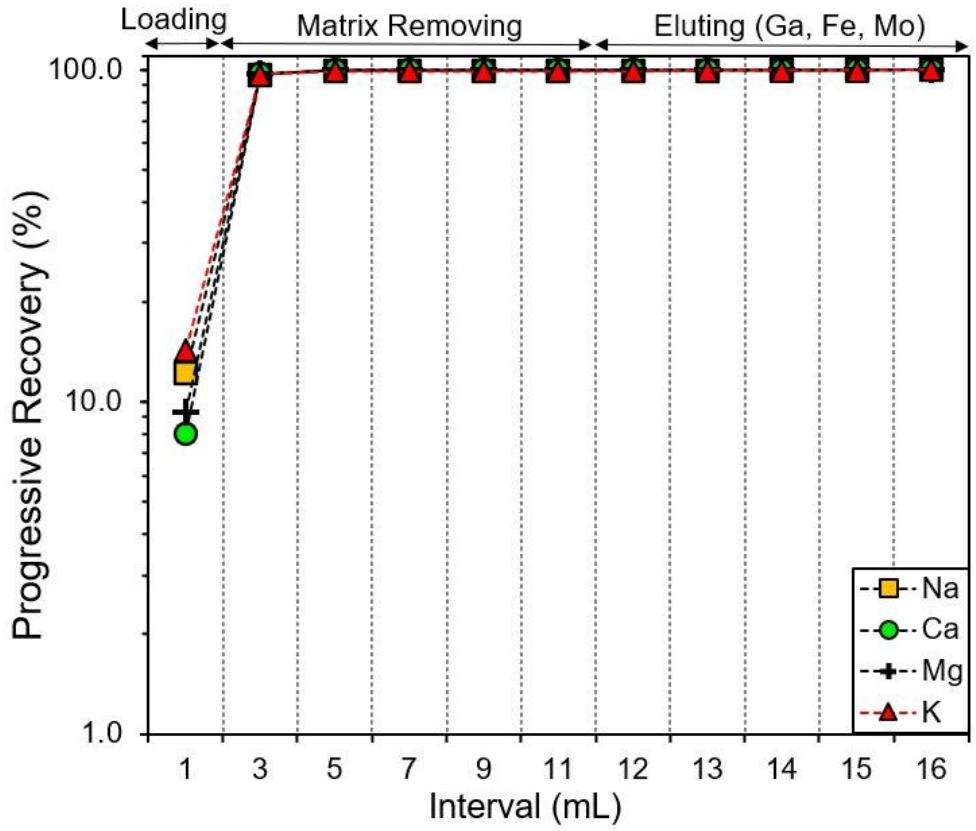

Figure A2. Elution of major matrix elements in column 1 (anion exchange).

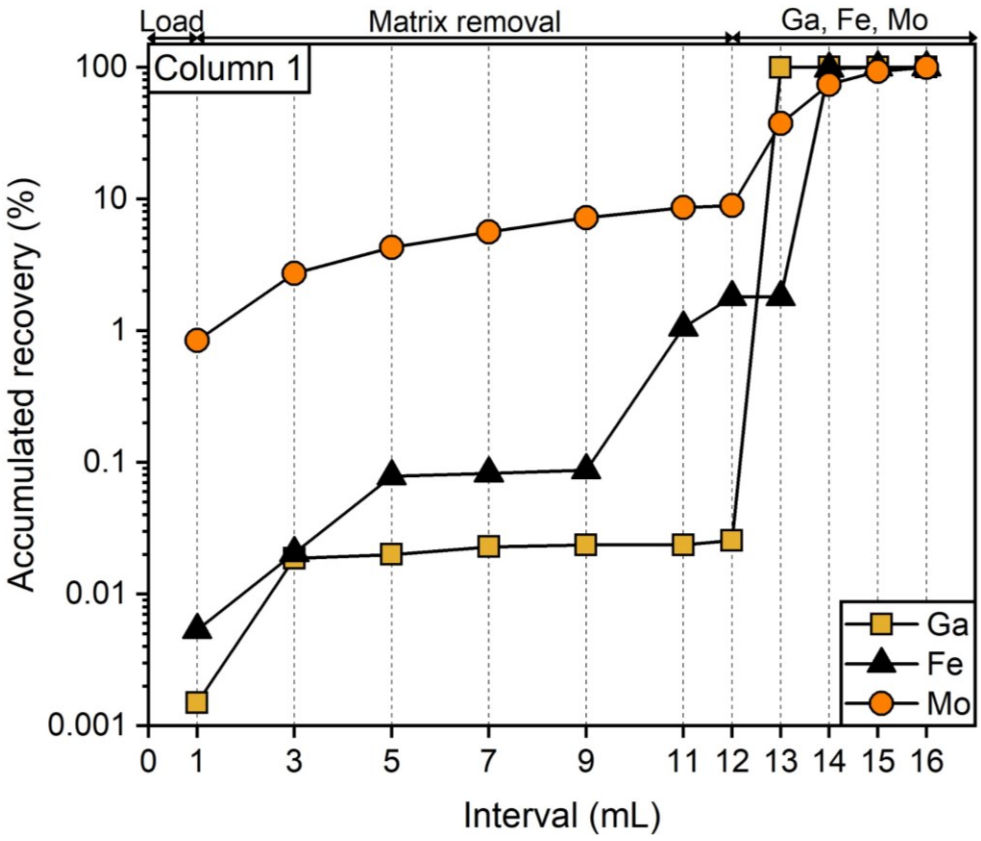

Figure A3. Elution of Ga, Fe, Mo in column 1 (anion exchange).

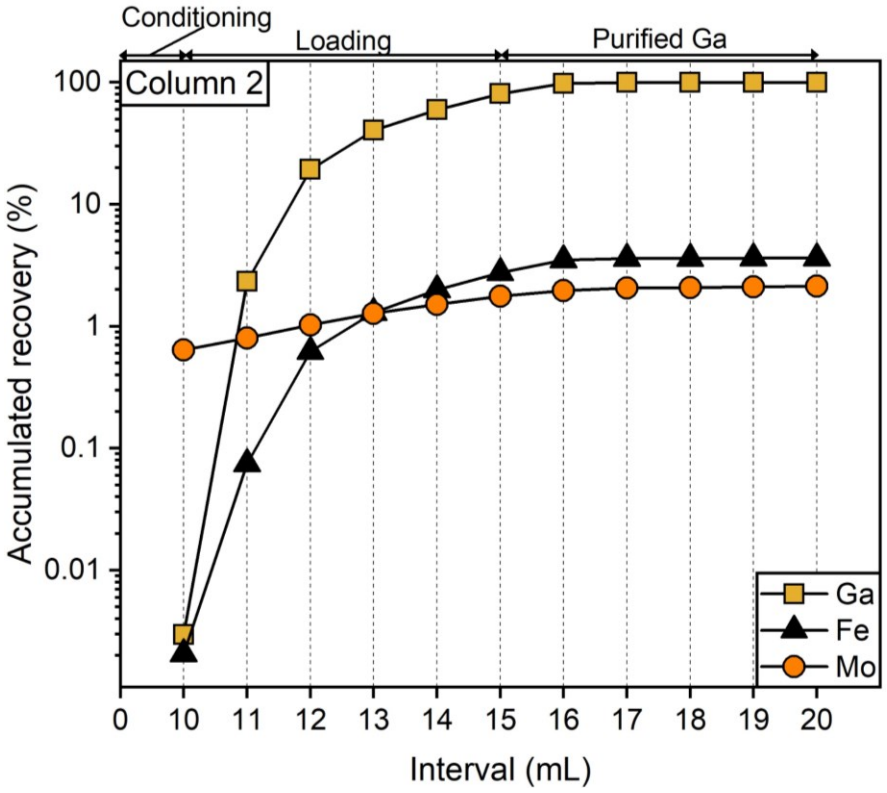

Figure A4. Elution of Ga, Fe, Mo in column 2 (cation exchange).

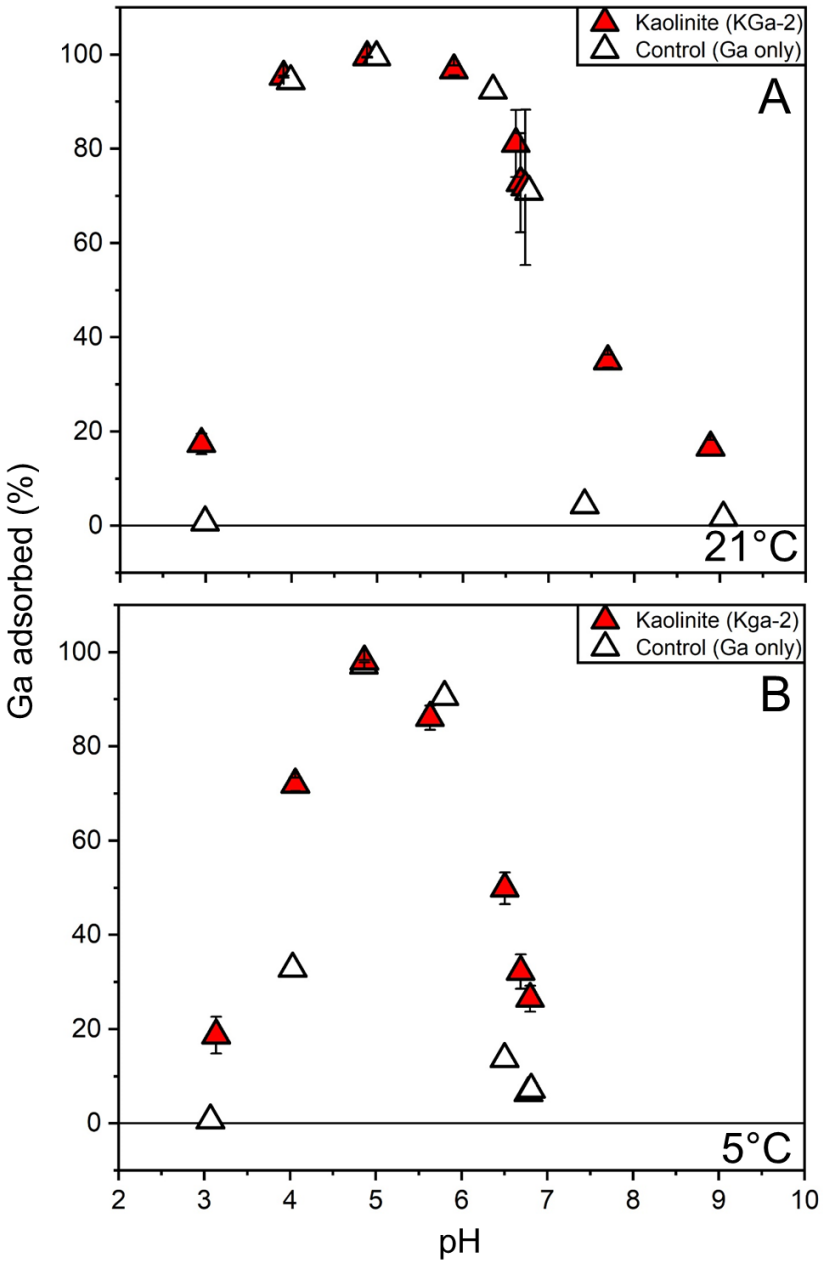

Figure A5. Ga adsorption experiments with kaolinite at different concentrations and temperatures. A) 3000 µg/L Ga, 21°C, B) 1000 µg/L Ga, 5°C (2SD, n = 3).

Appendix B

Tables

Table B1. Summary of kinetic Ga adsorption experiments (1000 µg/L) with high Ga/kaolinite mass ratio at 21°C.

Experiment	time	pH	$[Ga]_{initial}$	Ga/kaolinite	Ga adsorbed
	hours		µg/L	µg/g	%
KGa-2-1	0.4	5.9	1000	400	93
KGa-2-2	0.7	5.4			96
KGa-2-3	1	5.3			97
KGa-2-4	2	5.7			98
KGa-2-5	4	5.6			99
KGa-2-6	8	5.8			99
KGa-2-7	24	6.0			99
KGa-2-8	50	6.2			99
KGa-2-9	97	6.0			99
KGa-2-10	172	5.9			99
Blk (Ga only)	172	6.5			7.6

Note: Initial pH = 7

Table B2. Summary of control experiments containing only minerals in 0.01M NaCl, at 21°C.

Experiment	Mineral	[Solid]	pH	Al	Si	Ca	Fe	Ga
		g/L		µg/L				
3KG-NaCl	Kaolinite (Kga-2	0.034	3	4.3	12.3	11.0	2.5	2.4E-02
7KG-NaCl			7	0.4	13.3	16.4	2.3	4.5E-02
3SA-NaCl	Ca-Montmorillonite (Saz-1)		3	7.8	206.7	169.9	3.6	1.3E-02
7SA-NaCl			7	2.6	88.6	190.0	3.0	3.1E-02
3SI-NaCl	Crystalline Silica		3	4.9	10.9	12.5	3.1	2.1E-02
7SI-NaCl			7	0.6	31.4	13.5	2.7	4.7E-02
3AL-NaCl	Aluminum Oxide		3	1019.8	6.8	15.9	2.4	2.0E-02
7AL-NaCl			7	5.7	11.7	15.0	2.4	1.4E-02
3GT-NaCl	Goethite		3	0.6	6.2	15.0	5.1	1.4E-02
7GT-NaCl			7	0.3	9.4	12.5	2.7	7.2E-03

Table B3. Summary of 3000 µg/L Ga adsorption experiments with kaolinite (KGa-2), testing the influence of pH at 21°C.

Experiment	[NaCl]	pH	KGa-2	$[Ga]_{loaded}$	$[Ga]_{lost}$	Ga_{lost}	$\delta^{71}Ga$	2σ	n
	M		g	µg/m^2	µg/m^2	%	‰		
3A	0.01	3.0	0.03	133.20	22.38	16.80	1.88	0.21	2
3B		3.0	0.03	137.28	25.62	18.66	1.82	—	1
3C		2.9	0.03	127.31	21.31	16.74	1.78	—	1
3BlkNoClay		3.0	—	—	—	0.75	2.02	0.11	2
4A		3.9	0.03	133.19	127.11	95.44	—	—	—
4B		3.9	0.03	127.09	121.08	95.27	—	—	—
4C		3.9	0.03	125.79	119.77	95.22	—	—	—
4BlkNoClay		4.0	—	—	—	94.41	—	—	—
5A		5.0	0.03	129.10	128.30	99.38	—	—	—
5B		4.8	0.03	126.85	126.23	99.51	—	—	—
5C		4.9	0.03	135.75	134.95	99.41	—	—	—
5BlkNoClay		5.0	—	—	—	99.44	—	—	—
6A		5.8	0.03	127.40	123.85	97.21	—	—	—
6B		5.9	0.03	119.60	115.52	96.59	—	—	—
6C		6.0	0.03	122.73	118.05	96.19	—	—	—
6BlkNoClay		6.4	—	—	—	92.39	—	—	—
6.7A		6.7	0.03	127.96	95.26	74.45	—	—	—
6.7B		6.7	0.03	118.96	79.60	66.92	—	—	—
6.7C		6.6	0.03	112.36	86.53	77.01	—	—	—
6.7D		6.7	0.03	112.19	89.95	80.17	—	—	—
6.7E		6.8	0.03	111.88	71.25	63.68	—	—	—
6.7F		6.7	0.03	110.36	79.07	71.65	—	—	—
7A		6.6	0.03	122.44	101.32	82.75	—	—	—
7B		6.6	0.03	125.28	96.47	77.00	—	—	—
7C		6.6	0.03	122.14	102.00	83.51	—	—	—
7BlkNoClay		6.8	—	—	—	70.94	—	—	—
8A		7.7	0.50	128.73	44.33	34.44	—	—	—
8B		7.7	0.50	128.73	45.57	35.40	—	—	—
8BlkNoClay		7.4	—	—	—	4.40	—	—	—
9A		8.9	0.50	126.28	20.26	16.04	—	—	—
9B		8.9	0.50	126.28	21.68	17.17	—	—	—
9BlkNoClay		9.0	—	—	—	1.74	—	—	—

Note: BET area of KGa-2 = 23.5 m^2/g.

Note: Samples with "Blk" indicates the control experiments with Ga only.

Table B4. Summary of 3000 µg/L Ga adsorption experiments with kaolinite (KGa-2), testing the influence of ionic strength at 21°C.

Experiment	[NaCl]	pH	KGa-2	$[Ga]_{loaded}$	$[Ga]_{ads}$	% Ga_{ads}		$\delta^{71}Ga$	2σ	n
	M		g	µg/m^2	µg/m^2	meas.	model	‰		
0.01A	0.01	3.0	0.03	133.20	22.38	16.80	20.08	1.9	0.2	2
0.01B		3.0	0.03	137.28	25.62	18.66		1.8	—	1
0.01C		2.9	0.03	127.31	21.31	16.74		1.8	—	1
0.01BlkNoClay		3.0	—	—	—	0.80	—	2.0	0.1	2
0.1A	0.1	3.0	0.03	132.67	24.30	18.31	15.11	1.8	—	2
0.1B		3.0	0.03	136.79	14.88	10.88		1.8	—	1
0.1C		3.0	0.03	137.38	16.27	11.85		1.8	—	1
0.1BlkNoClay		3.0	—	—	—	1.17	—	1.9	—	1
0.3A	0.3	3.1	0.03	136.77	8.94	6.54	12.29	2.0	0.3	2
0.3B		3.0	0.03	141.60	12.30	8.69		1.8	—	1
0.3C		3.0	0.03	137.01	10.84	7.91		1.8	—	1
0.3BlkNoClay		3.0	—	—	—	-1.30	—	1.8	0.2	2
0.5A	0.5	3.0	0.03	129.17	3.85	2.98	11.63	1.8	0.1	2
0.5B		3.0	0.03	135.24	5.39	3.99		1.8	—	1
0.5C		3.0	0.03	123.49	6.41	5.19		1.8	—	1
0.5BlkNoClay		3.0	—	—	—	-1.18	—	1.9	—	1
0.8A	0.8	3.1	0.03	132.67	6.48	4.89	11.67	1.8	0.1	2
0.8B		3.0	0.03	137.35	10.20	7.43		1.8	—	1
0.8C		3.0	0.03	132.90	10.91	8.21		1.8	—	1
0.8BlkNoClay		3.0	—	—	—	0.20	—	1.8	0.1	2
1A	1.0	3.0	0.03	131.18	5.73	4.36	11.91	1.8	0.1	2
1B		3.1	0.03	137.28	5.60	4.08		1.7	—	1
1C		3.1	0.03	139.12	6.79	4.88		1.7	—	1
1BlkNoClay		3.0	—	—	—	1.00	—	2.3	—	1

Note: Samples with "Blk" indicates the control experiments with Ga only.

Table B5. Ga recoveries and interfering matrix element ratios of SRM NIST-994 and secondary standards purified using procedures A and B.

Summary			Measured element/Ga mass ratios						
Procedure	Experiment	Ga Recovery	Cu	Zn	Fe	Mo	Ba	Mn	Na
A	Syn BHVO2-a	107	3.9E-02	4.7E-02	5.4	1.3E-02	1.1E-03	8.5E-04	0.8
A	Syn BHVO2-c	103	0.2	0.1	6.5	1.2E-02	1.3E-03	2.6E-03	3.4
A	0.3N+0.7B-a	104	0.1	0.1	4.1	1.1E-02	5.6E-04	3.2E-03	0.5
A	0.5N+0.5B-a	102	4.2E-02	3.5	4.0	1.0E-02	1.3E-03	9.5E-04	3.7
A	0.7N+0.3B-a	100	4.9E-02	3.8E-02	3.2	1.1E-02	4.2E-03	1.9E-03	0.5
A	NIST-994-a	94	5.0E-04	0.1	0.1	1.1E-02	1.6E-04	2.4E-04	0.4
A	NIST-994-c	93	5.8E-03	0.2	0.1	1.1E-02	2.6E-03	2.3E-04	0.5
A	1X-a	98	5.4E-03	0.1	0.2	1.3E-02	2.8E-04	2.6E-04	0.5
A	10X-a	103	4.6E-02	4.9E-02	0.3	1.4E-02	2.4E-04	1.1E-03	1.2
A	20X-a	98	0.1	3.9E-02	0.3	1.3E-02	2.5E-04	3.3E-04	0.8
B	Syn BHVO2-b	104	0.1	0.3	2.3	2.0E-02	2.0E-03	1.0E-03	1.5
B	Syn BHVO2-d	103	0.1	0.1	2.3	1.8E-02	1.2E-03	1.2E-03	1.4
B	0.3N+0.7B-b	102	2.8E-02	4.3E-02	1.4	1.6E-02	4.0E-04	4.0E-04	0.5
B	0.5N+0.5B-b	102	0.1	3.7E-02	1.5	1.3E-02	5.5E-04	1.7E-03	0.4
B	0.7N+0.3B-b	101	4.3E-02	0.2	1.2	1.8E-02	5.3E-04	1.4E-03	0.6
B	NIST-994-b	97	6.6E-04	0.1	0.1	1.7E-02	3.7E-04	3.8E-04	0.5
B	NIST-994-d	96	1.4E-03	0.2	0.1	1.6E-02	3.6E-04	3.7E-04	0.5
B	1X-b	99	7.5E-03	0.2	0.1	1.8E-02	2.1E-03	3.7E-04	0.6
B	10X-b	100	4.1E-02	0.1	0.2	1.9E-02	2.1E-03	8.3E-04	0.9
B	20X-b	98	0.1	4.7E-02	0.1	2.0E-02	3.7E-04	4.1E-04	0.5
Suggested element/Ga mass ratios:			Cu	Zn	Fe	Mo	Ba	Mn	Na
			0.25	0.1	5	1.2	0.02	0.01	–

* Suggested ratios are from (Feng et al., 2019; Yuan et al., 2016; Zhang et al., 2016). Highlighted cells indicate ratios outside of suggested values. Recommended Na/Ga has not been reported, indicated by a dash.

Table B6. Ga/element ratios of matrix elements which can also induce polyatomic interferences during Ga isotope analysis, compared between procedure A and B.

Experiment	Al/Ga		Si/Ga		P/Ga		K/Ga		Ca/Ga	
	Proc. A	Proc. B	Proc. A	Proc. B	Proc. A	Proc. B	Proc. A	Proc. B	Proc. A	Proc. B
Syn BHVO2	0.2	0.4	0.9	1.2	3.0	3.6	0.4	0.6	0.4	0.8
0.3N+0.7B	0.2	0.1	0.7	1.3	2.7	3.8	0.4	0.3	0.5	0.3
0.5N+0.5B	0.3	0.1	0.9	1.2	2.8	4.3	1.8	0.4	5.0	0.4
0.7N+0.3B	0.1	0.1	0.7	1.5	2.8	4.6	0.3	0.5	0.4	0.8
NIST-994	0.1	0.1	0.8	1.1	2.4	3.6	0.3	0.4	0.4	0.6

Note: Cells highlighted in red indicate that the elemental ratio is higher than in Procedure A.

Table B7. Ga recoveries and interfering matrix element ratios for samples of purified adsorption experiments and Ga stocks testing the influence of pH.

Summary			Measured element/Ga mass ratios				
Experiment	Mineral	Ga Recovery	Cu	Zn	Fe	Mo	Ba
3KGA50	Kaolinite (KGa-2)	97	8.1E-03	7.0E-02	6.9	2.3E-03	4.5E-03
4KG-50		96	3.0E-03	5.0E-02	4.8	1.2E-03	1.7E-03
5KG-50		95	2.7E-03	1.0E-01	5.6	9.5E-04	1.2E-03
6KG-50		95	2.9E-03	4.0E-02	6.9	7.6E-04	1.1E-03
7KGA50		96	9.5E-04	4.6E-03	5.5	7.3E-04	2.7E-04
8KG-50		99	1.3E-03	3.4E-03	5.3	6.2E-04	2.9E-04
9KG-50		97	8.0E-04	8.6E-03	6.5	2.2E-02	1.8E-03
6SA-50	Ca-Montmorillonite (Saz-1)	99	2.3E-03	1.8E-01	7.2	7.8E-04	2.0E-02
7SAA50		99	2.4E-03	8.1E-02	6.3	4.1E-04	1.8E-03
8SA-50		97	2.3E-03	4.6E-02	5.8	6.1E-04	3.3E-03
9SA-50		98	9.8E-04	5.0E-02	5.9	4.5E-04	5.5E-04
3ALA50	Aluminum Oxide	96	2.7E-03	5.6E-02	5.5	7.7E-04	5.1E-03
4AL-50		95	1.5E-03	6.9E-02	6.0	4.4E-04	3.8E-03
5AL-50		95	2.0E-03	8.3E-03	8.5	2.2E-03	6.8E-04
7ALA50		94	6.7E-03	5.4E-03	7.4	1.3E-03	1.4E-03
8AL-50		90	1.9E-03	2.8E-02	5.7	7.7E-04	2.4E-03
9AL-50		92	3.6E-03	1.3E-02	5.4	8.0E-04	3.9E-04
3STK50	Ga stock	96	5.7E-04	1.1E-02	5.4	4.6E-04	8.3E-04
4STK-50		93	2.3E-03	4.8E-02	5.9	2.1E-04	2.4E-03
5STK-50		93	9.4E-04	0.1	6.2	4.9E-04	3.5E-03
6STK-50		87	1.1E-03	0.1	6.2	2.0E-04	6.8E-04
7STK50		94	3.1E-03	0.1	5.8	4.0E-04	1.1E-03
8STK-50		94	5.9E-04	5.5E-03	6.1	3.6E-04	3.7E-04
9STK-50		94	8.6E-03	0.1	6.5	6.6E-05	8.0E-03
Suggested element/Ga mass ratios:			Cu	Zn	Fe	Mo	Ba
			0.25	0.1	5	1.2	0.02

* Suggested ratios are from (Feng et al., 2019; Yuan et al., 2016; Zhang et al., 2016). Highlighted cells indicate ratios above suggested values. The first character of the experiment name indicates experimental pH.

Table B8. Ga recoveries and interfering matrix element ratios for samples of purified adsorption experiments, controls (Ga only), and Ga stocks testing the influence of ionic strength.

Summary			Measured element/Ga mass ratios				
Experiment	Mineral	Ga Recovery	Cu	Zn	Fe	Mo	Ba
0.01A	Kaolinite (KGa-2)	99	–	0.1	0.2	1.8E-02	3.2E-04
0.01B		103	–	2.7E-02	0.1	1.6E-02	5.9E-03
0.01C		97	–	3.7E-02	0.2	1.7E-02	7.4E-04
0.1A		103	–	3.4E-02	0.2	1.6E-02	5.3E-04
0.1B		99	–	8.2E-02	0.2	1.6E-02	3.6E-04
0.1C		100	–	2.7E-02	0.2	1.8E-02	–
0.3A		105	–	2.6E-02	0.2	1.7E-02	1.6E-03
0.3B		101	–	1.2E-02	0.2	1.6E-02	4.8E-05
0.3C		105	–	2.7E-02	0.2	1.6E-02	–
0.5A		101	–	2.6E-02	0.2	1.6E-02	4.3E-05
0.5B		101	–	2.6E-02	0.1	1.6E-02	1.8E-04
0.5C		103	–	0.2	0.1	1.5E-02	1.7E-04
0.8A		101	–	2.4E-02	0.2	1.5E-02	–
0.8B		101	–	6.0E-02	0.2	1.7E-02	2.1E-04
0.8C		104	–	3.9E-02	0.2	1.5E-02	1.4E-04
1A		102	–	2.3E-02	0.2	1.6E-02	2.7E-04
1B		103	–	0.1	0.2	1.5E-02	7.3E-04
1C		100	–	3.5E-02	0.2	1.5E-02	1.5E-04
0.01BlkNoClay	N/A	97	–	0.1	0.2	1.5E-02	2.7E-04
0.1BlkNoClay		95	5.7E-04	0.4	3.5	1.6E-03	1.1E-03
0.3BlkNoClay		104	–	0.1	0.2	1.6E-02	–
0.5BlkNoClay		100	6.4E-04	3.6E-02	3.1	1.4E-03	3.6E-04
0.8BlkNoClay		102	9.8E-04	0.1	0.2	1.9E-02	5.4E-04
1BlkNoClay		103	1.1E-03	0.1	2.7	9.3E-03	5.5E-04
0.01GaSTK	N/A	98	1.2E-03	4.5E-02	3.1	2.4E-03	3.6E-04
0.3GaSTK		101	4.3E-03	0.1	0.8	1.6E-02	1.3E-02
0.5GaSTK		106	1.5E-03	0.1	2.6	4.5E-03	1.9E-04
0.8GaSTK		104	9.4E-04	4.4E-02	0.4	1.6E-02	4.0E-04
Suggested element/Ga mass ratios:			Cu	Zn	Fe	Mo	Ba
			0.25	0.1	5	1.2	0.02

* Suggested ratios are from Feng et al. (2019). Highlighted cells indicate ratios above suggested values. Dashes indicate elements that were undetectable in concentration analysis. The first character in the experiment name indicates experimental ionic strength. Experiment names with "Blk" and "STK" indicate the control (Ga only) and Ga stock, respectively

Table B9. Ga/element ratios of matrix elements which can also induce polyatomic interferences during Ga isotope analysis.

Experiment	Category	Mineral*	Al/Ga	Si/Ga	P/Ga	K/Ga	Ca/Ga
Syn BHVO2-a	Mixing fraction (isotope data quality)	N/A	0.2	0.9	3.0	0.4	0.4
0.3N+0.7B-a			0.2	0.7	2.7	0.4	0.5
0.5N+0.5B-a			0.3	0.9	2.8	1.8	5.0
0.7N+0.3B-a			0.1	0.7	2.8	0.3	0.4
NIST-994-a			0.1	0.8	2.4	0.3	0.4
3KGA-50	Variable pH adsorption with 50 µg/L Ga	Kaolinite (KGa-2)	3.7	0.4	9.5	0.8	1.1
4KG-50			0.3	0.2	9.3	—	1.0
5KG-50			0.3	0.4	9.1	—	0.6
6KG-50			0.5	0.2	8.4	—	0.9
7KGA50			0.2	0.3	9.1	—	0.2
8KG-50			0.1	0.2	9.3	—	0.2
9KG-50			0.2	0.3	9.7	—	0.3
6SA-50		Ca-Montmorillonite (Saz-1)	1.4	0.3	9.3	—	0.7
7SAA50			1.1	0.5	9.0	—	0.4
8SA-50			0.3	0.5	9.2	—	0.3
9SA-50			0.3	0.4	8.4	—	0.4
3ALA50		Aluminum oxide	1.2	0.5	9.5	—	0.7
4AL-50			0.2	0.4	11.9	—	0.6
5AL-50			0.2	0.3	14.0	—	0.3
7ALA50			3.0	0.3	14.1	0.7	0.6
8AL-50			0.2	0.6	9.6	—	0.3
9AL-50			0.4	0.2	9.2	—	0.04
0.01A	Variable ionic strength adsorption with 3000 µg/L Ga	Kaolinite (KGa-2)	0.03	0.5	3.7	—	0.5
0.01B			0.03	0.4	3.7	—	0.1
0.01C			0.03	0.4	3.8	—	0.1
0.1A			0.3	0.5	3.7	—	0.3
0.1B			0.03	0.3	3.7	—	0.5
0.1C			0.02	0.5	3.7	—	0.1
0.3A			0.04	0.4	3.7	—	0.3
0.3B			0.01	0.4	3.7	—	—
0.3C			0.03	0.3	3.6	—	0.02
0.5A			0.1	0.5	3.5	—	0.1
0.5B			0.02	0.6	3.6	—	0.1
0.5C			0.01	0.5	3.7	—	0.3
0.8A			0.01	0.4	3.3	—	0.1
0.8B			0.2	0.5	3.9	—	0.3
0.8C			0.03	0.5	3.5	—	0.2
1A			0.02	0.4	3.8	—	0.0
1B			0.04	0.4	3.6	—	0.6
1C			0.04	0.4	3.8	—	0.1

* Only applies to adsorption experiments. Dashes indicate elements that were undetectable in concentration analysis.

Table B10. Summary of experiments testing the influence of pH on the Ga/Al ratio during adsorption at 21°C.

Experiment	Mineral	Ga_{added}	$Ga_{remaining}$	Al_{added}	$Al_{remaining}$	Ga_{lost}	Al_{lost}	$(Ga/Al)_{in}$	$(Ga/Al)_{fin}$
		µg	µg	µg	µg	%	%	mass ratio	
3KG50cc	Kaolinite (Kga-2)	24.1	21.5	23.1	25.0	11	-8	1.04	0.9
5KG50cc		25.0	8.5	23.6	15.0	66	36	1.06	0.6
7KG50cc		25.5	21.4	24.0	1.0	16	96	1.06	21.2
3SA50cc	Ca-montmorillonite (Saz-1)	24.5	1.1	23.5	8.0	95	66	1.04	0.1
5SA50cc		25.6	1.5	24.2	0.3	94	99	1.06	5.1
7SA50cc		25.2	16.4	23.8	0.7	35	97	1.06	23.4
3SI50cc	Crystalline Silica	24.6	3.5	23.6	489.4	86	-1974	1.04	0.01
5SI50cc		25.2	0.6	23.8	1.9	98	92	1.06	0.3
7SI50cc		25.6	8.0	24.1	0.3	69	99	1.06	28.2
3AL50cc	Aluminum Oxide	24.3	16.8	23.3	416.6	31	-1685	1.04	0.04
5AL50cc		25.0	7.3	23.7	22.6	71	4	1.06	0.3
7AL50cc		25.2	7.0	23.7	0.9	72	96	1.06	7.9
3GT50cc	Goethite	24.6	18.9	23.6	24.1	23	-2	1.04	0.8
5GT50cc		25.4	0.0	24.0	10.7	100	56	1.06	3.04E-03
7GT50cc		25.2	1.3	23.7	0.1	95	100	1.06	11.7
3BlkNoClay50cc	N/A	24.2	23.8	23.3	22.6	2	3	1.04	1.1
5BlkNoClay50cc		24.5	22.4	22.8	21.1	8	8	1.07	1.1
7BlkNoClay50cc		24.5	21.3	23.0	3.1	13	87	1.06	6.9

Where $(Ga/Al)_{in}$ and $(Ga/Al)_{fin}$ indicate initial and final ratios, respectively. "Blk" in the sample name refers to controls with no mineral and 50 µg/L Al and Ga. Numbers in experiment labels indicate experimental pH.